

# POLITECNICO DI TORINO

---

Dipartimento di Ingegneria Meccanica ed Aerospaziale

Corso di Laurea Magistrale

in Ingegneria Biomedica

Tesi di Laurea Magistrale

**Internal fixation of acetabular fractures: performance assessment  
through Finite Element Analysis**



Relatrice:

Prof.ssa Terzini Mara

Correlatrice:

Prof.ssa Bignardi Cristina

Candidato:

Andrea Di Pietro

---

Anno Accademico 2019/2020

# Index

---

<b>Abstract.....</b>	<b>3</b>
<b>1. Introduction.....</b>	<b>4</b>
1.1 Hip anatomy .....	4
1.2 Acetabular fractures .....	7
1.3 Non conservative treatments .....	11
1.3.1 Indication for surgery .....	11
1.3.2 Surgical treatment.....	12
1.3.3 Surgical accesses .....	13
1.4 Striker acetabular plates.....	15
1.5 Perren’s strain theory .....	16
1.6 Theory on Finite Elements Analysis .....	19
1.6.1 Linear elastic problem .....	20
1.6.2 Non-linear analysis .....	21
<b>2. Methods .....</b>	<b>25</b>
2.1 The four configurations .....	25
2.2.1 Hip bone geometry.....	27
2.2.2 Plate geometry .....	28
2.2.3 Screw, cartilage and femoral component geometries.....	35
2.3 Mesh generation .....	37
2.3.1 Plates mesh .....	37
2.3.2 Screws mesh.....	38
2.3.3 Pelvis mesh.....	40
2.3.4 Cartilage and femur meshes.....	41
2.3.5 Summary of meshed components.....	42
2.4 Materials and properties .....	43
2.5 Contacts definition .....	44

2.6	Boundary Conditions .....	46
2.6.1	Preloading of the screws .....	46
2.6.2	Single leg stance loading .....	49
2.7	Strain calculation .....	51
2.8	Assessment parameters .....	53
<b>3.</b>	<b>Results.....</b>	<b>54</b>
3.1	Stress distribution.....	54
3.1.1	Preloading of the screws .....	54
3.1.2	Single leg stance loading .....	60
3.2	Displacements field .....	65
3.2.1	Preloading of the screws .....	65
3.2.2	Single leg stance loading .....	68
3.3	Analysis at fracture gap .....	71
3.3.1	Axial strain.....	71
3.3.2	Shear strain .....	74
<b>4.</b>	<b>Discussion.....</b>	<b>77</b>
<b>5.</b>	<b>Conclusions .....</b>	<b>87</b>
	<b>Bibliography.....</b>	<b>88</b>

# Abstract

---

Acetabular fractures have a high impact on patient quality life, but at the same time are quite rare (3/100000/year). It has been estimated that only 3% of fractures observed in traumatology involve the acetabulum and it has been observed that, due to progressive rising of osteopenia and osteoporosis, the incidence of acetabular fractures resulting from a fall of fewer than 10 feet increased. On the contrary, a reduction of acetabular fractures occurred since the advent of mandatory seatbelt, with young people being the most affected in fractures caused by high velocity trauma, such as car accidents. From a pathophysiological point of view fractures of the acetabulum are caused by the impact of the femoral head on the articular surface, and the severity and typology of injury is determined by the femur position at the moment of impact: external rotation provides anterior fracture patterns whilst internal rotation is associated with posterior fracture patterns. Being acetabular fractures high energy injuries, they are often correlated with other pathologies such as damage to cartilage that can lead to future osteoarthritis and that could increase related morbidity; thus, for these reasons, it appears of primary importance developing good and reliable treatments for this disease.

This thesis work aims at the evaluation of the biomechanical performances of non-conservative treatments of acetabular fractures through a Finite Element approach. Six combinations of two acetabular fractures typologies (the elementary transverse fracture and the T-shaped associated fracture) and two pelvic plates models (the standard suprapectineal plate, already widely used in the non-conservative approach, and the Striker PRO suprapectineal quadrilateral surface plate) were analysed, also focusing on different screw fixation configurations (C1 and C2). The implemented models have been tested in a single leg stance condition that represents an activity that the patient could perform few weeks after surgery.

The comparison between configurations has been executed through the assessment of three main parameters, focusing substantially on the solicitation on the pelvic bone: The Von Mises stress and the displacement field of the bone and the fracture gap strains have been considered. The main outcome is identifiable in the major performance of SQBP C2 configuration, whose infrapectineal portion is able to better distribute the stress, avoiding dangerous solicitations on the bone. In terms of fracture gap strain analysis, the SQBP C2 combination can be considered the best compromise either for transverse and for T-shaped fractures. In conclusion, in relation to an elementary transverse fracture, adopting the SQBP C1 configuration should be preferable, whilst the most appropriate treatment for T-shaped fractures could be identified with the SQBP C2 configuration.

# 1. Introduction

---

## 1.1 Hip anatomy

Pelvic ring is a bony complex formed by two arches conventionally delimited by acetabular surfaces: the anterior one is made by ileo-ischio-pubic branches, three bones originating the hip bone with their fusion between tenth and sixteenth year of age; the posterior surfaces instead is composed of sacrum, iliac wings and sacrum-iliac joints.

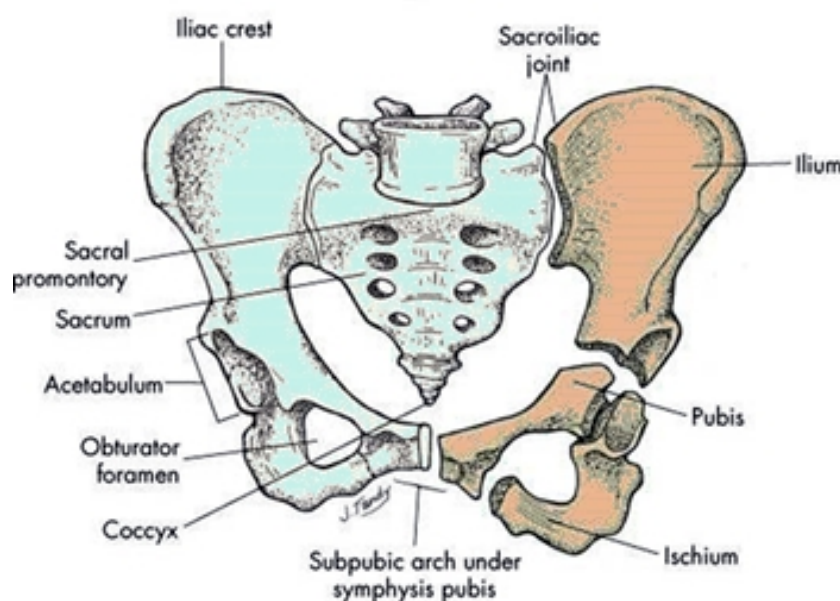


Figure 1.1 Pelvic bone anatomy

The pubis is formed of a body, an upper branch and a lower branch that delimit the anterior-medial portion of the obturator foramen. On the medial side there is the symphysis face of the bone which articulates with the contralateral one with the interposition of an interpubic disc. Above the symphysis face there is the pubic tubercle and this continues with the comb crest that laterally becomes an arcuate line of the ileum. At the point of passage between the upper branch and the ileum is located the ileopectineal or ileopubic eminence.

The ileum consists of a body and a wing. The body contributes to the formation of the acetabulum and has a supra-acetabular groove on the outside and an arcuate line on the inside. The wing presents externally a gluteal face with the three gluteal lines (lower, anterior and posterior), internally the iliac fossa and in the posterior portion the auricular surface that articulates with the sacrum.

The iliac crest begins anteriorly with the anterior superior iliac spine (ASIS, below which there is the anterior inferior iliac spine, AIIS) and continues posteriorly, forming an outer and inner lip. The outer

lip has a lateral protrusion called the iliac tubercle. The iliac crest ends posteriorly with the upper posterior iliac spine (SIPS), beneath which is present the lower posterior iliac spine (SIPI).

The ischium consists of a body and a branch which, joining with the lower branch of the pubis, delimits the obturatory foramen at the bottom. The ischial spine separates the large ischial incision from the small one. The ischial tuberosity is part of the ischial branch.

The sacrum originates from the fusion of the five sacral vertebrae. Anteriorly it presents a concave pelvic face, posteriorly a convex dorsal face. The surface that articulates with the last lumbar vertebra with the intervertebral disc interposition is called the base of the sacrum. The distal apex articulates with the coccyx. The portion of the sacrum next to the forams is called the sacral wing and is formed by the fusion of transverse processes. In the dorsal face there are five longitudinal ridges formed by the fusion of spinous, articular and transverse processes. The lumbo-sacral joint is the most anterior point of the spine, which is the reason it is called the promontory. Laterally to the wings are located the auricular surfaces that articulate with the ileum.

The acetabulum is the melting point of the three ileum, ischium and pubis bones. It is delimited by the edge of the acetabulum and contains the acetabular fossa, which is surrounded by the semi-lunar surface, covered by articular cartilage. Commonly, in the acetabulum the front and rear wall, the roof, the posterior upper segment (joins the roof and the rear wall) and the posterior lower segment (includes the last part of the rear wall and the rear horn of the articular surface) are distinguished. Acetabular fractures involve most of the walls of the articular surface and the bone segments supporting the acetabulum.

For a better understanding of the acetabular fractures Letournel and Judet described the acetabulum as contained between the oblique arms of an "inverted Y" (Fig. 1.2), formed by a posterior column, the ileo-ischiatic component and a longer anterior column extending from the anterior part of the iliac crest to the pubic symphysis; the upper part of the posterior column is joined to the posterior part of the anterior column slightly above its half.

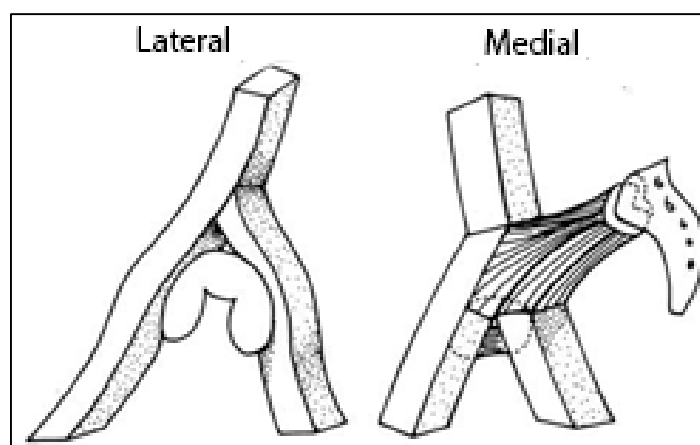


Figure 1.2 Letournel and Judet "inverted Y" hemipelvis

The pelvic ring does not have great intrinsic stability and therefore is made stable by the presence of ligamentous structures. The pelvic stabilizing structures are the pubic symphysis, posterior sacroiliac ligaments, anterior sacroiliac ligaments and sacrospinous and sacrotuberal ligaments. The first two structures are the most important for maintaining the conformation and stability of the pelvic ring.

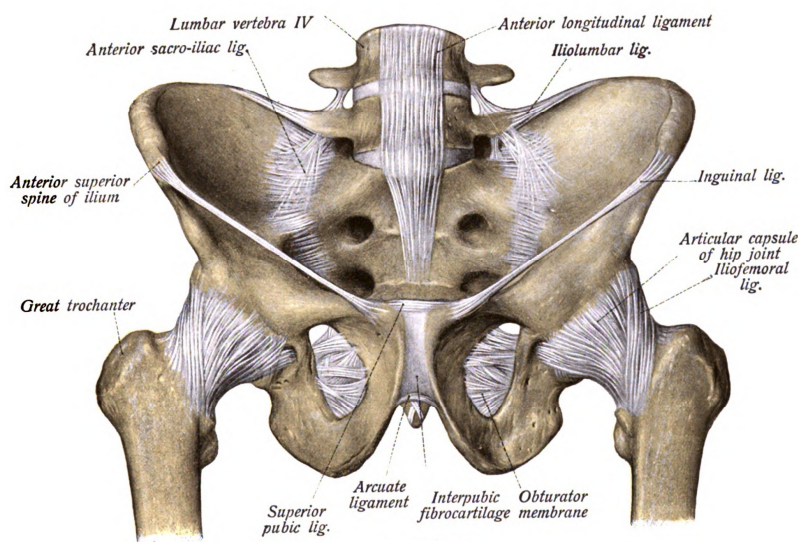


Figure 1.3 Ligamentous structures in the hip

The two hemipelvis articulate anteriorly in the pubic symphysis with the interposition of a fibrous cartilage disc called interpubic disc generally less than 5 mm thick, on average thinner in men than in women. Cranially and caudally the symphysis is reinforced by the upper pubic ligament and the arcuate ligament of the pubis, respectively. The sacroiliac joint is an ampharthrosis surrounded by a very strong fibrous capsule, reinforced by the anterior, interosseous and posterior sacroiliac ligaments. The movement of this joint during gait is rather limited. The posterior part of the pelvic ring was compared by Tile [1,2] to a bridge with two pylons consisting of the posterior superior iliac spines, a tensostructure consisting of the sacroiliac ligament complex and the bridge itself consisting of the sacrum. This tensostructure, which is probably the strongest ligamentous structure of the human body, is further reinforced by the ilio-lumbar ligaments which are inserted into the transverse processes of L5 and the iliac crest. The sacrospinous ligament connects the lateral margin of the sacrum to the ischial spine and prevents external rotation of the hemipelvis. The sacrotuberal ligament, on the other hand, resists both the rotational forces applied along the horizontal plane and the shear forces applied along the vertical plane. The inguinal ligament runs from the anterior iliac spine to the pubic tubercle. Below this is the inguinal canal which laterally contains the musculorum lacuna and medially the vasorum lacuna separated by the ileopectoralis bendelletta. The musculorum lacuna contains the ileopsoas muscle and the femoral nerve, the vasorum lacuna contains, in the latero-medial direction, the artery and then the femoral vein. The forces acting on a hemipelvis during a traumatic event are arranged in three main directions: external rotation, internal rotation and shear forces in the vertical plane. In high-energy trauma, the forces often act on different planes simultaneously.

1. **External rotation:** it can be caused by a force applied directly on the posterior iliac spines or, more frequently, by a forced external rotation of the thigh. The result is a fracture of the hemipelvis that is defined as an "open book". This is characterized by the destruction and opening of the pubic symphysis and, if the force is sufficiently intense, by the rupture of the anterior sacro-iliac and sacro-spinous ligaments.
2. **Internal rotation:** it is determined by lateral compression forces, acting directly in the lateral-medial direction on the wing or iliac crest or indirectly through the head of the femur as a result of trauma to the lower limb which may therefore result in acetabular fractures. These forces result in compression fractures of the posterior complex and, anteriorly, fractures of the ipsilateral and contralateral ileo-ischio-pubic branches.
3. **Shearing forces on the vertical plane:** acting along the main trabecular lines of the pelvis, they can cause the destruction of the posterior ligament complex and give important breakdowns of bone fragments together with marked soft tissue damage.

## 1.2 Acetabular fractures

Pelvic ring fractures are pathological entities of rare occurrence, occurring with an incidence of about 20-37 per 100,000 individuals per year [3,4]. Less than 10% of these involve the acetabulum, with an incidence of about 3 per 100,000 individuals per year [5]. In 63% of the cases there are fractures of the associated type, instead 37% concern of simple type fractures. Fractures of both columns are the most frequent, representing 25% of acetabular fractures, followed by posterior wall fractures [6,7]. The age groups most affected are between 15 and 30 years of age (37%) and between 50 and 70 years of age with a slight predominance for the male sex (56.7%). The percentage frequency with respect to all fracture events, varies from 0.3% to 6%, but in polytraumatized patients the percentage of involvement of the pelvic ring, and potentially of the acetabulum, rises to 20%. A high percentage of patients, mostly young subjects, victims of high-energy trauma, have concomitant injuries, in particular it has been estimated that 69.4% have head, chest or limb trauma [8]. The first cause of acetabular fracture are road accidents, especially those with lateral impact, in which mainly young individuals are involved and which commonly cause associated fractures of the pelvic ring or other body districts, as a consequence of the high energy of such traumatic events. The incidence of severe pelvic injuries in the context of road trauma is constantly increasing [9,10]. The second cause in order of frequency is precipitation trauma. In particular, in young people it is usually precipitation from great heights, while in older subjects it is not uncommon to find fractures caused by moderate or low-energy trauma, such as simple falls to the ground, caused by physiological bone weakening due to osteoporosis and often in association with other fractures involving the lower limbs, which in these cases may be the cause or consequence of the fall [7,11]. For a long time the traditional classification of acetabulum fractures has identified two broad categories: central dislocation and posterior dislocation of the pelvis with acetabulum fractures. Already in 1951 Cauchoix and Trouchet realised that not all aspects of acetabular fractures could be traced back to this classification and that it was necessary to recognise the existence of intermediate forms. In the following years, various authors

proposed different classifications, up to the one suggested by Letournel, which today is universally recognized as the most important both in the diagnostic phase and in order to set a correct surgical strategy [12]. This classification proposes the subdivision of acetabular fractures into two large groups: elementary fractures and associated fractures. Elementary fractures are those in which a part or the entire column supporting the acetabulum appears interrupted or detached from the rest of the pelvis. Associated fractures are given by the coexistence of at least two elementary fractures [13,14,15,16].

According to Judet and Letournel's classification, it is possible to distinguish the following elementary fractures:

- Type A: Back wall
- Type B: Back column
- Type C: Front wall
- Type D: Front column
- Type E: Transverse

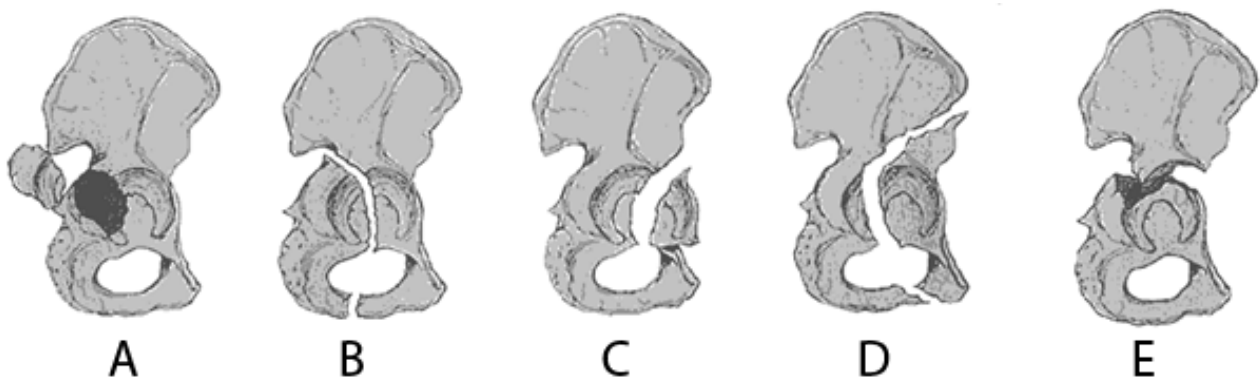


Figure 1.4 Elementary fractures classification described by Judet and Letournel

They have also included the associated fractures that with a more complex geometry, require the concurrence of at least two elementary shapes. The five main associations are:

- Type A: Column and back wall.
- Type B: Transverse and posterior wall (with a dislocation of the femoral head posteriorly or centrally).
- Type C: T-type.
- Type D: Front column + rear transverse emitter.
- Type E: Bicolumn.

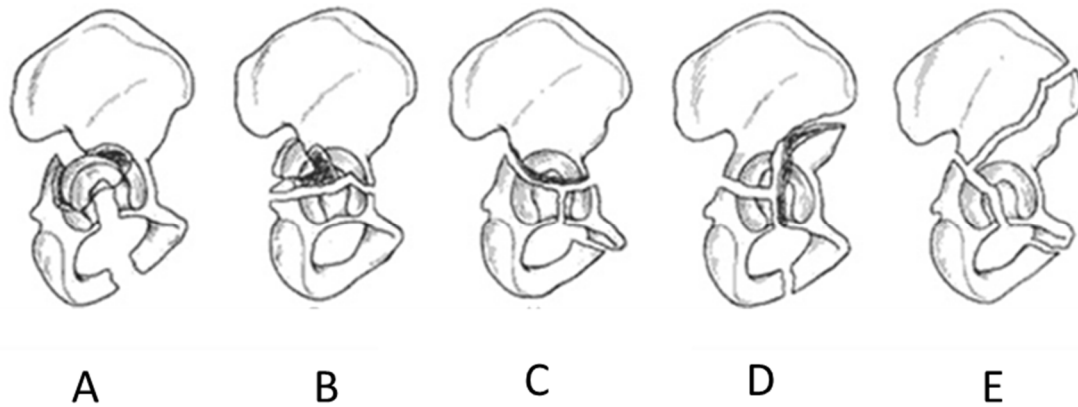


Figure 1.5 Associated fractures classification described by Judet and Letournel

Although several fractures of the associated type involve both columns of the acetabulum, the term bicolumnar fracture, in this classification, identifies that fracture in which none of the articular fragments of the acetabulum retains any bone continuity with the axial skeleton: a rhyme of fracture divides the ileum, so that the sacroiliac joint is no longer connected to any articular fragment. The classification proposed by Letournel was subsequently modified by the A.O. school, which developed an alphanumeric classification system for fractures of the acetabulum based on the severity of the fracture and which partly resume the types defined by Judet and Letournel [17].

1. **Type A:** partially articular with one column:

- A1: posterior wall
- A2: posterior column
- A3-1: front wall
- A3-2: front column

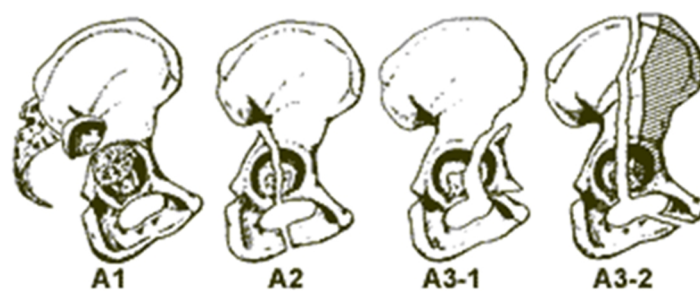


Figure 1.6 A.O. School classification - Type A fracture

2. **Type B:** partially articular, crosswise oriented with roof portion attached to the intact ileum:

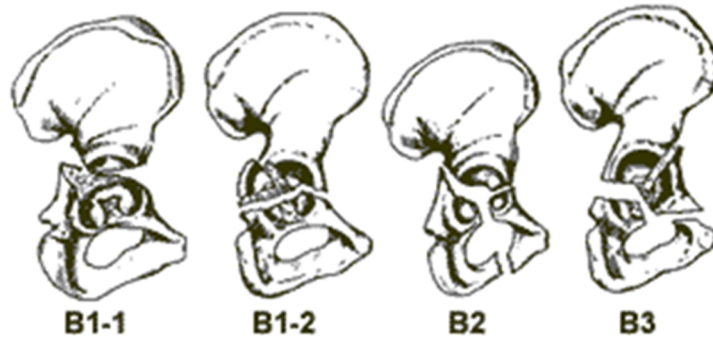


Figure 1.7 A.O. School classification - Type B fracture

- B1-1: transverse
- B1-2: transverse + rear wall
- B2: T-shaped
- B3: front column + rear hemitransverse emitter

3. **Type C:** full articular with both columns (the so-called floating acetabulum):

- C1: both columns, fracture line at iliac crest level.
- C2: both columns, fracture line at the lower anterior iliac spine.
- C3: both columns, fracture line inside the sacroiliac joint.

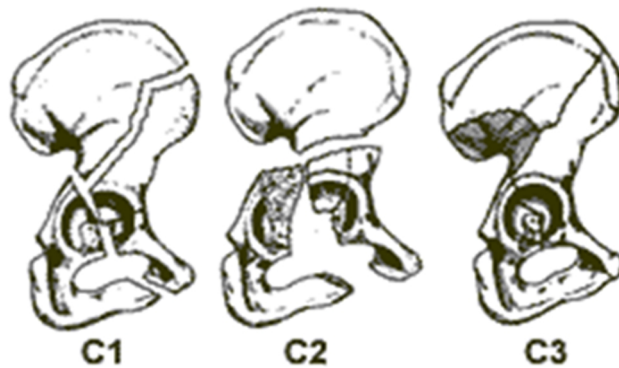


Figure 1.8 A.O. School classification - Type C fracture

## 1.3 Non conservative treatments

Acetabulum fractures remain among the most challenging fractures for the orthopaedic surgeon to treat successfully [18]. The complexity of the cup anatomy and the proximity of noble structures such as vessels, nerves and pelvic organs is the basis for an increased risk of severe complications (in addition to those that can be produced by trauma) both intra-operatively and post-operatively, so that in the past the vast majority of acetabular fractures were treated conservatively. The results of this type of treatment, however, were modest, since the acetabulum is the pelvic part of the coxo-femoral joint, and its reduction is not precise and heavily affects hip function, which was always more or less compromised. More generally, all pelvic lesions, due to the particular anatomy that places the osteo-legamentous structures in close relation with the vascular structures, are always associated with a certain amount of bleeding that can be of venous, arterial or mixed origin. The sequence and type of treatment of a pelvic ring fracture are therefore essentially established on the basis of two factors: the hemodynamic conditions of the patient and the type of possible pelvic instability [19,20,21]. These evaluations are of great importance since the interventions that can be performed differ enormously in terms of speed of execution, difficulty and invasiveness. Moving on to the surgical indication, it should be noted that the acetabular fracture, by definition, is an articular fracture, therefore it requires anatomical reduction and stable synthesis in order to obtain the best results, since, according to the results of numerous studies [22,23,24,6] fractures that present even the slightest incongruity are destined to develop early arthrosis. It's only in rare cases where the fracture is compound (fragment distance less than 2 mm) and stable conservative treatment can be followed, (i.e. when the anterior column is partially involved), that the affected hip movement is possible without any pain. Of course, there must be no sinking of the articular surface, which in all cases requires surgical treatment, otherwise there will be joint incongruity and the subsequent rapid development of post-traumatic coxarthrosis. The timing of the operation depends on the patient's general condition and on the execution of the necessary investigations to understand the type of fracture. There is no urgency to perform the surgery, except in the case of simultaneous hip dislocation, which must be reduced. The surgical treatment should be carried out in the days immediately following the patient's arrival and in any case no later than 3 weeks, as after this period the reduction of fragments is much more difficult, the reference points become not easy to recognize and the results are no longer satisfactory as in an early treatment [18].

### 1.3.1 Indication for surgery

The possibility of surgical treatment should be considered by analyzing not only the type of acetabular fracture and its breakdown, but also by contemplating characteristics such as the age of the patient, the associated comorbidities, the clinical picture resulting from the trauma, the anesthesiological difficulties and the surgical intervention itself. For the reasons mentioned above,

trauma surgery of the acetabulum should preferably be performed in specialized centers where a specially trained and experienced team in this branch operates. The indication for surgical treatment is usually given in cases with unstable fractures of the acetabulum and in the absence of congruence. Apart from the reduction by external maneuvers of a posteriorly dislocated femoral head which must be performed by emergency procedure, regardless of the type of acetabular fracture, only three conditions have the character of surgical urgency [25]:

- an irreducible dislocation of the femoral head;
- an unstable reduction of the dislocated femoral head;
- a posterior dislocation of the femoral head associated with a segmental fracture of the femoral head (pipkin fractures).

Sometimes these indications are not respected in practice due to the presence of other patient problems that may take precedence over acetabular reconstruction. Except for the cases mentioned above, no acetabular fracture is ever an urgent case and the demanding surgery involved in its treatment should never be performed in the middle of the night by a tired or inexperienced team. The ideal is to operate between the second and sixth day after the trauma, once the pelvic bleeding has stopped spontaneously. In the meantime, it is not necessary to put the limb in traction, and the patient simply needs to block his legs by pillows. Internal osteosynthesis surgery should be considered if an important joint incongruence is evident from the beginning [26]. In the absence of marked signs of impact or abrasion, and especially in young adults with relatively compound fractures, reduction surgery and internal osteosynthesis should be preferred [27]. A reduction of less than 3 mm is the threshold used to evaluate the success of the intervention [22,24,28].

### **1.3.2 Surgical treatment**

The coxofemoral joint is an important joint that bears a great load, both in maintaining the upright station and during walking. If it is left in a state of subluxation or joint inconsistency the inevitable long-term consequence will be arthrosis. Most surgeons agree that an accurate reconstruction of the joint surfaces is the best guarantee for the restoration of normal function of a traumatised joint [22]. The aims of surgical treatment are the exact reconstruction of the articular surface of the acetabulum and the achievement of stable internal fixation, allowing early post-operative movements and the possible use of continuous passive mobilization. A proper osteosynthesis of the surface can only be achieved through a perfect reconstruction of the acetabular components [16,29]. The cup is an elementary anatomical structure, particularly difficult to attack: access to the fracture site must therefore be established after an in-depth study of the radiograms in the three projections, antero-posterior, wing and obturator, with the possible aid of more sophisticated instrumental investigations (CT, 3D CT) and after a correct classification of the type of fracture [25]. Since this is a particularly complex pathology, both diagnostically and therapeutically, it would be desirable for acetabular fractures to be treated in specialised centres, equipped with appropriate equipment and

highly experienced staff. The intervention consists of open reduction and internal synthesis with plates and screws (Open Reduction Internal Fixation - ORIF) [12]. The reduction techniques involve transkeletal, longitudinal or femoral neck traction, or the use of the large distractor or even manual traction. It is necessary to have special instruments, specially designed for pelvic surgery, since the forces present in the pelvis are considerable and the proximity of noble structures requires maximum attention. Once the reduction of the acetabular fracture has been obtained, it is essential to control it by means of a brightness amplifier, as it is not always possible to directly visualise the result of the reduction. The number and configuration of screws and plates to be used as osteosynthesis depends on the type of fracture. The screws are used to stabilise fragments such as the walls of the acetabulum, taking care not to penetrate into the acetabular cavity, while the plate will serve to protect the previous synthesis. There is no precise rule on how many screws and plates to use, given the wide variety of possible fractures; the purpose of osteosynthesis must be to properly stabilise the fracture to allow the patient to move the hip painlessly from the first days after surgery and to be able to mobilise it with crutches afterwards. The stability of the osteosynthesis and the quality of the reduction achieved are the fundamental prerequisites for achieving the best results at distance of time [18].

### ***1.3.3 Surgical accesses***

Several surgical accesses have been described for the bloody treatment of acetabular fractures. Of all the access routes to the cup, none is able to highlight the acetabular cavity in all its shape. For this reason, before treatment, it is important to study the lesion well, adapting the surgical plan to the specific type of fracture being treated. The ileo-inguinal approach was developed by Emile Letournel, based on dissections of corpses, in order to obtain anterior access for acetabulum fractures. Surgical exposure requires a great deal of attention to the mobilisation of the femoral vessels and nerve, as well as the spermatic funiculus in males or the round ligament in females. With the patient in supine decubitus, the incision starts at the central point of the iliac crest, curves towards the anterior superior iliac spine, continues parallel to the inguinal ligament and ends 2 cm above the pubic symphysis (purple line in Fig 1.9).

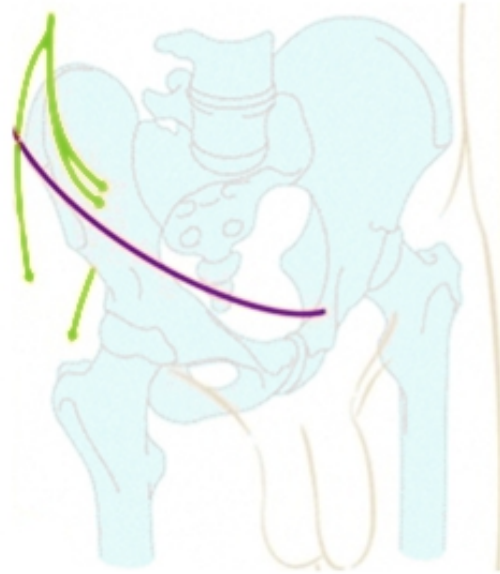


Figure 1.9 Ileo-inguinal approach incision

Conversely in the anterior intra-pelvic approach modified by Stoppa the patient is placed supine on a radiotransparent operating bed. The surgeon positions himself on the side opposite the fractured acetabulum. With this approach the surgeon has to protect the obturatorial vascular-nervous beam and the lumbosacral trunk for the duration of the operation. The oblique incision is 2 cm above the pubic symphysis and extends from the ipsilateral outer groin ring to the contralateral outer ring (purple line in Fig 1.10)

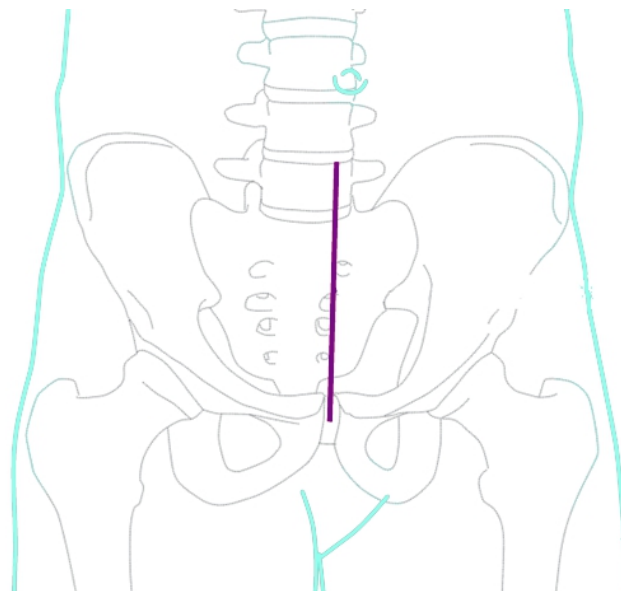


Figure 1.10 Intra-pelvic approach modified by Stoppa incision

## 1.4 Striker acetabular plates

In this thesis two different plates were considered, both belonging to the Striker company which developed the Pelvic Reduction and Osteosynthesis (PRO) plating system: the suprapectineal quadrilateral buttress plate (SQBP) and the Matta suprapectieal pelvic plate (SPP) or standard suprapectineal plate. The standard suprapectineal pelvic plate (SPP) according to the brochure provided by Striker [30] is a pre-contoured plate built in annealed stainless steel with 2.5 mm thickness and 12 mm spacing between the holes. They are realized in this way to be provided of the flexibility to adapt to the patient-specific hip bone. They have been projected to take into account both male and female average anatomy utilizing two kinds of curvatures (R88 for females and R108 for males). Round and tapered plate edges are designed to facilitate plate sliding submuscularly. Another characteristic is the possibility of wide screw angulation within the 3.5 mm diameter screw hole : especially for wall fixation it can be placed up to 70° from the hole axis in order to reach the preferred angulation.



Figure 1.11 *Suprapectineal pelvic plate by Striker (SPP plate)*

The suprapectineal quadrilateral buttressing plate has basically the same features of the standard one but additionally can boast of an other part lying on the infrapectineal side of the pelvis linked with the other through two bridges.



Figure 1.12 *PRO Suprapectineal quadrilateral buttressing plate by Striker (SQBP plate)*

The design of these plates allows them to buttress the quadrilateral surface and are chosen primarily in the treatment of the following fractures:

- Anterior column;
- Anterior column and posterior hemi-transverse;
- Associated both column;

- High transtectal transverse that exits in the posterior column near the sciatic notch.

This plate is provided of 16 screw holes, pre-angled in order to leave away the acetabulum, and accept both 3.5 and 4.5 mm screws with the same angulation as the standard plate. The central perpendicular hole is designed for the attachment to the handle for plate insertion but it can also be used as a screw hole. A characteristic of this plate, thanks to the 90° bent triangular component, is that provides simultaneous fixation in both the anterior and posterior columns by mechanical connection. The suprapectineal portion of the plate buttresses the anterior column (a), and respectively the infrapectineal portion (b) does with the quadrilateral surface (Fig. 1.13).

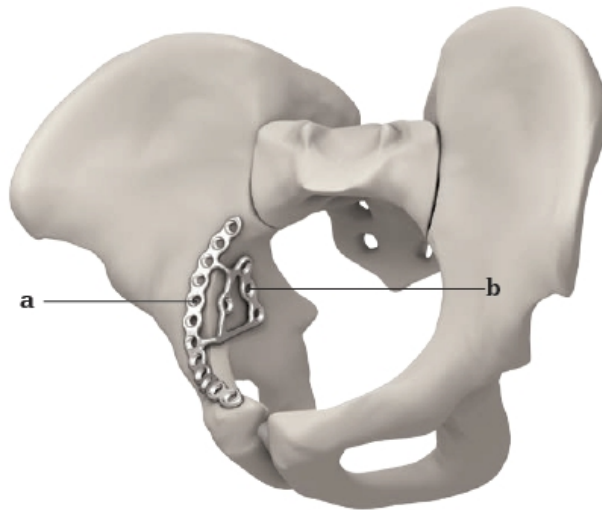


Figure 1.13 *Suprapectineal (a) and infrapectineal portions of SQBP plate*

As well described by Gras et alii [31], the main approach adopted using this 3D suprapectineal plate (SQBP) corresponds to the anterior intra-pelvic approach whether the fracture is elementary; instead, when it deals about high column fractures or insufficient fracture reduction, the methodology to operate in addition with the first window of Letournel's ilioinguinal approach, has been widely chosen. In this study, furthermore, has been reported that in 87% of cases considered, it has not been necessary to bend this plate in-situ during the surgical operation because of its native precontoured feature that already follows the standard hip connotations. This suprapectineal plate, moreover, allows a standard fixation along the iliopectineal line and buttressing the quadrilateral surface stabilizes the posterior column fractures underneath the 90° bent portion of plate.

## 1.5 Perren's strain theory

In scientific literature is widely accepted the idea that a fracture healing is not a standardized phenomenon, but it might follow different approaches. At the basis of this concept some theories can be investigated, such as the Perren's one, according which the environment that surrounds a fracture, could lead to a specific way of healing or a non-healing. In fact, some studies [32,33,34]

affirm that the bony healing is a complex phenomenon mainly mediated by two factors: a mechanical and a biological one. These recent scientific findings take inspiration from the ancient Wolff theory [35] written in 1892, that suggest a correlation between bone and mechanical stimuli. More precisely Wolff declared that distribution and orientation of trabecular bone adapt dynamically to the applied external load and that bone structures remodel themselves with particular orientation and distribution in order to minimize internal stress. Decades later, Frost [36] resumed and expanded the Wolff's laws by defining its concept of "mechanostat", according which bone is in continuum balance between remodelling made by osteoclasts and lamellar bone formation thanks to osteoblast activity: the one or the other behaviour is triggered by a defined external stimulus. Although Perren's theory is specific to bone fractures differently from Wolff's law and Frost's mechanostat theory, as explained by Elliott [37] they all provide an unified explanation of the complex mechanism related to bone healing; in fact is not rare the possibility of fracture non-unions, especially in case of multi-fragmentary fractures as *"today, the hypertrophic pattern of non-union is widely accepted to be due to mechanical factors and the atrophic pattern to be avascular "* [37]. In other words, there is a mechano-biological balance that governs the fracture healing, where the presence of biological factor and the entity of mechanical stimuli imply either the possibility of fracture non-union or the reaching of a typology of stability instead of the other. The two kinds of stabilities that take part in this complex balance are the absolute and relative ones. Absolute stability is of direct type as it is exclusively related to the generation of new lamellar bone through the formation of haversian channels on the fracture surface, without the intermediate generation of bony callus. It is obtained by stabilizing the fracture with rigid internal fixation without leaving fracture gap (i.e. using compression plate) in order to prevent any movement to the fracture rhyme. This stability is related to a primary healing and there is no certainty it deals about a short-term healing. Instead, relative stability is correlated to indirect stability, it consists of several intermediate steps before the complete healing in lamellar bone. It is reached through biological phenomena: initially granular tissue is formed, a precursor of soft and hard bone callus called woven bone, and then it is converted into compact bone after cartilage deposition; substantially, the mechanism is that the tissue formed after fracture progressively stiffens till the strain is low enough (2 to 5 %) to allow bone formation [37]. In practice, from a clinical perspective this is reached through a "flexible" internal fixation (i.e. using bridge plate) that allows some movements of the fracture rhyme. The healing time related to this approach could also be shorter than the absolute stability. Depending on the typology of internal fixation adopted, that is using a bridge plate rather than a compression plate, it is possible to impose a relative stability instead of an absolute one. This theory is also called interfragmentary movement analysis (IFM) because it studies the movements of the various fragments of bony stumps, but nevertheless does not refer exclusively to the concept of movement expressed in mm, instead it is widely explained also through the concept of strain present in the fracture gap. Strain is so mathematically defined:

$$\varepsilon = \frac{l_F - l_I}{l_I} * 100$$

Where  $\varepsilon$  is the percentage elongation or contraction of the fracture gap and  $l_F$  and  $l_I$  are respectively the final gap distance and the initial gap distance of the fracture.

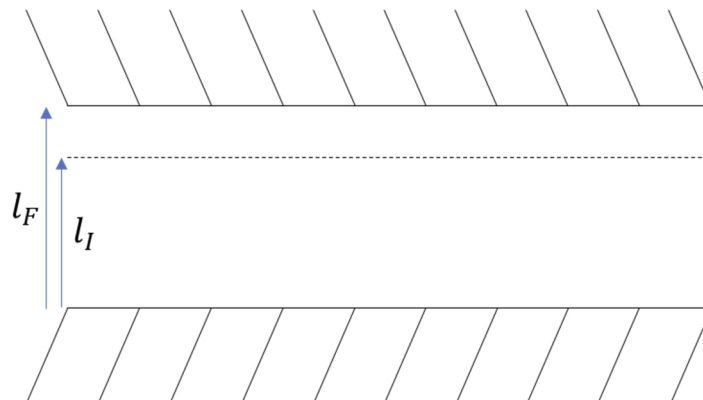


Figure 1.14 Fracture gap axial strain

The strain theory takes in consideration in addition to the module of movement also its direction; in fact, both axial strain and shear strain are been defined as mechanical stimuli respectively in perpendicular and transverse direction to the fracture plane. In our case, as the screw placements are quite distant to the fracture gap, the internal fixation methodology of the plate could be considered closer to a bridge plating rather than to a compression plating method; and thus, this internal fixation modality in relation to the developing of a relative stability could be evaluated. In literature there are several and even contradictory theories dealing with a quantification of the optimal strains that would promote callus formation. Regarding the axial strain, Perren’s theory refers to an optimal range comprised between 2 and 10 % in compression. In fact according to Perren [32], fracture needs to be subjected to a minimal axial compression (2%) that is the lower threshold to obtain the callus induction, but at the same time axial compression should not cross the upper limit of 10 % in order to allow bony bridging [38, 39].

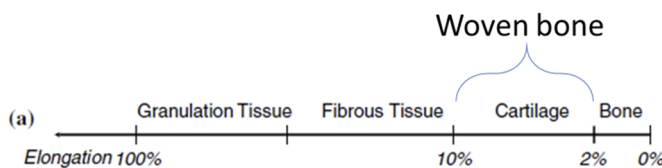


Figure 1.15 Axial strain optimal range [2 -10] % for woven bone formation. Image taken from [44]

Other studies [40,41,42,43] instead suggest that having too large shear strain at the fracture gap should be dangerous for reaching the relative stability. In fact, high transversal movements on the fracture rhyme could determine rupture of the growing blood vessels, fundamental for bone callus formation [33]. For that, a criterion to define shear strain behaviour in fracture rhyme is the minimalization of these strains. In literature [44,45] also the octahedral shear strain is considered for the evaluation of a quantitative analysis and it is expressed that for optimal bony healing it should remain between the range 0.04 – 3.75 %.

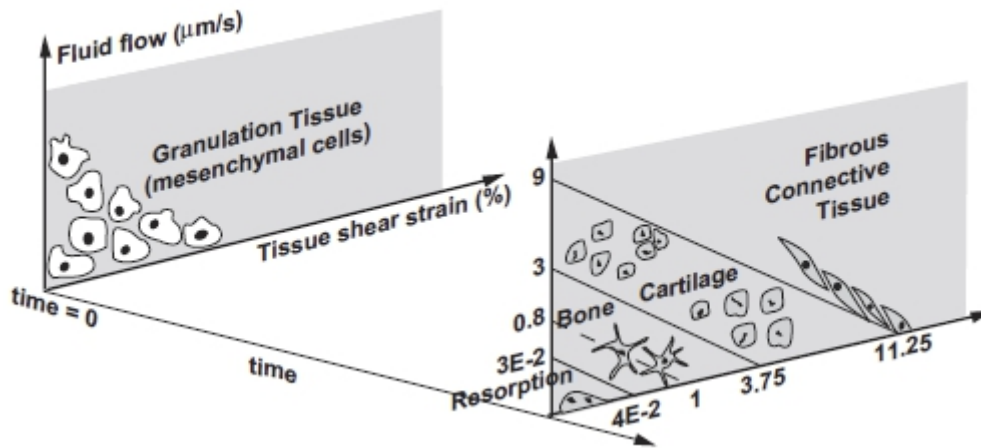


Figure 1.16 Octahedral shear strain optimal range [0.04-3.75] % for woven bone formation. Image taken from [44]

## 1.6 Theory on Finite Elements Analysis

Finite element analysis is a widespread methodology in engineering, adopted above all in solid mechanics, that uses tools belonging to the finite element methods (FEM) that allow numerical solution of differential equation systems, unsolvable in closed-form expression. It is based on the reproduction of real phenomena even with complex geometric domain, into its in-silico representation, in order to study or predict its physical behaviour. The first step of FEA analysis is the pre-processing phase, then the solving phase comes and eventually the post-processing one. More specifically the pre-processing step is the crucial and longest one because fundamentally here the mesh of our model is obtained after having defined and realized all the geometries that take part to the project. The mesh generation is very important because on its nodes are calculated the differential equations which provide the solution of the problem, thus for that reason it is deduced that the quality of mesh is relevant for a satisfying result. FEA analysis is not a pure and fully-faithful representation of reality, in fact it consists of a discretization of 'something' that in reality appears as a continuum; so in FEA environment equations are solved in some specific points called nodes, constituting mesh seed, and then thank to shape functions, adopting polynomial functions, results can be extended all over the other points of the domain. Once generated the mesh, defined the material properties and applied the specific boundary conditions such as forces and bonds that define our problem of interest, the solving environment that provides the numerical solution of the differential equations is set up, converting them into polynomial ones. The post-processing steps consists in the evaluation of results by the user, extrapolating the information of interest such as stress and deformation. In most of cases, under certain conditions, problems with a linear-elastic approach have been treated but in other situations this is not more valid because of the presence of elements and features that bring non linearities between stress and deformation, such as happens in this thesis study.

### 1.6.1 Linear elastic problem

The linear elastic static formulation consists in determination of tension, deformation and displacements fields of an elastic linear material solid, bonded and loaded with an external force. As mentioned before the linear elastic behaviour occurs only in particular conditions called also elastic static problem where the following hypothesis are guaranteed:

1. Linear, elastic, isotropic behaviour of materials
2. Infinitesimal displacements
3. Absence of contacts and structural instabilities
4. Absence of dynamic effect
5. Invariant time behaviour

The elastic linear problem follows three main laws to get the numerical solution: the first equations to consider are the *undefined equations of equilibrium* that affirm that the external load is in equilibrium to the internal tensions in the element (Fig.1.17):

$$\nabla \sigma + F = 0$$

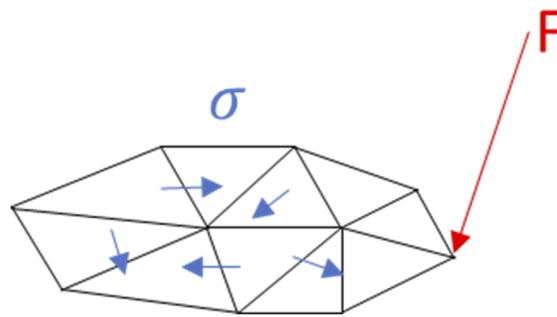


Figure 1.17 Internal equilibrium of stress in a meshed structure

Where  $\sigma$  is the stress tensor and  $F$  the vector of the external load applied.

The second equation considered is the compatibility equations, in case of little displacements, they define that the strain field as a differential operation of the displacement field can be conceived:

$$\varepsilon = \text{diff } u$$

Where  $\varepsilon$  is the deformation field and  $u$  is the displacements field.

The third fundamental law used in linear elastic formulation is just the *stress-strain relation* or *constitutive equation* which correlates the stress and strain fields:

$$\sigma = E \cdot \varepsilon$$

Where  $\sigma$  is the stress field,  $\varepsilon$  is the deformation field and  $E$  is the Young Modulus of the material. The solving method of linear analysis is based on the discretization of the domain into elements delimited by nodes; known  $F$  (external force vector) applied to the structure and the bonded nodes,

it is possible to obtain the nodal displacements vector  $f$  through the *generalized Hook's law*, knowing the rigidity matrix  $K$  of the structure (Fig. 1.18):

$$f = K^{-1} \cdot F$$

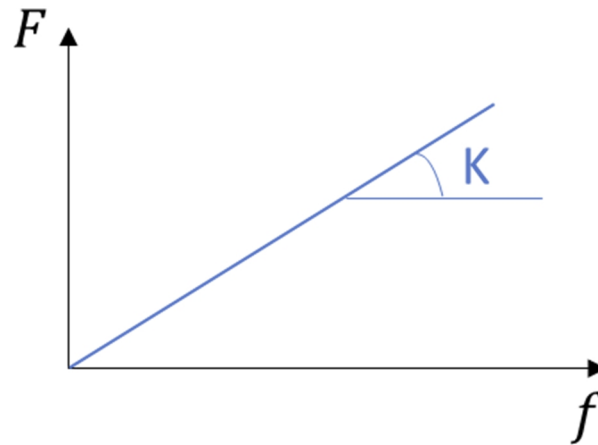


Figure 1.18 Generalized Hook's law representation

Once obtained  $f$  it is possible to extract through the former equations (compatibility, equilibrium and constitutive), the displacements, stress and deformation field of the nodes (Fig. 1.19) ; the final step consists of the extension of the solution to all the other points of the domain using linear or non-linear form functions.

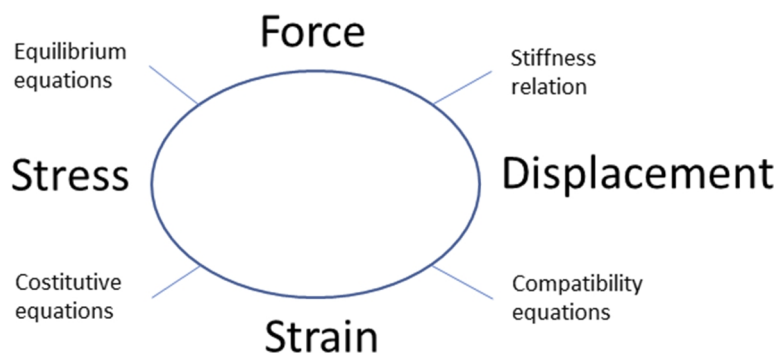


Figure 1.19 Relationship between analysis parameters and equations involved

### 1.6.2 Non-linear analysis

Non-linear analysis follows some laws that actually diverge from the linear approach. Non-linear analysis are necessary when there are such cases in which the linear relationship between stress and deformation is no more satisfied and in other words reversing the stiffness matrix  $K$  is not more possible. These conditions are:

1. Material non-linearities:
  - Plastic material
  - Non-linear elasticity
2. Geometrical non-linearities:
  - Large strains and displacements
  - Presence of local buckling
3. Boundary condition non-linearities:
  - Distributed load
  - Load follower
  - Presence of contacts

The main solving approach is called Newton – Raphson method and it is basically an incremental-iterative algorithm. This method provides that the entire load applied is divided into more pieces, one for every load step increment, in order to improve stability of the model and to consider the problem linear within the step considered. It is important to say that convergence to solution is not guaranteed and whereas it is reached, the difference between applied load  $P$  and structural response  $K \cdot u$ , where  $K$  is the stiffness and  $u$  is the displacement, has to be less than a prefixed error  $e_{MAX}$ .

Although this thesis study deals with a 3D model with non-linearities mainly due to contacts between screws and plate, just for the demonstrative purpose in showing the solving methodology of a non-linear analysis, a single dimension case could be considered for simplicity; for example a spring with stiffness  $K$  dependent on the displacement  $u$ , and loaded with an external force  $P$  can be studied; Therefore, finding the displacements  $u$  is the aim of the analysis.

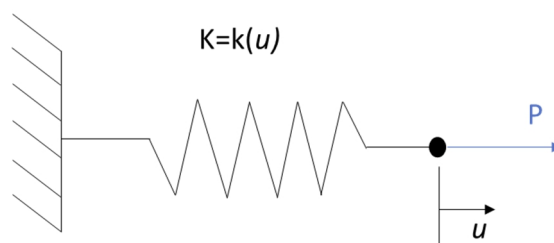


Figure 1.20 Representation of a non-linear stiffness spring

Two important elements present in this method, which are of fundamental importance are the secant ( $k$ ) and tangential stiffness ( $k_t$ ).

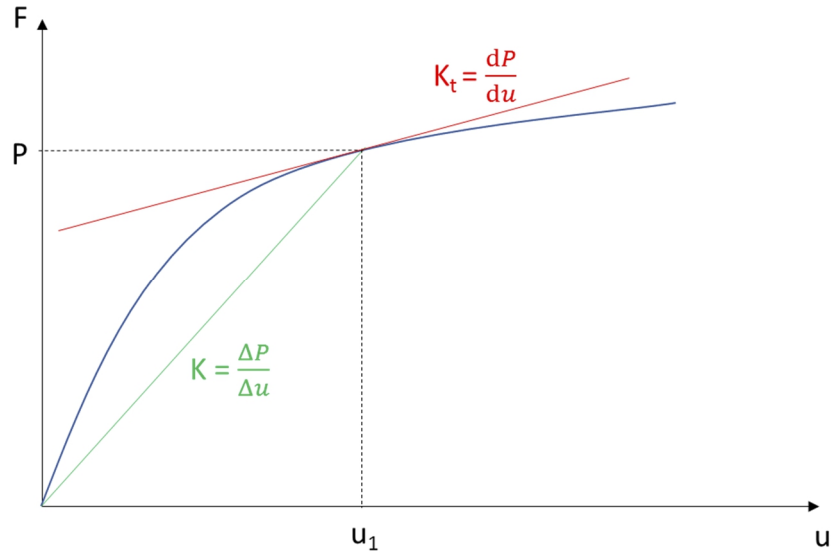


Figure 1.21 Graphical representation of secant ( $k$ ) and tangential stiffness ( $k_t$ )

In this figure, the non-linear relationship between force  $P$  and displacement  $u$  can be appreciated. Secant stiffness is defined as the ratio between force increment and displacement increment, instead tangential stiffness is defined as the slope of the  $P$ - $u$  curve in a defined point. It follows that in a linear problem, secant and tangential stiffness calculated at the same point are coincident.

So, knowing that  $P = k \cdot u$  in a linear elastic problem, it is possible to define:

$$k_t = \frac{dP}{du} = u \frac{dk}{du} + k$$

$$k = \frac{\Delta P}{\Delta u}$$

The Newton Raphson method can be conceived basically as two nested for loops, explained by the following scheme:

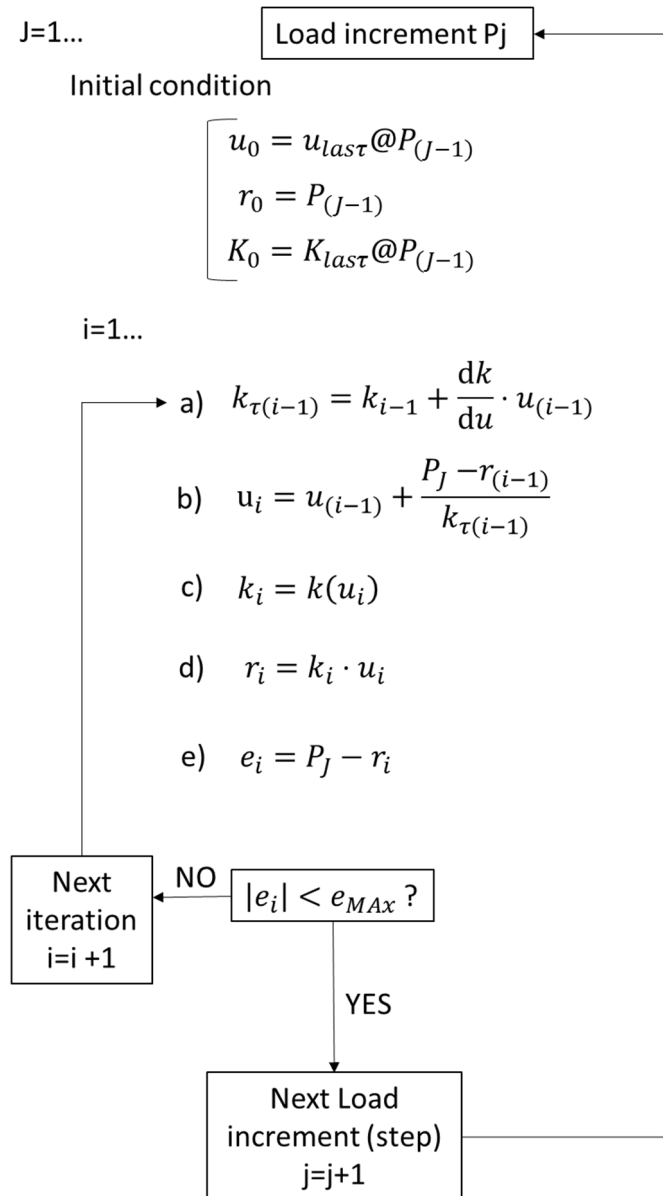


Figure 1.22 Newton Raphson algorithm for non- linear analysis

It starts with the initialization of the initial displacement  $u_0$ , structure response  $r_0$  and tangent stiffness  $k_0$  which at the initial increment  $j=1$ , are all set to zero. Then the first iteration ( $i=1$ ) begins in which the new tangent stiffness  $k_{\tau 0}$  (a), the new predicted displacements  $u_1$  (b), the new secant stiffness  $k_1$  (c) at the new displacement, the new structural response  $r_1$  (d), and the relative error  $e_1$  (e) are calculated. At the end of this iteration if the error is less than the tolerance it starts a new step, instead a new iteration begins ( $i=2$ ). When the convergence of the solution for the first step is reached, in which the first piece of load is considered, a new step ( $j=2$ ) begins with the first iteration ( $i=1$ ). Now the initial conditions are not set to zero but coincide with the last values obtained in the last iteration of the previous step. This algorithm runs until are completed all the load steps allowing to complete the imposed load.

## 2. Methods

---

### 2.1 The four configurations

As already mentioned, the aim of this thesis work is to compare different combinations of acetabular fractures (the elementary transverse and the so called T-shaped ones), with two different plates (the standard pelvic plate (SPP) and the suprapectineal quadrilateral surface buttressing plate (SQBP)) that are respectively anchored to the bone through two different screws configurations (C1 and C2) (Fig. 2.1).

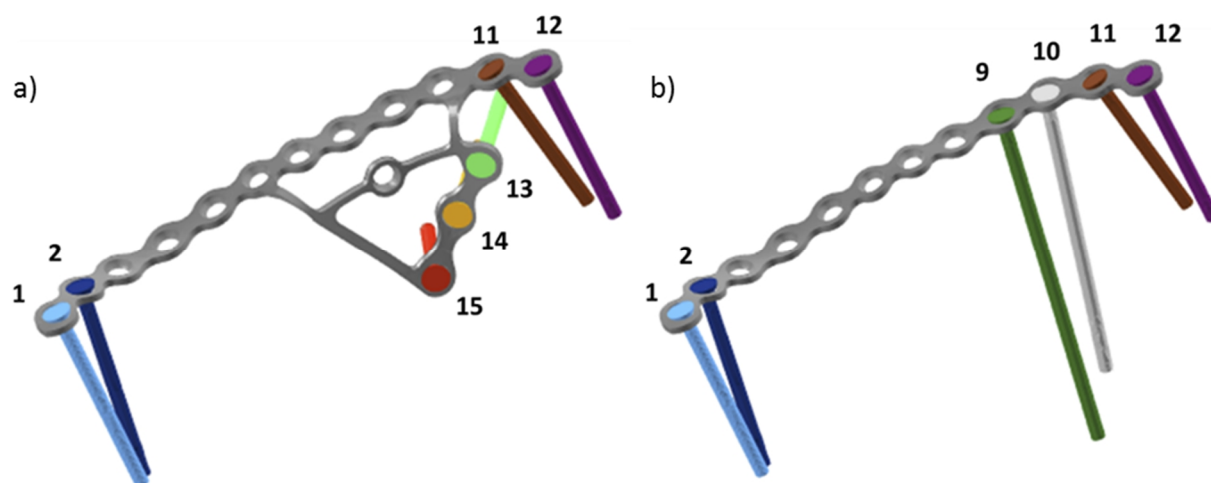


Figure 2.1 a) Screw configuration C1 b) Screw configuration C2

- The configuration C1 is composed of seven screws, among them four are placed at the two extremity of the plate on the iliopectineal brim (1, 2, 11, 12 in fig. 2.1 a), two per side, and the other three (13, 14, 15 in fig. 2.1a) are inserted on the quadrilateral surface of the ilium, making care not to penetrate the acetabulum.
- The configuration C2 is composed of six screws, each one belonging to the arcuate line of ileum; two long screws in the middle portion of the plate (9, 10 in fig. 2.1b) are longer than the others, reaching up to 89 mm in length.

Combining plate typologies and screws configurations, six models were implemented, two of which represent the mixed configuration of suprapectineal quadrilateral surface buttressing plate without the three screws inserted into the quadrilateral surface of the ilium. This latter was implemented in order to evaluate the stabilization contribution of the infrapectineal side of the plate when not anchored to the bone.

The six configurations implemented are shown in figure 2.2.

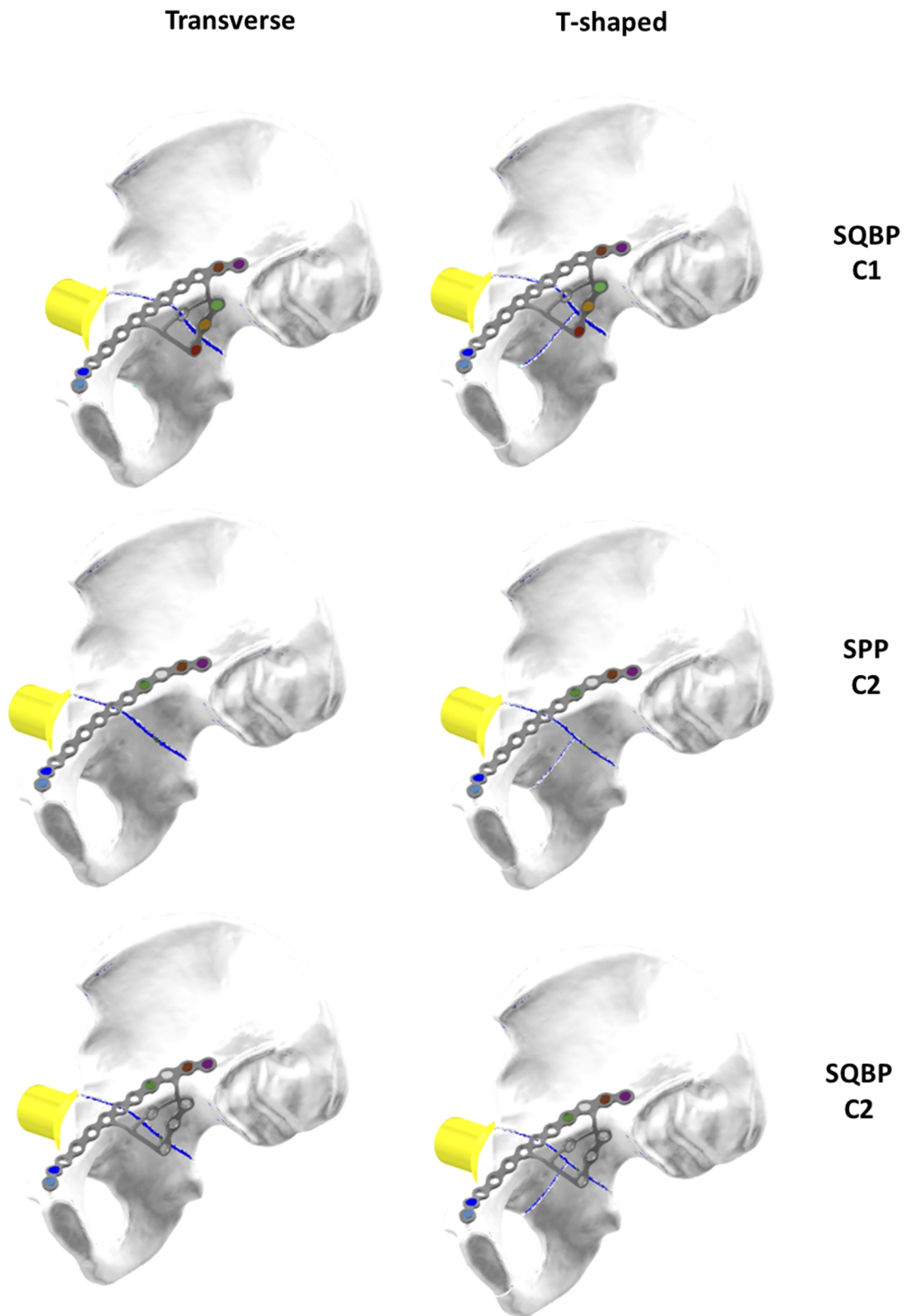


Figure 2.2 Representation of the six combinations of fracture types, plates and screw configurations adopted

The above mentioned models have been generated using finite element methods techniques which has involved the usage of different software and several methodologies.

### 2.2.1 Hip bone geometry

A standard Sawbones (Sawbones®vEurope AB, Malmoe, Sweden) pelvis geometry was selected for this study (SKU: 3415-1).

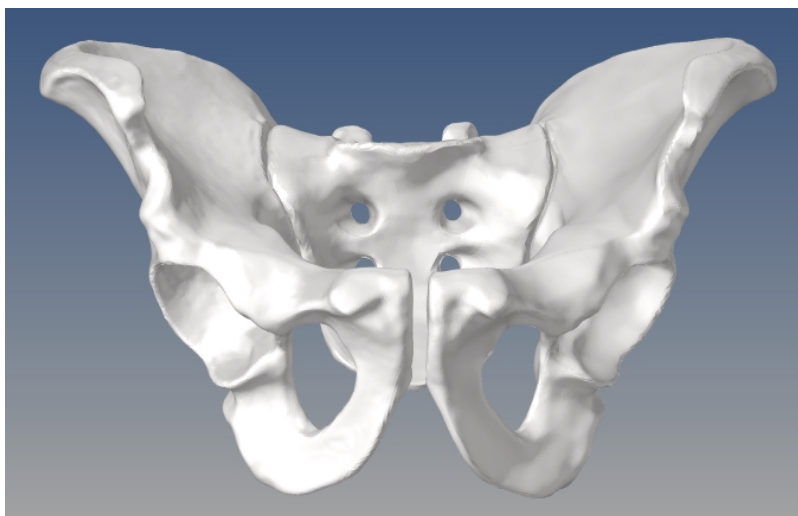


Figure 2.3 *Sawbones® vEurope AB, Malmoe, Sweden pelvis geometry*

For this analysis aim, only the right hemipelvis was used: in fact, the provided plate belongs to that side of the pelvis. The main operation made on the bone is the creation of the holes for screws insertion because these ones allows the thigh compression of the plate on the hip bone. In a real situation the surgeon achieves this by drilling a portion of bone underneath the plate holes and then tightening the threaded screws on the bone. The strategy adopted to translate this operation in the software domain is the Boolean difference between the hip bone and the screws solids. The realization of the screw surface is described afterward, so in this moment is enough considering the screws not to have any thread and so could be thought simply as cylinders.

The result of this operation can be observed in the following figure 2.4 where the bone surface presents as many holes as the number of screws (red dashed circles).

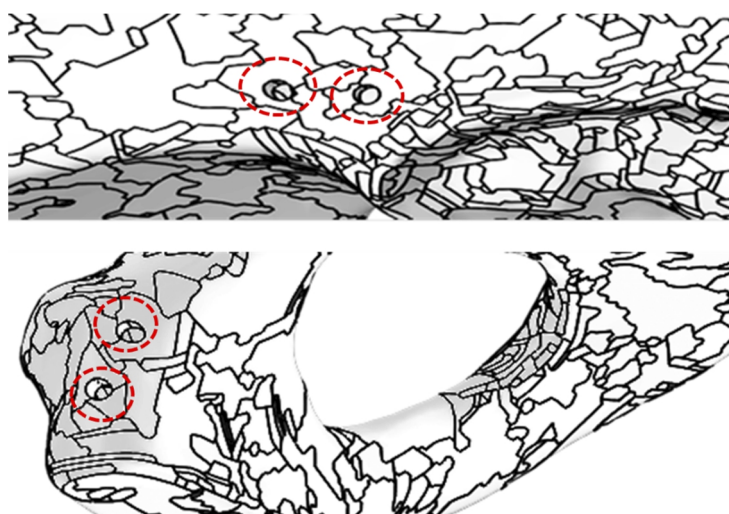


Figure 2.4 *Bone geometry holes after drilling (in red dashed circles)*

### 2.2.2 Plate geometry

The initial step of the work deals with the reproduction of the two plates in analysis, without any external devices beyond the PC. In fact, all the reconstruction follows the principles of reverse engineering: starting from the real object (SQBP plate) and studying the characteristic shapes, several methodologies have been applied to reproduce appropriately every feature in the CAD environment. The reproduction of the two Stryker plates in 3D CAD has involved several steps, employing two different software: Hypermesh (Altair Engineering, Inc., Troy MI, United States) and Rhinoceros (Rhinoceros 3D, Associates, Seattle, WA). The initial part of the 3D reconstruction has been performed in Rhinoceros. The following steps refer to the creation of the SQBP plate, which has the most sophisticated geometry having substantially a lateral portion in addition.

**Step 1:** The measurements of the plate have been taken with a caliper for the creation of the initial pattern of the plate in its longitudinal portion, composed of 12 holes; To obtain this design a repetition of circumferences and parabolas has been used. The plate is 14.5 mm long with a centre to centre distance between holes of 11 mm; the holes are 3.5 mm radius long.

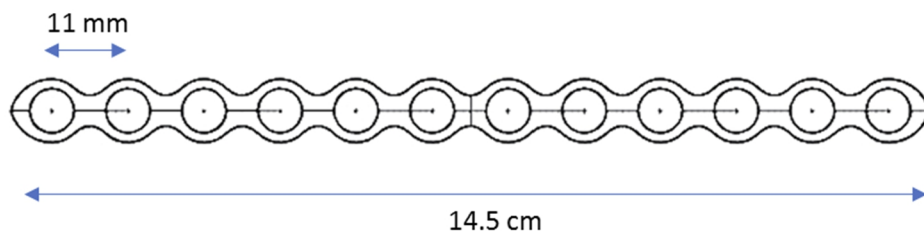


Figure 2.5 Plate initial geometry

**Step 2:** Using polylines in addition to the same procedure adopted before, the second portion composed of 4 holes has been constructed on the same plane (x-y) of the longitudinal one. With the Extrude command (2 mm thickness) the initial solid has been obtained (Fig. 2.6).

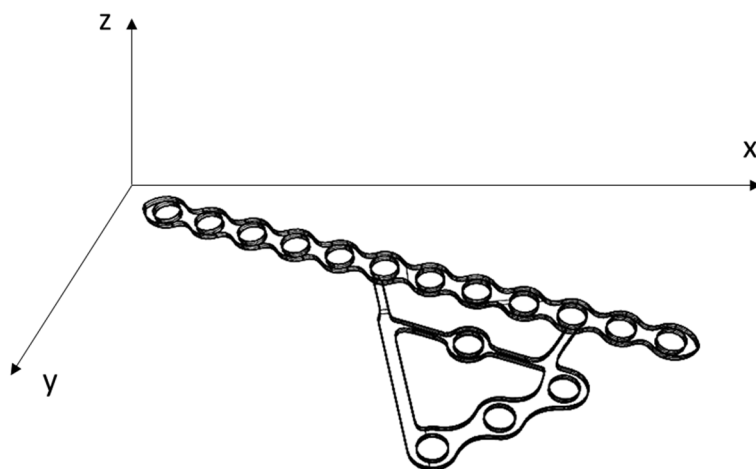


Figure 2.6 Initial solid plate with the infrapectineal and suprapectineal portions

**Step 3:** The inferior face of the plate has been modified reducing the inferior holes diameter to 5 mm, keeping the upper holes diameter equal to 7 mm; afterwards, the superior and inferior side holes have been conjoined through a hollow surface (in red in Fig. 2.7) allowing the positioning of the screw head.

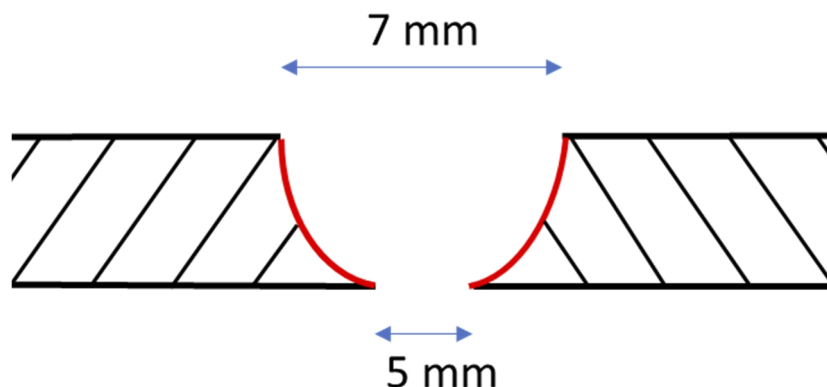


Figure 2.7 Plate hole countersink shape with upper diameter 7 mm and lower 5 mm

**Step 4:** Exploiting the “bend” command, three bending operations were performed:

1. In the first case the longitudinal part has been bent on the plane in order to recreate an anatomic curvature which follows the arcuate line of the ilium. The bending has been performed in the plane x-y along the z axis so that at the end of this procedure the plate is still within the plane x-y (Fig. 2.8).

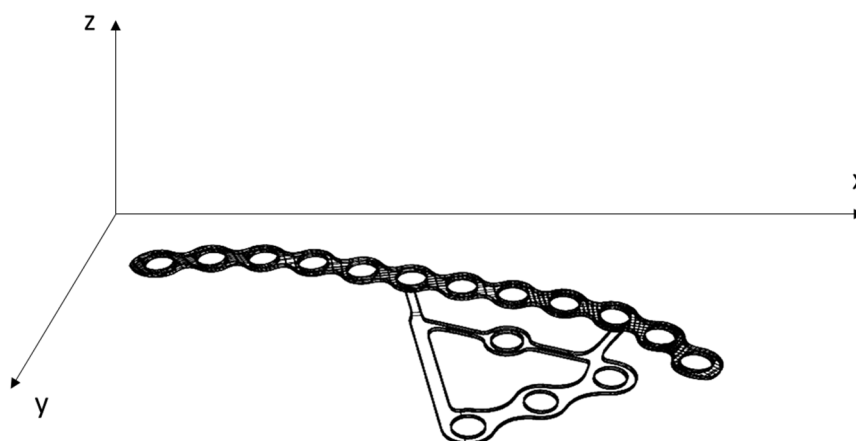


Figure 2.8 Plate first bending in x-y plane

2. In the second one, the lateral part of the plate (infrapectineal portion) has been bent with an almost 90° curvature with respect to the plane x-y.
3. Eventually this lateral infrapectineal part of the plate has been newly inflected along the z axis to fit to the quadrilateral surface of the ilium (Fig 2.9).

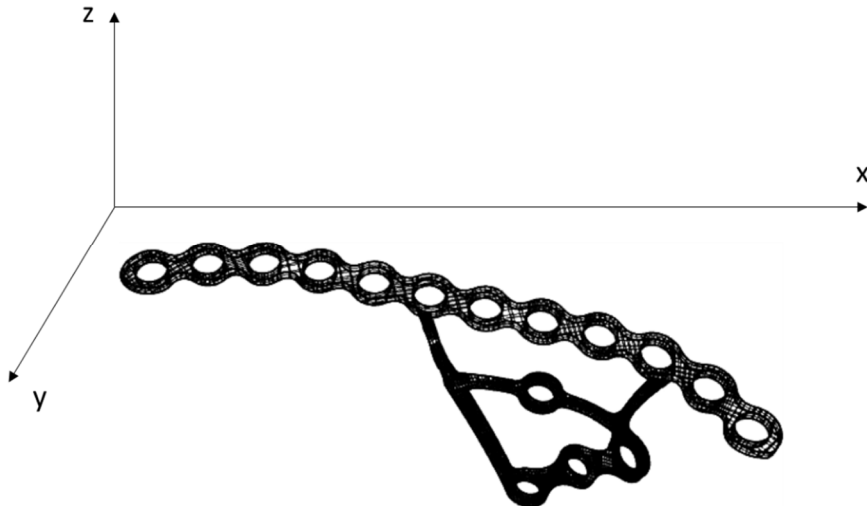


Figure 2.9 Plate infrapectineal portion third bending along z axis

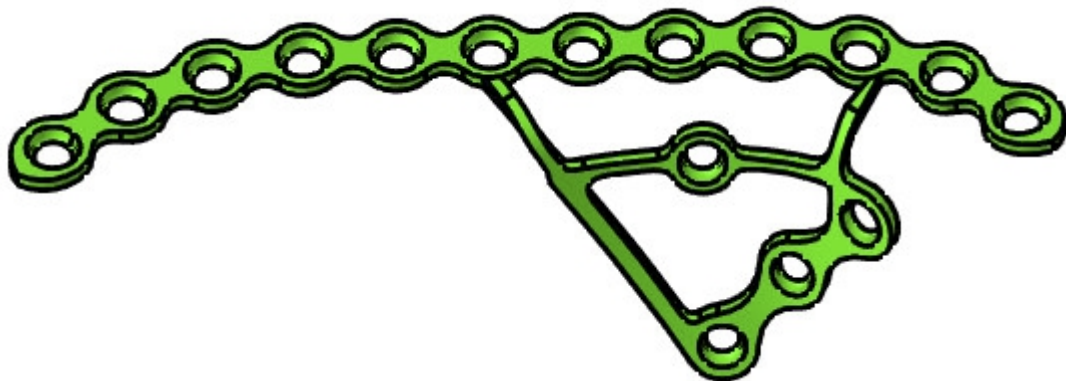


Figure 2.10 Plate geometry shapes obtained at step 4

The so obtained plate model, represented in figure 2.10 has already anatomic properties in its shape but still the two bridges connecting the two portions of the plate seem not to reflect the real geometry.

**Step 5:** Commands such as *polylines*, *curveOnSurface*, *controlPointCurve* have been used for the generation of the edges of the model, and others like *loft*, *curve*, *extrude*, *edgeCurve*, *Plane* have been used to construct the surfaces making more smoothed and harmonious the connection between the two parts of the model (Fig. 2.11).

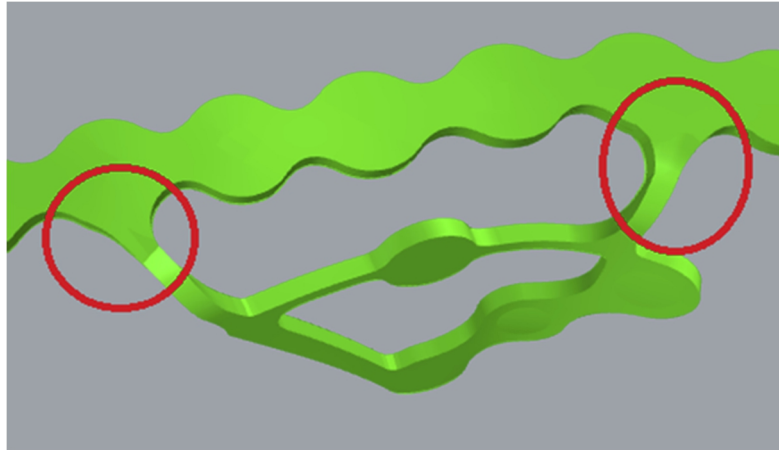


Figure 2.11 Smoothing of connections of the two portions (infrapectineal and suprapectineal) of the plate (in red circles)

**Step 6:** In this step the bending of the plane x-y has been executed, in order to adapt it to the iliopectineal margin of the pelvis provided. The command drape has been used in Rhinoceros software to copy, in just one surface, the shape of the zone of interest of the pelvis, that is the quadrilateral surface of the ilium with its own articulate pattern (Fig. 2.12).

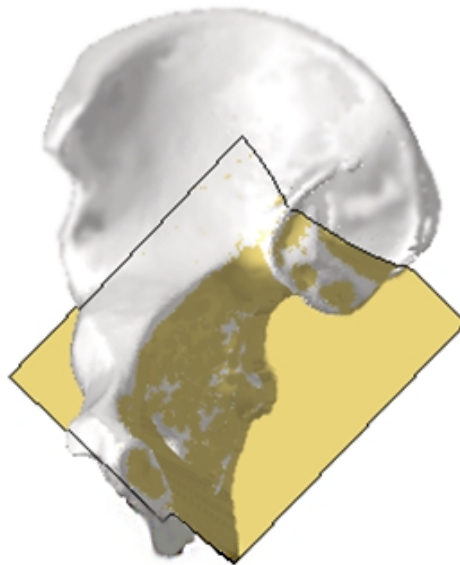


Figure 2.12 Utilization of drape surface (in gold) to copy bone shapes (in white)

In Hypermesh software, using the *Hypermorph* section and *freehand* command the suprapectineal side of the already meshed plate was bended so as to follow the surface extracted before. In detail some particular nodes of the plate have been projected on the surface using *move node to surface* option and *mvbias* and *fxbias* parameters have been set ad hoc (Fig. 2.13).

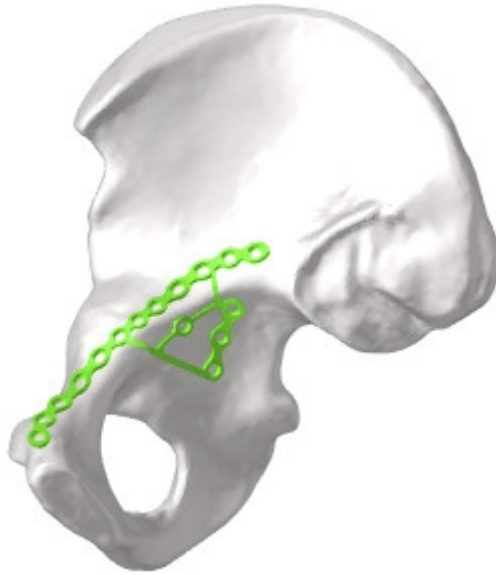


Figure 2.13 Bent plate with deformed hole countersinks at end of Step 6

**Step 7:** The following step has been executed to improve the holes countersink geometry because through the last bending procedure (Step 6) the plate holes have been deformed making them unsuitable to accommodate the screws heads. From the plate version with all holes filled, it has been follow the here described algorithm to create the hemispherical holes countersinks in which the screw head could fit:

1. Determination of external circumference in the plate circular shape by interpolating points belonging to the edge of the superior surface with further determination of its own centre; the commands adopted are *circle: fit points* and *centermark* (Fig 2.14).

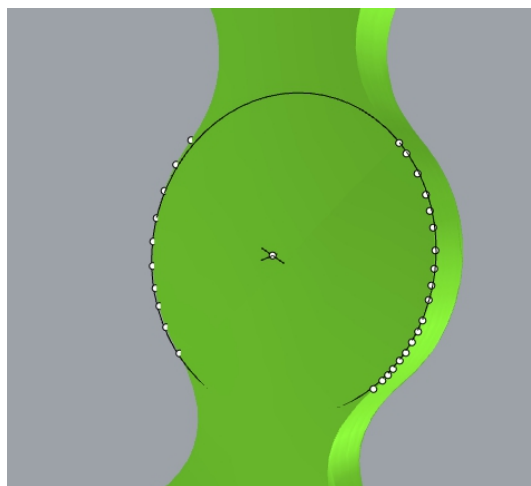


Figure 2.14 Determination of the external circumference

2. Generation of circumference of 3.5 mm radius, concentric to the external one just created and determination of its own normal passing through the centre, using *extrude* command (Fig. 2.15).

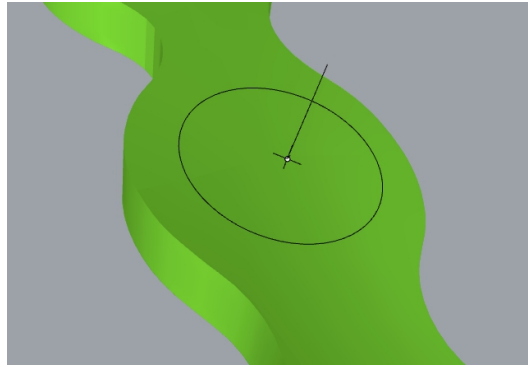


Figure 2.15 Determination of the upper circle with its normal axis in its centre

3. Creation of a second 2.5 mm radius circumference in the intersection point between the normal axis and the inferior plate surface which is coaxial with the superior one (Fig. 2.16).

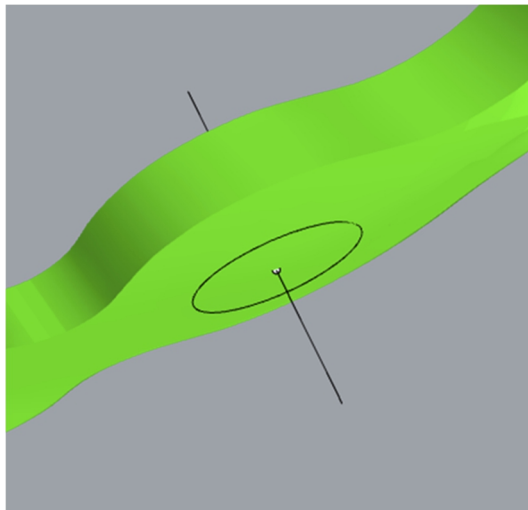


Figure 2.16 Determination of the lower circle coaxial with the upper one

4. Generation of the sphere passing through the two circumferences (command *sphere*) after its radius calculation. To perform radius ( $r$ ) calculation and define where to place its centre ( $a$ ), geometric functions have been exploited, which take in input the two diameter ( $s$ ,  $t$ ) and the distance between the two circumference ( $p$ ) (Fig. 2.17):

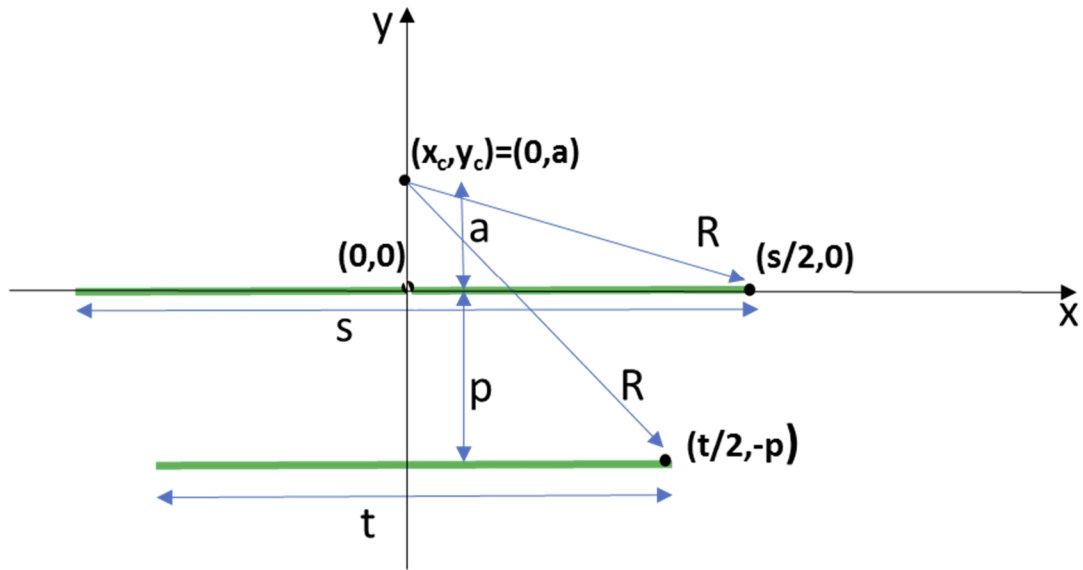


Figure 2.17 Geometrical scheme of the sphere passing through the two circumferences from a frontal point of view

Known values:  $s, t, p$

Unknown variables:  $a, R$

Eq. Generic circumference with centre  $x_c$  and  $y_c$  :

$$(x - x_c)^2 + (y - y_c)^2 = R^2$$

Eq. first circumference passing through  $(\frac{s}{2}, a)$ :

$$\left(\frac{s}{2} - 0\right)^2 + (0 - a)^2 = R^2 \quad (1)$$

Eq. second circumference passing through  $(\frac{t}{2}, -p)$ :

$$\left(\frac{t}{2} - 0\right)^2 + (-a - p)^2 = R^2 \quad (2)$$

Joining (1) and (2) :

$$a = \frac{(s^2 - t^2) - p}{8p} \quad \text{and} \quad R = \sqrt{\frac{s^2}{4} + a^2}$$

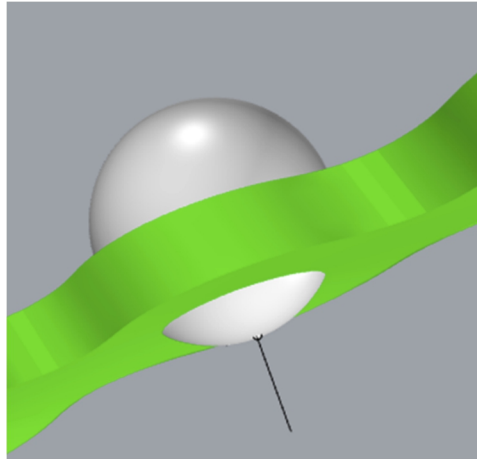


Figure 2.18 Representation of the created sphere into the plate geometry

5. Boolean difference implementation, in order to create final countersinks in the plate, between the 16 spheres and the bent plate itself (Fig 2.19).

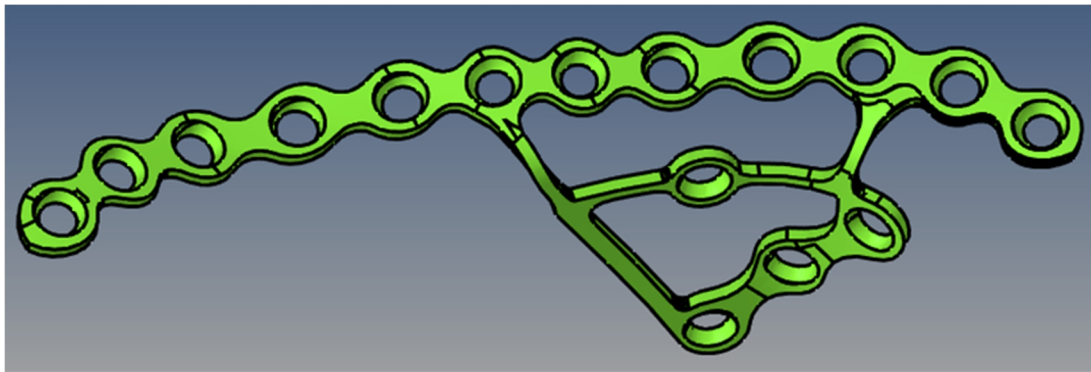


Figure 2.19 Final geometry of SQBP plate

### 2.2.3 Screw, cartilage and femoral component geometries

Other than the plates and the hip bone, already discussed, it has a fundamental role in the model implementation the presence of cartilage, screws and neck and femoral head. The first one has been created directly by mesh without passing through geometrical environment, conversely the latter two components have been constructed with a composition of surfaces.

As regard the screw, it has been modelled as a cylinder (diameter 5 mm and variable length) with a hemispherical head (diameter 7 mm) in order to fit and twirl in the plate hole countersink, so as to reach the desired angulation of fixation. Therefore, in order not to weigh down the model, it has been chosen not to recreate the outer thread of the screw, simplifying the real geometry and considering it a bolt element as already used in literature (Fig. 2.20a) [46,47].

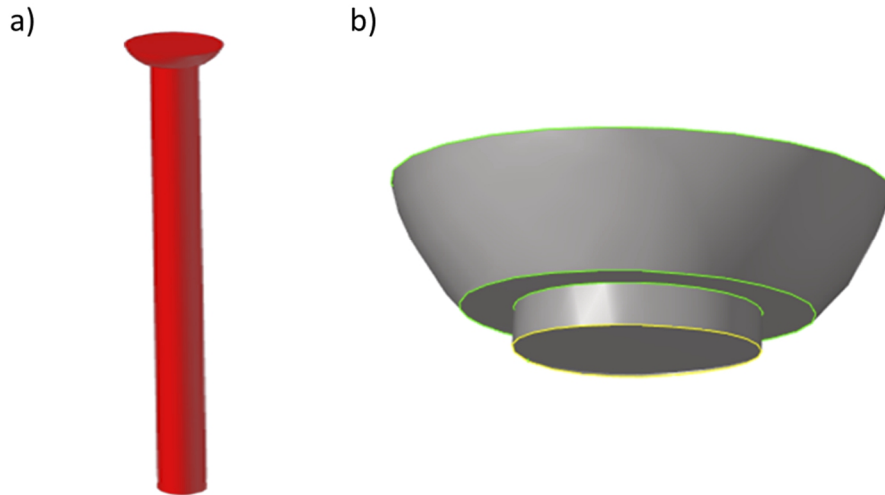


Figure 2.20 a) Screw geometry b) Circle (in yellow) for screw preloading

In each screw a circle was positioned almost at the extremity of the body of the screw, useful in the following for the implementation of the pretension surface, needed for the screw preloading (Fig. 2.20b).

The femoral component has been created through the union of a sphere, as a femoral head, and a cylinder, representing the femoral neck. Initially, the femoral head has been created by calculating the sphere passing through four superficial points of the acetabular cup, then the so obtained sphere has been rescaled at the 95% to make sure not to have initial contacts or penetrations into the acetabulum. After the creation of a superficial mesh of the femoral head it has been chosen a distal node on which generate the femoral neck, computing the normal direction at that node through the cross product between two vectors tangential to the sphere.

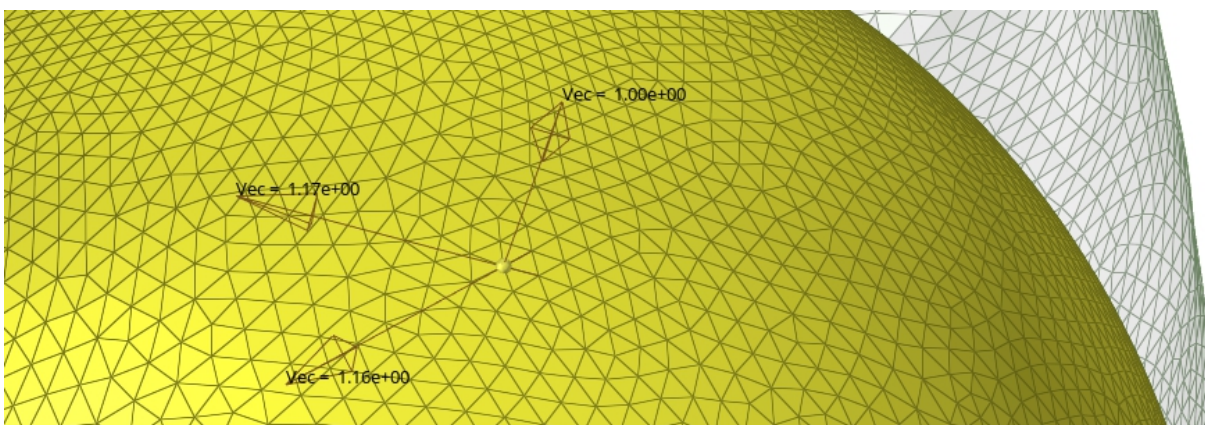
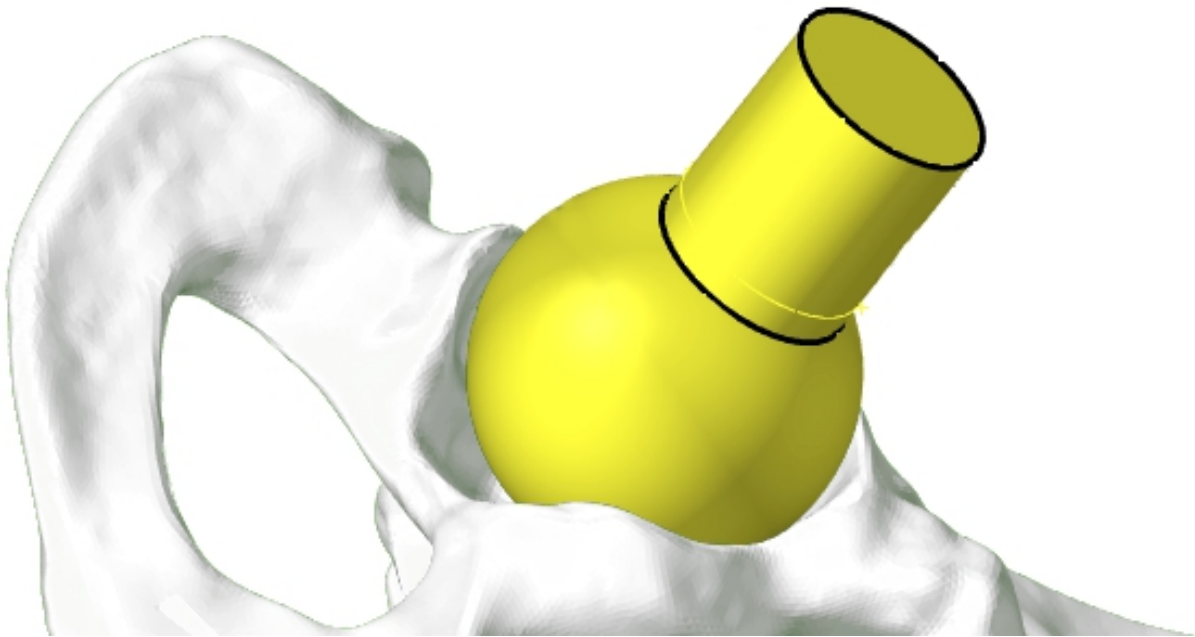


Figure 2.21 Representation of the normal vector to an element of the femoral head mesh

On this node, a circumference with 15 mm of radius and direction coincident to the normal vector previously calculated has been traced, and then extruded obtaining the 40 mm long cylinder. The last step consisted in the Boolean union of the cylinder and the sphere to get the final femoral component (Fig 2.22).



*Figure 2.22 Representation of femoral head positioned into acetabular cup*

It is clear that the just created femoral component is not anatomically faithful but it will only play the role of load transmitter to the acetabulum. However, the femoral region will not be addressed in the results analysis. Furthermore, this does not represent an anatomical zone to study in this work so is not dutiful a strictly detailed shape.

## **2.3 Mesh generation**

### **2.3.1 Plates mesh**

The volumetric mesh of the plate has been created after its geometrical definition. Due to its sinuous shapes characterized by curves, parabolas and circumferences, first order tetrahedral elements have been selected, elements that would be able to faithfully replicate the plate geometry (Fig 2.23).

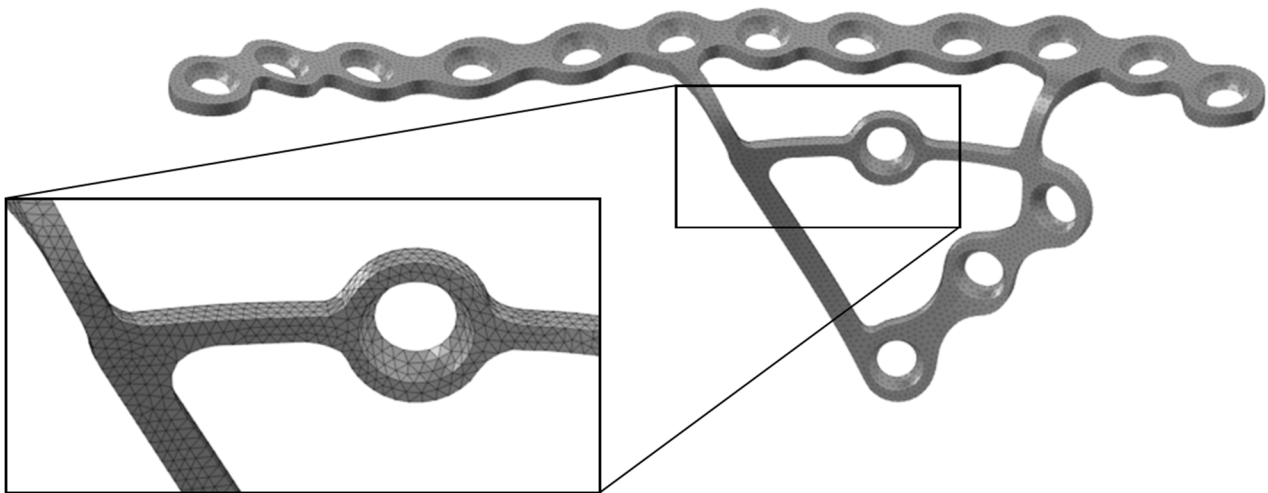


Figure 2.23 SQBP plate mesh with zoom on tetrahedral elements

From the so obtained mesh, the SPP mesh was derived by erasing the lateral infrapectineal portion of the SQBP plate and adjusting the lateral contour; it follows that the two SQBP and SPP plates are perfectly the same along the iliopectineal brim (Fig. 2.24).



Figure 2.24 SPP plate mesh

### 2.3.2 Screws mesh

Once created the geometry of all the screws, with their own lengths, positions, and angulations in accordance with the clinical practice, their volumetric meshes has been created adopting first order tetrahedral elements. Differently from the plate mesh, screws meshes have been manually modified in order to create a shared mesh with the bone: in the intersection surfaces all the nodes have been made coincident (Fig. 2.25). This strategy allows to limit computational resources with a lighter analysis and reduced computational times.

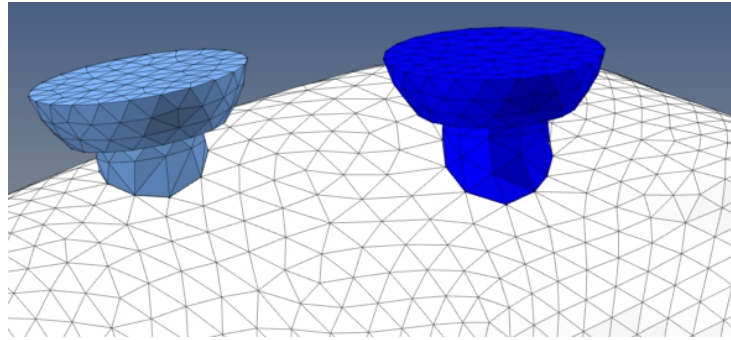


Figure 2.25 Shared mesh between screws and bone components

As already mentioned, the screw configurations taken in exam in this study are two, called C1 and C2 (Fig. 2.1). The screws have different length according to their specific locations and assolve to different tasks: the long screws 9 and 10, respectively 89 and 79 mm, long guarantee a tight grip to the most distal zone of the bone, especially in the T-shaped fracture with the distal stump; the screws 13, 14 and 15 have the role to buttress the quadrilateral side of the ileum and their length has to be restrained in order to avoid any perforation of the acetabulum; eventually, the screws common to the two configurations (number 1, 2, 11, 12) placed on the two extremities of the plate along the ileopectineal brim, permit a solid grip of the plate-bone system, bringing the fracture to be treated with a bridging plate as the positions of these screws are away from the fracture site. Table 2-1 lists the lengths of each screw.

Screw N°	1	2	9	10	11	12	13	14	15
Length (mm)	48	48	89	79	40	43	29	29	22

Table 2-1 List of screws lengths

A characteristic of the screws-plate system is the presence of an upper limit of screw angulation with respect to the normal direction: although in the real case, thanks to the particular shape of the countersink of the hole, it's allowed a range of angulation up to 35° in all the directions, in this FEM model the screw can twirl only up to 14 ° in order to not generate any penetration in the plate (Fig. 2.26).

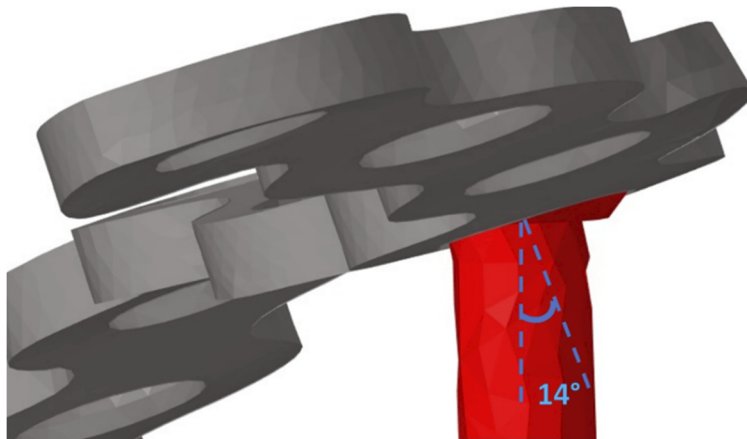


Figure 2.26 Representation of the maximal screw angulation with respect to the normal axis of plate hole

### 2.3.3 Pelvis mesh

The hemipelvis geometry was meshed in the Hypermesh pre-processor with first order tetrahedral elements. As previously stated, screw-bone interfaces share the same superficial mesh, thus avoiding any definition of contact between these components.

On the obtained mesh, the two fractures typologies were created by manually deleting elements, as visible in figure 2.27. The fracture gap thickness thus obtained is not perfectly constant between the models: the resultant fracture gaps thickness varies from 2 to 3 mm (Fig. 2.27 and 2.28).

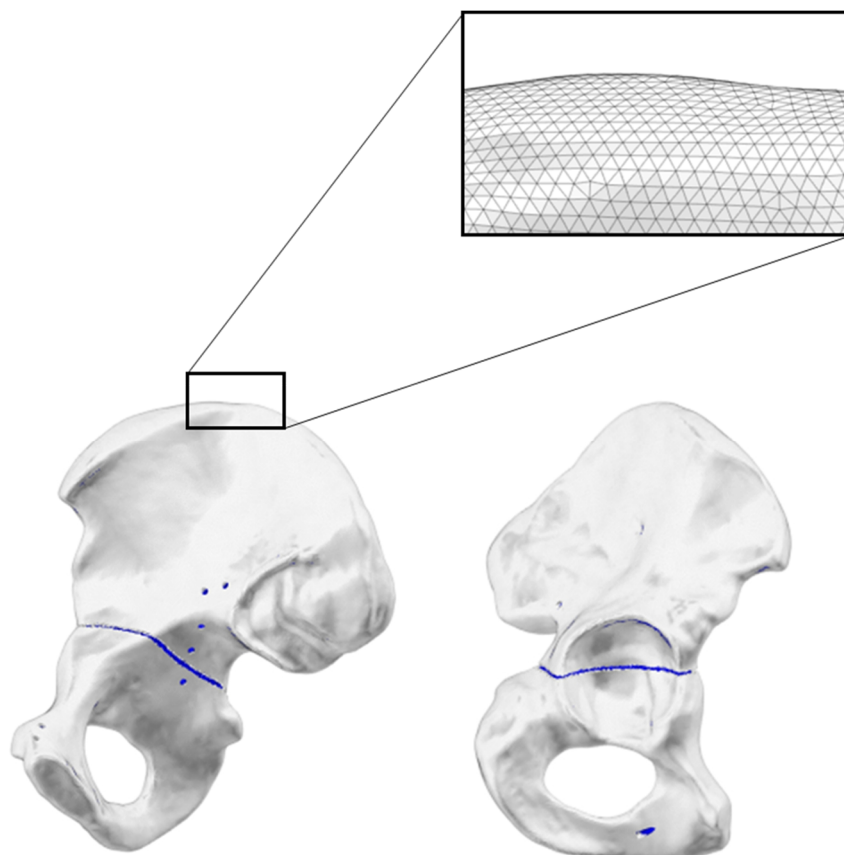


Figure 2.27 Medial (left) and lateral (right) views of elementary transverse fractures with zoom on mesh tetrahedral elements

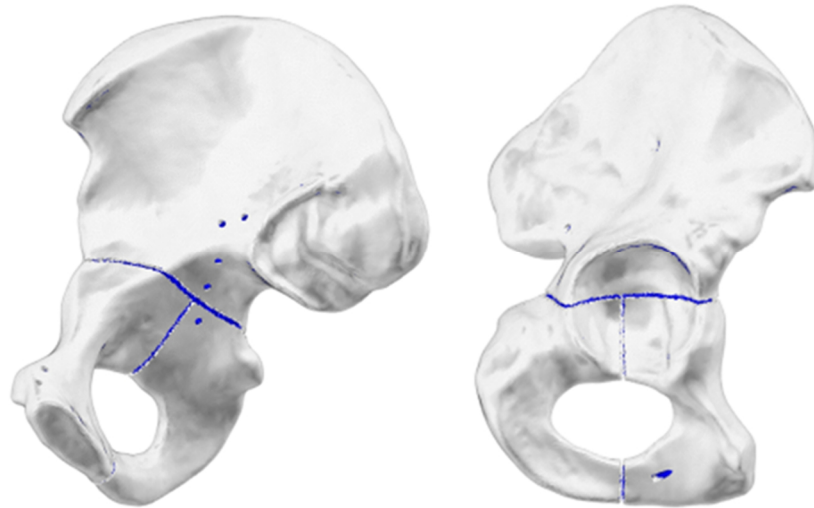


Figure 2.28 Medial (left) and lateral (right) views of associated T-shaped fractures

### 2.3.4 Cartilage and femur meshes

After several trials, it has been decided to introduce in the acetabulum also a cartilaginous entity, able to distribute the load coming from the femoral head to the acetabulum, in a physiologic manner. From an anatomical point of view, the cartilaginous entity present in the hip joint can be split into two parts: a femoral and a pelvic portion. The mean thickness pelvic component is equal to  $1.26 \pm 0.04$  mm, while the femoral one is characterized by a mean thickness of  $1.18 \pm 0.06$  [48].

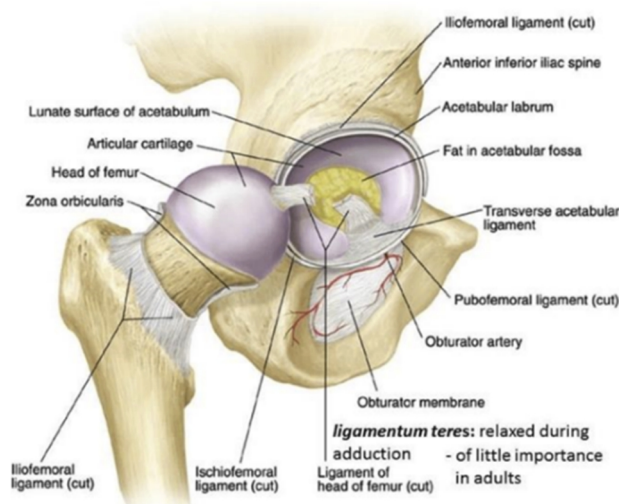


Figure 2.29 Anatomic representation of pelvic and femoral components of cartilage

As it is possible to see from the figure 2.29, these two portions of cartilage have a non uniform shape: on the extremities of femoral head, the cartilage is composed of a thinner layer and even disappears in the centre of the acetabulum. Being the load distribution the aim of cartilage introduction, only a single component of constant thickness equal to 2 mm was implemented, attributing the entire thickness of the two components to the acetabulum. In order not to weight down the model, the

mesh of the cartilage has been build as a solid layer offset of the central portion of the 2D mesh of acetabulum, generating first order wedge elements (Fig. 2.30).

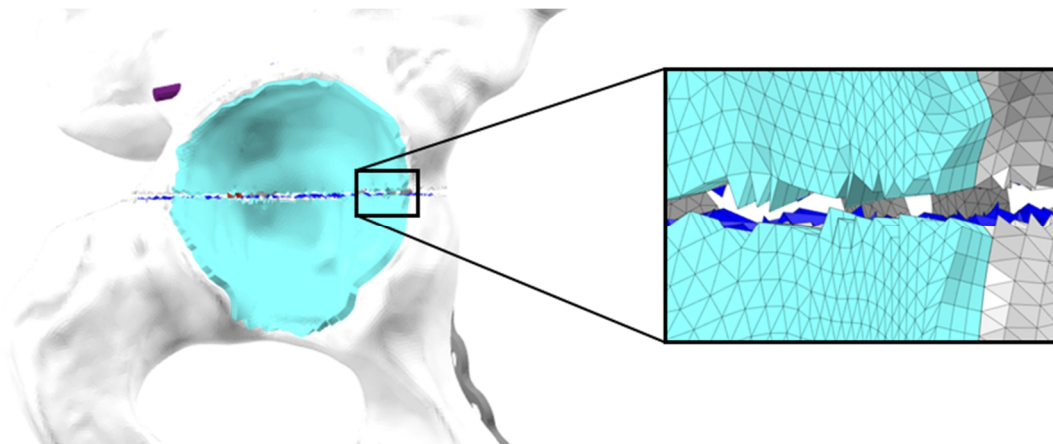


Figure 2.30 Representation of cartilage mesh with zoom on wedge elements

The neck and the femoral head mesh have been constructed by meshing directly the geometries obtained, consisting in a sphere joined with a cylinder, with first order tetrahedral elements.

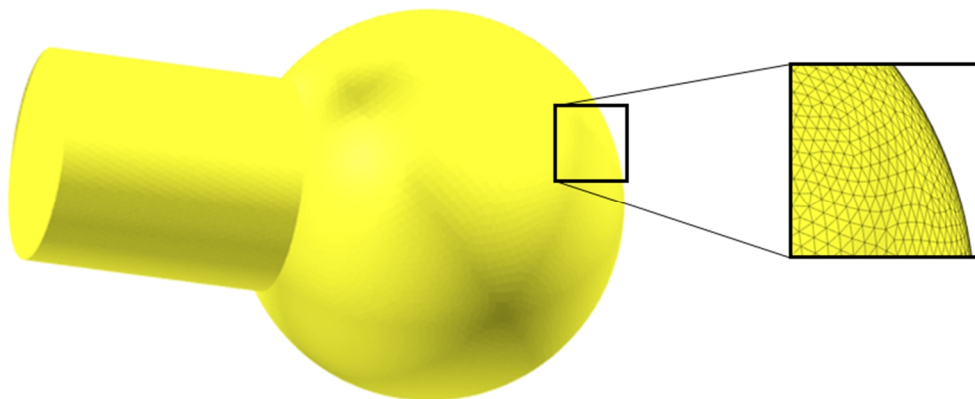


Figure 2.31 Representation of femoral component mesh with zoom on tetrahedral elements

### 2.3.5 Summary of meshed components

In this paragraph are shown, resumed in the table 2-2 all the different components in relation to their number of elements, global edge length and typology of element adopted.

Component	# Elements	Global Edge Length (mm)	Element Type
Transverse fractured Bone	1774743	1.5	Tetra4
T-shaped fractured Bone	1772012	1.45	Tetra4
Configuration screw C1	22043	0.89	Tetra4

Configuration screw C2	27666	0.73	Tetra4
Plate SQBP	49715	0.66	Tetra4
Plate SPP	37070	0.56	Tetra4
Cartilage in transverse fracture	24915	0.65	Penta6
Cartilage in T-shaped fracture	24520	0.7	Penta6
Head and femoral neck	169818	1.65	Tetra4

*Table 2-2 Summary of number of elements, global edge length and element type of various component implemented*

## 2.4 Materials and properties

Elastic materials with isotropic properties were assigned to each component of the model. Only exception is the cartilage, which has been represented as a non-linear hyperelastic material. The following table resumes the mechanical properties for each elastic isotropic material:

<b>Material</b>	<b>Elastic modulus E (MPa)</b>	<b>Poisson's ratio <math>\nu</math></b>	<b>Density <math>\delta</math>(Kg/m<sup>3</sup>)</b>
Cortical bone [49]	16700	0.3	1600
Cancellous bone [49]	1000	0.055	640
Screws and plate [50]	193000	0.29	8000

*Table 2-3 Summary of mechanical and physical properties of the three elastic materials implemented*

As regards the cartilage, in literature [51] it is widely accepted that cartilage behaviour can be represented at best by a hyperelastic material of the Neo-Hookean type. A hyperelastic material behaviour is described by the strain energy density function from which the stress-strain relation can be derived. The compatibility relation between stress and strain can be represented by the graph shown in Figure 2.32:

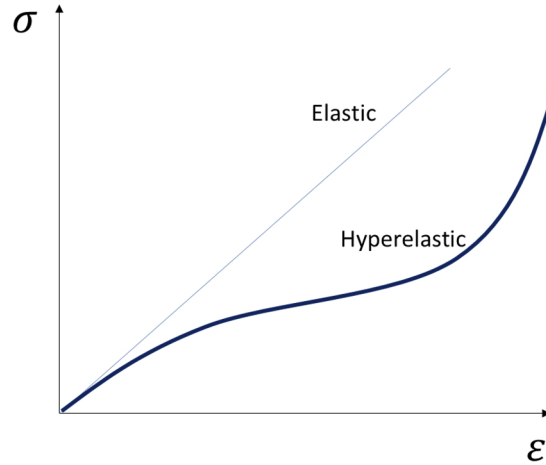


Figure 2.32 Stress-strain relationship of hyperelastic material (bold line) and elastic material (thin line)

The hyperelastic material has the property to behave as a soft one in low load condition and as a stiffer one under higher loads. The main reason of applying the hyperelastic behaviour to the cartilage is its capability of bearing high loads, such as body weight, and at the same time limiting the resultant deformations.

In Abaqus (Dassault Systèmes, Vélizy-Villacoublay, France) environment, the solver software, this strain energy density function is defined through two variables,  $c_{10}$  and  $D_1$ , that are specific of the cartilage. This two values are related to the Young Modulus  $E$  and the Poisson ratio  $\nu$  by the following relations [52]:

$$c_{10} = \frac{E}{4(1 + \nu)}$$

$$D_1 = \frac{6(1 - 2\nu)}{E}$$

After several trials using as  $E$  the values 5, 10 and 20 MPa and  $\nu$  equal to 0.46, a parameters couple of  $E= 12$  MPa and  $\nu=0.46$  has been selected [53] that provided the most reliable result; it followed that  $c_{10} = 2.05$  and  $D_1 = 0.1$ .

## 2.5 Contacts definition

When possible (i.e. when a glued contact could be imposed) the contact implementation was avoided by adopting a shared mesh. The contacts presence, indeed, implies that the analysis becomes non-linear. Nevertheless, the definition of contacts in this model is essential and indispensable to impose the right interactions between all the components.

There are four different regions in which contacts have been implemented:

1. The contact between plate and screws allows the compression of the plate on the bone needed to execute its biomechanical task. The contact between plate and screw occurs between the head screw and at the plate hole countersink, both with hemispherical shape,

as visible in figure 2.33. This contact has been conceived as a contact pair with friction. The static coefficient of friction between screws and plate, made both of stainless steel 304, has been set equal to 0.1 [54] considering a lubricated condition produced by biological fluids.

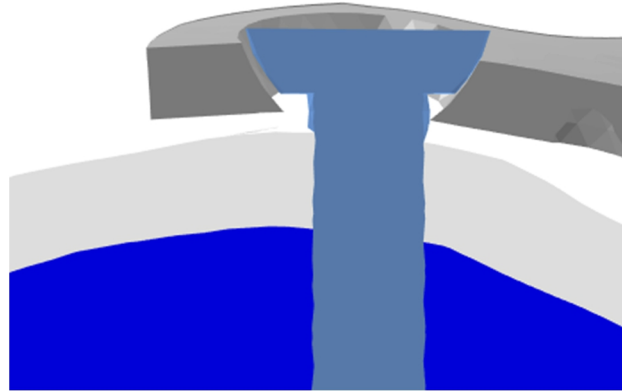


Figure 2.33 Section of internal fixation system inserted in cortical and cancellous bone

2. The contact between the plate and the cortical bone was set in order to permit the adherence of the plate on the bone, integrating the action of the screws. Also in this case has been used a contact pair, with static coefficient of friction equal to 0.37 [55].
3. The contact between the cartilage and the femoral component, fundamental to transmit the external load to the acetabulum, was implemented as a contact with an almost negligible static friction, equal to 0.02 [55, 56].

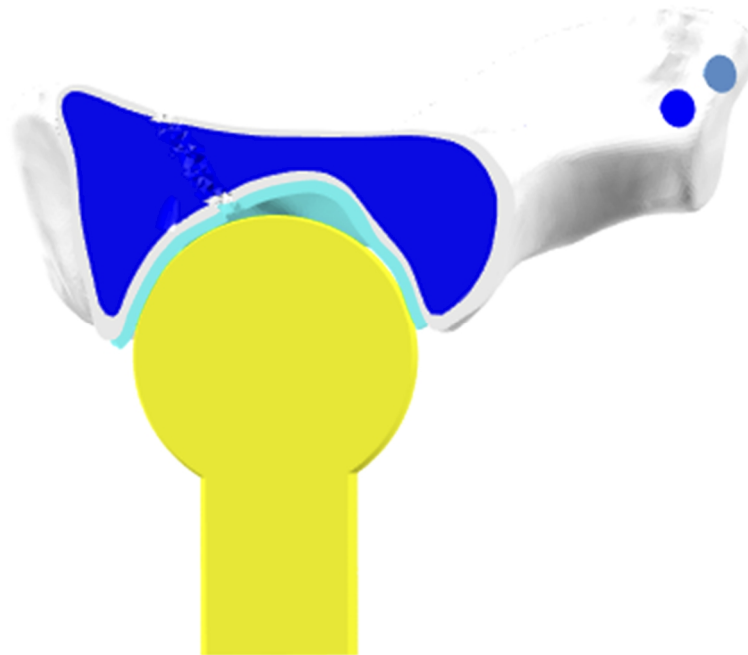


Figure 2.34 Section of femoral head inserted into the acetabular cup in contact with cartilage

4. For the T-shaped fractures models, it has been necessary to set up also a self-contact in the fracture region to avoid penetration between two stumps. Obviously, this is a condition to

avoid because it would describe an unreal phenomenon and would generate unfaithful results. Therefore, the static coefficient of friction utilized between the bones has been set to 0.4 [55].

## 2.6 Boundary Conditions

The hip is a very complex entity from a biomechanical point of view because involves many different anatomical structures as muscles, tendons, cartilages and ligaments, that are always in dynamic balance. It follows that trying to analyse the real biomechanical behaviour of a fractured hip with an internal fixation system should be considered a hard challenge. The simulation in Abaqus environment has involved two distinct loadsteps: the preloading of the screws and the loading of the hip, reproducing a single leg stance.

### 2.6.1 Preloading of the screws

The preloading of the screw is the first load to consider, because it allows the tightening of the screws into the bone. The screw preloading was performed exploiting bolt elements: a pretensioned surface located near to the screw head was selected and an axial compression along the screw axis was imposed. In the Abaqus environment, this action is produced by a shortening of the elements of the mesh where the bolt load is positioned on.

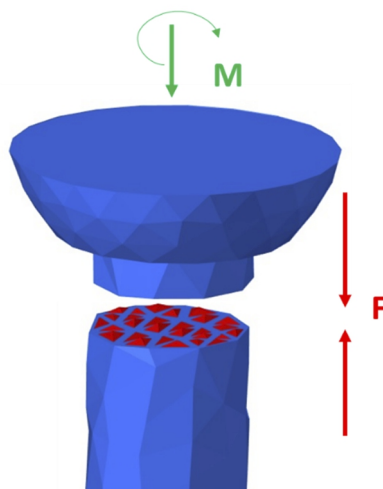


Figure 2.35 Preloading force of the screw ( $F$ ) induced by external applied torque ( $M$ )

From clinical data, it has been found the resulting moment torque applied to the screw during fastening, being equal to 4 Nm. Unfortunately, the parameter requested by the solver Abaqus is not the moment torque but the axial compression force acting in the screw. In literature seems still not be so well unified the relation between the applied moment torque and preloading force in an orthopaedic screw. Due to this aspect, it has been performed an accurate research in literature linking together several papers in order to arrive to a reliable conclusion. In Hughes work [57], it is described that the torque applied by the surgeon (e.g. 4Nm) is not all used to produce the pre-tensioning of the screw, in fact it is formed by:

- Torque to overcome thread friction

- Torque to produce bone threading
- Torque lost at the interface with the plate
- Torque useful for pre-tensioning

Further, it is hypothesized that in the most unfavourable condition only 5% of the applied torque is useful for pre-tensioning.

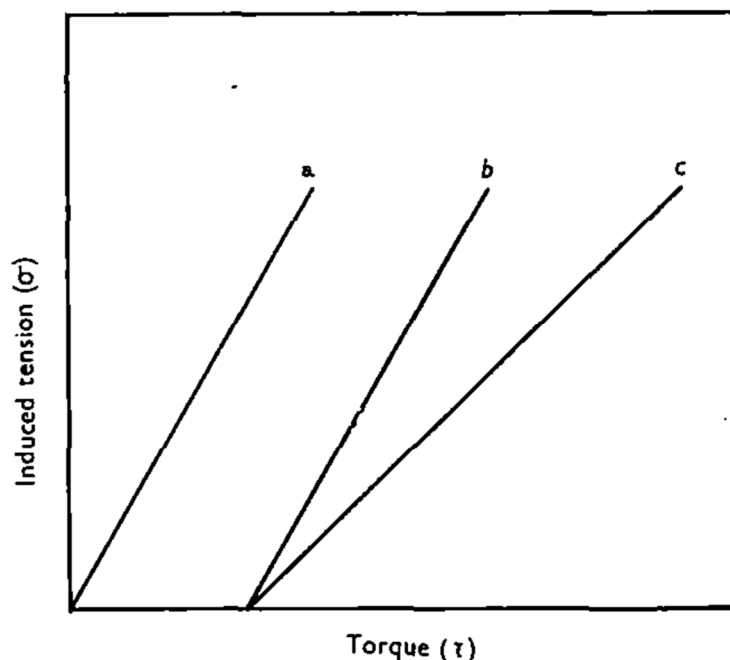


Figure 2.36 Applied torque – Induced tension relationship. Image taken from [57]

The relation between applied torque and induced tension in the screw is described by the scheme above and substantially it shows three main behaviours (Fig. 2.36):

- Ideal situation;
- Screw inserted in a not threaded hole without friction between screw head and plate;
- Screw inserted in a not threaded hole with friction between screw head and plate.

Karnezis and colleagues [58] found an experimental relationship between torque and axial preload in a 4.5 mm (internal diameter) screw.

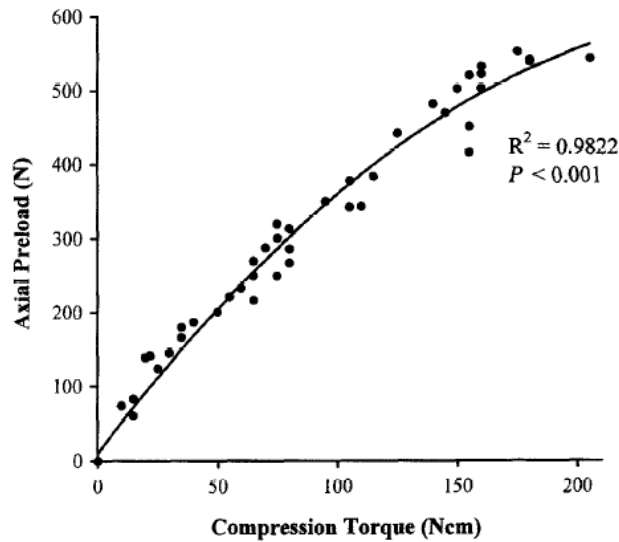


Figure 2.37 Experimental compression torque – axial preload relationship. Image taken from [58]

Since the force referred in the article is belonging to a 4.5 mm internal diameter screw, and conversely the internal diameter of the screw taken in consideration is 2.5 mm, the following passages have been made:

1. Finding the relationship tension induced - useful torque by dividing the axial preload value with the cross-section area of the 4.5 mm diameter screw. This has been possible because has been used the relation  $F = \sigma \cdot A$ , where  $F$  is the axial preload,  $\sigma$  is the induced stress in the screw, and  $A$  is the cross-section area that correspond to the section of the screw.

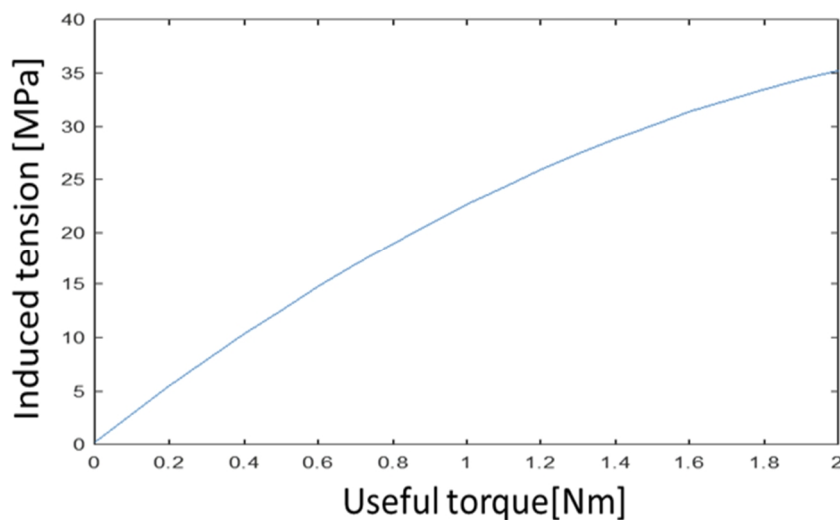


Figure 2.38 Useful torque – induced tension relationship in the screw

2. Multiplying the obtained tension by the cross-section of the 2.5 mm diameter screw to get the desired relationship between axial preload and useful torque

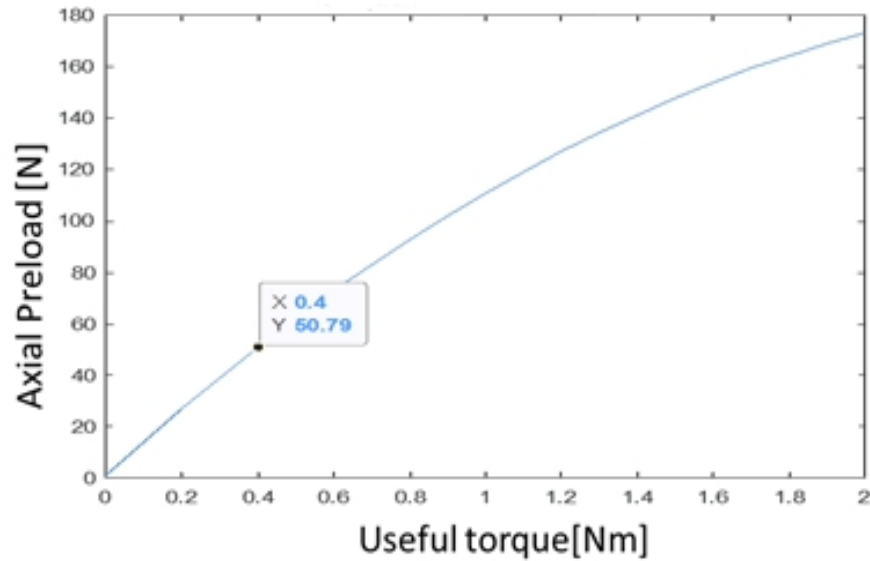


Figure 2.39 Useful torque – axial preload relationship in the screw of 2.5 mm diameter

So, it is hypothesized that the useful torque in screw tightening to be only the 10 % (a compromise between worst and middle case depending above all on the ability of surgeon and the modality of operation) of the applied torque [57]. Thus, because of the presence of friction between screws and plate and possible faults in bone hole threading, the initial value of 4 Nm becomes 0.4 Nm of useful torque, that would correspond to an axial preload equal about to 50 N. Thus, this value of 50 N has been introduced in Abaqus environment to set up the tightening force of the screws. The hypothesis that a high torque value is not sufficient to determine a high pretension force value in the screw is also endorsed by Beaupre work [59].

### 2.6.2 Single leg stance loading

In literature [60, 61] it is possible to observe a great variety of approaches for the setting up of the boundary conditions in a pelvis model; it is indeed possible to make analysis with several depths of details. Some studies consider ligaments as rigid connections or muscles and tendons as springs of specific stiffness, acting from the point of origin to the one of insertion [60]; even, some adopt the entire pelvis and other only a hemipelvis. It's obvious to affirm that all these details are dependent on what is the study aim.

In the models defined in this thesis, either for computational costs and not to further weight down a non-linear analysis, it has been decided to focus just on the right hemipelvis.

Fundamentally, the two aspects to analyse are how to load the hemipelvis and how to constrain it. As regards the bonding method, it was chosen to fix the six degrees of motion (three transactional and three rotational) of two groups of nodes, belonging to a portion of the pubic symphysis and to the iliac crest [60] as shown by the image below (Fig. 2.40).

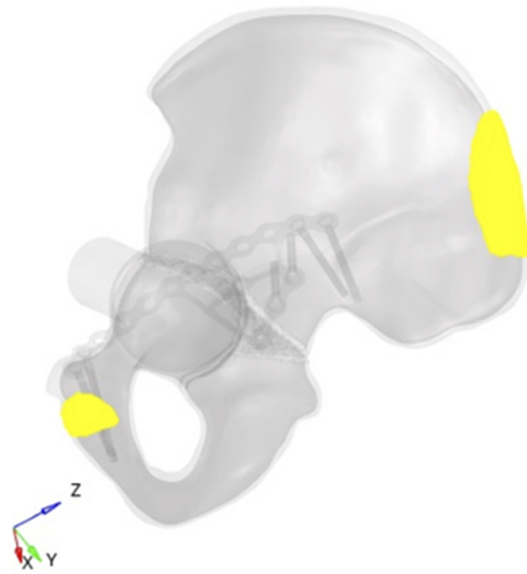


Figure 2.40 Bonded zones in the hip: iliac crest and pubic symphysis

Afterwards, it has been proceeded with a research to try to implement a physiological load that would simulate a real activity. Bergmann et alii [62] have studied through instrumented hip implants, the various reaction forces acting on the acetabulum during activities and among those the single leg stance. This kind of movement is really interesting because can be performed by the operated patient also after few weeks from the surgical operation.

The reaction force during single leg stance obtained by Bergmann takes in consideration all the contractile structures that compose the upper thigh and the hip beyond the presence of body weight; thus, for that reason it can be considered a physiological load. It is defined in a local coordinate system applied at the centre of the femoral head as shows the image below (Fig. 2.41).

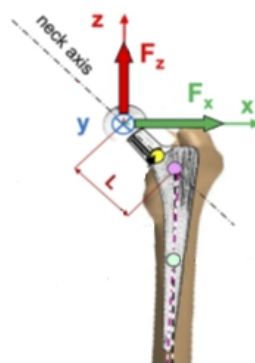


Figure 2.41 Single leg stance hip reaction force spatial components [62].

Here, the x axis corresponds to the medial - lateral direction, the y axis is the antero-posterior direction and the z axis defines the cranio-caudal direction.

As regards the values of the force in the three directions, they have been obtained from several subjects rescaling the result of each subject in order to associate the value of force registered at a body of 100 kg. This operation has been necessary to standardize the different values of forces (expressed in terms of maximum and minimum) and to compare them among the subjects. Then, in this thesis work the average value between the maximum and minimum for every component of force have been calculated. The resultant module of the force corresponds to 2032 N and the various

components of force are  $F_x=651$  N,  $F_y=-126.5$  N,  $F_z= 1921$  N. These components of force have been placed at the centre of the femoral head, after having reproduced the same coordinate system (Fig. 2.42).

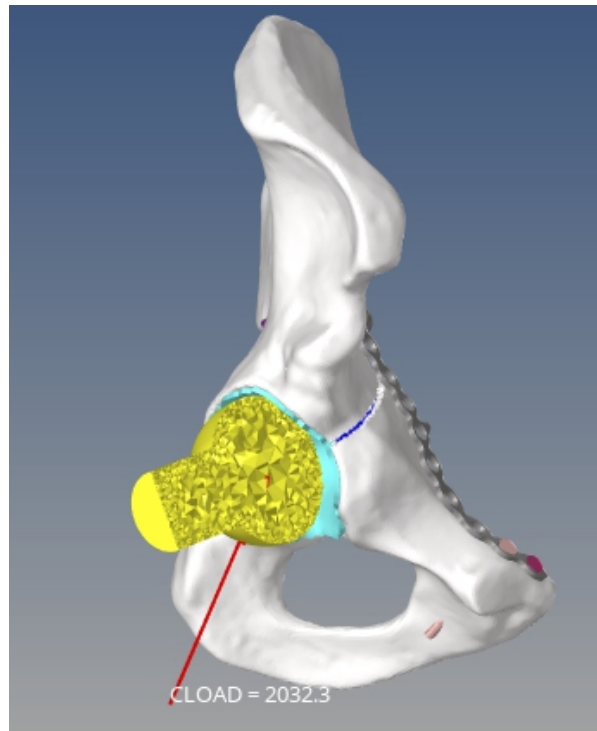


Figure 2.42 Hip joint reaction force acting in the centre of femoral head

## 2.7 Strain calculation

As reported in the introduction, a part of this work concerns the evaluation of the behaviour of fracture gaps during the loading step. In this section, the strain computation at the fracture it is detailed.

Local coordinate systems have been set at the fractures, considering a unique coordinate system for the elementary transverse fracture (in blue in figure 2.43a) and two coordinate systems for the T-shape fracture portions (the transverse fracture and the disruption of obturator foramen, respectively in blue and in red in figure 2.43b).

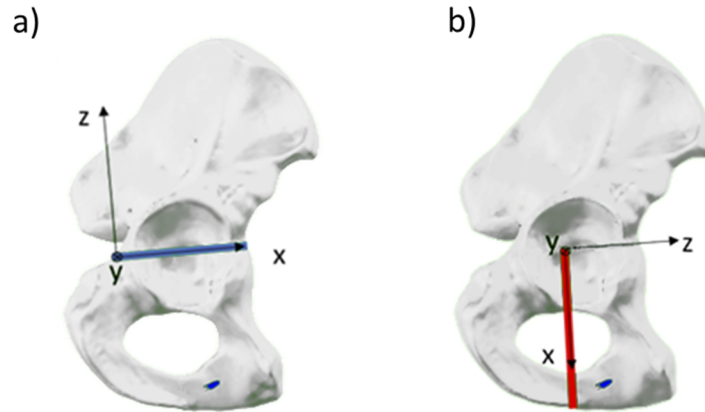


Figure 2.43 a) Relative coordinate system of transverse fracture b) Relative coordinate system of pelvic ring disruption

According to these local coordinate systems, the z direction is orthogonal to the fracture plane, while the x and y directions belong to this plane. Substantially z axis describes movements of compression and traction at the fracture rhyme, conversely x and y axis represent movements that would bring misalignments of the bone stumps on the fracture plane.

To implement the gap analysis along the fracture brim, 22 equidistant couples of points have been selected for the transverse fracture and 15 for the foramen disruption; the same couples of points have been used for each model within the same fracture type. In each couple, the points connection line crosses the fracture gap (Fig 2.44).

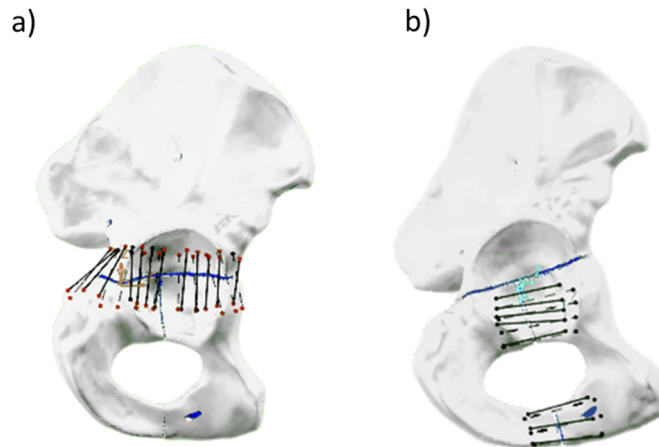


Figure 2.44 a) 22 chosen couples of points crossing on the transversal fracture b) 15 chosen couples of points crossing on the pelvic ring disruption

Since the model are six, but each fracture portion is analysed separately, totally the number of strain analysis are nine.

At first, all the fracture gaps have been measured, then the average fracture gap for every fracture portion was computed: elementary transversal, associated transversal and disruption of obturator foramen. The two typologies of strain determined are the axial and the shear strain: the axial strain represents the parting and approaching of the bone stumps

along the fracture plane normal; conversely, the shear strain gives information on the movements acting on the fracture plane that might bring mismatch of the stumps. In Hyperview, the post-processing software, the incremental distances of the couples of points have been measured and strains were then computed in Excel. The axial strain has been calculated directly as the percentage variation in length along z direction over the respective mean fracture gap; for the shear strain the module between strains along x and y direction has been calculated in order to obtain a unique value representing the fracture plane.

Through a Matlab script, the so obtained strains have been classified in specific ranges: optimal, acceptable, and unacceptable range, as defined in the table below.

Range	Axial strain [%]	Shear strain [%]
optimal	[-2 -10]	0
acceptable	(-10 -15]	(0 15]
unacceptable	(-15 -∞)	(15 +∞)

*Table 2-4 Summary of axial and shear strain ranges adopted*

## 2.8 Assessment parameters

The task of this thesis is resumable as the assessment of the performance of different internal fixation methods, through a single leg stance loading configuration. To describe at best the biomechanical behaviour of these models, it is necessary to take in consideration different parameters with their own specific features.

1. **Von Mises Stress:** the stress in the hip bone was analyzed through the so called Von Mises stress, which is a scalar value that combines all the nine components of the stress tensor; it is useful to compare directly to the yield strength of the material to understand whether material rupture could manifest. Having too high stresses at bone should be avoided because it could lead to breakdown or loosening of the internal fixation.
2. **Displacement field:** the displacement field of the bone can give information on the state of deformation of the bone and whether are present phenomena of rigid motion principally related to bone stumps. It should be preferable to achieve low values of displacement, that would describe a minimal unstable condition.
3. **Strain at the fracture gap:** as previously described, according to Perren's strain theory [33], the analysis of the fracture gap allows to assess the behaviour of the internal fixation system in the perspective of inducing the correct fracture healing. The strains evaluated as extensively described in the previous section have been compared through boxplots representing the distribution of strains. The study of the number .

# 3. Results

---

The results achieved in this study will be presented into two main comparisons: (1) the SQBP C1 vs SPP C2 comparison gives information on the entire method of internal fixation; (2) the SPP C2 vs SQBP C2 comparison addresses the incidence of the infrapectineal portion of the SQBP plate on the system stability.

## 3.1 Stress distribution

The results are here presented as Von Mises stress distributions, shown through a colorimetric code. The value therefore can be understood by the presence of a legend: colder colours represent minimal values, hotter colours stand for higher values of Von mises stresses.

### 3.1.1 Preloading of the screws

The first loading step of the analysis is the fastening of the screws through their pre-tensioning. Within this step, no differences emerged between the two fractures, therefore only the elementary transverse fracture results will be shown for the three internal fixation configurations (SQBP C1, SPP C2 and SQBP C2) (Figures 3.1, 3.2 and 3.3).

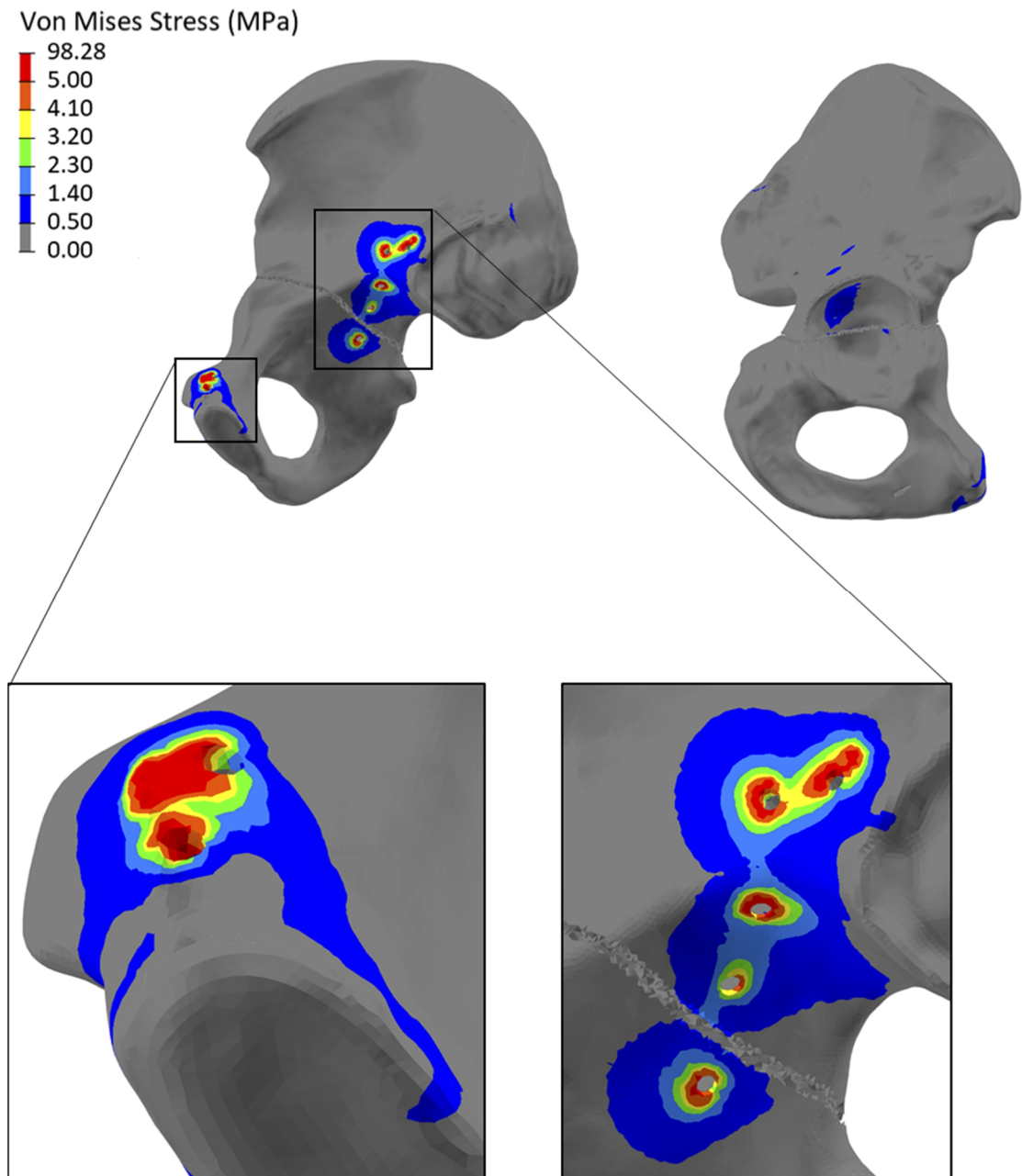


Figure 3.1 Medial (left) and lateral (right) side of hemipelvis using SQBP C1 during pre-tensioning; ZOOM: pubic tubercle (left) and quadrilateral surface (right))

The maximal values registered are located at the pubic tubercle, near the screw number 2, with 98 MPa and at the upper extremity of the arcuate line of the ilium, close to screw number 12, with 90 MPa. These two zones are the ones where the plate-bone contact arrives earlier, so these are the ones mainly subjected to the compression operated by the plate.

In correspondence of all the holes in the cortical bone it is possible to observe the result of the pre tensioning of the screws on the bone, consisting in the generation, at the border of the holes, of maximal stresses from 5 MPa up to 16 MPa, which then decrease radially.

From the lateral view it is possible to note the effect of the pre-tensioning generated by the infrapectineal screws (hole number 13, 14 and 15) in the acetabulum and in the lower body of ilium: Von Mises stresses up to 3 MPa are reached in these regions.

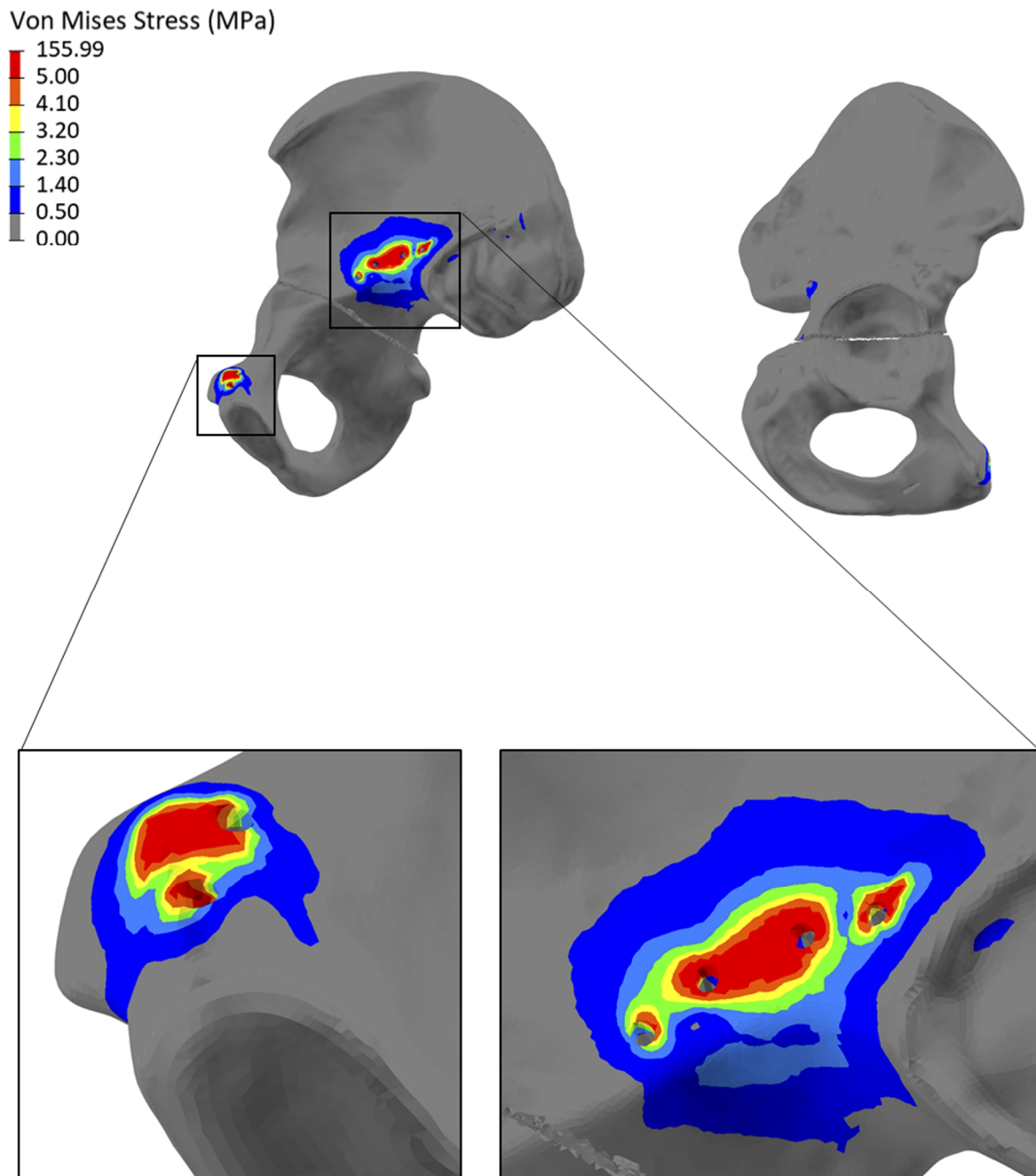


Figure 3.2 Medial (left) and lateral (right) side of hemipelvis using SPP C2 during pre-tensioning; ZOOM: pubic tubercle (left) and iliopectineal brim zoom (right)

The maximal values obtained in the configuration SPP C2 is 156 MPa at the pubic tubercle, due to the compression of the plate on the bone. Differently from the configuration C1 in correspondence of acetabulum there is no sollicitation produced by any screws and further, it can be noted a zone with stresses reaching about 5 MPa between the tenth and eleventh holes due to the contact with plate. Thus, it follows that in this configuration the plate-bone contact is primarily acting just on the pubic

tubercle. The effect of the screws fastening on the cortical bone, is resurable to a stress generation ranging between 6 MPa and 21.4 MPa in proximity of the holes.

The use of the SQBP plate and the configuration C2 of screws disposition, generates the Von Mises stress distribution shown in Fig 3.3.

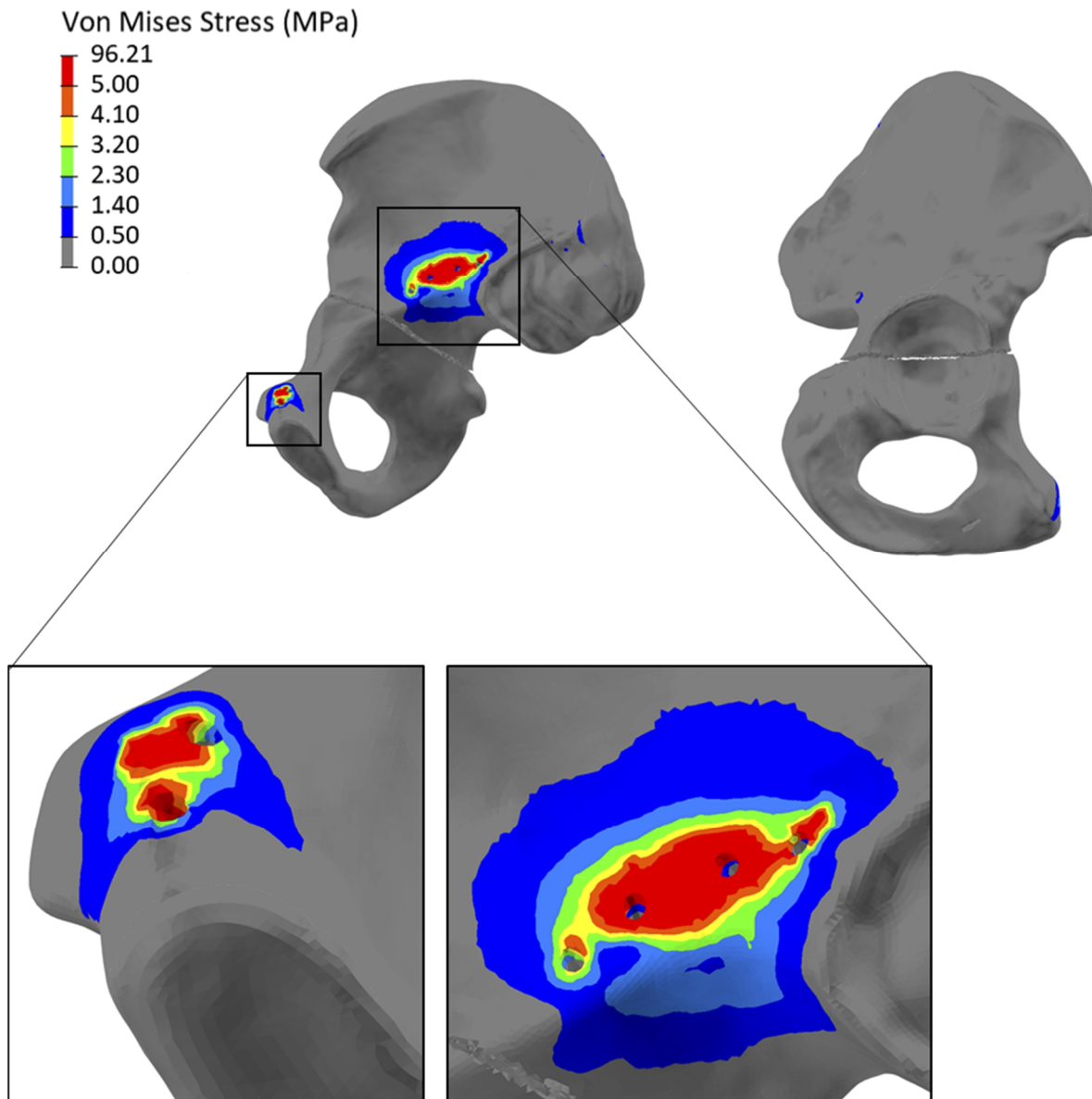


Figure 3.3 Medial (left) and lateral (right) side of hemipelvis using SQBP C2 during pre-tensioning

At a first sight the behaviour of this configuration is very similar to the previous one. The two main differences are referred to the regions of bone – plate contact, both on the pubic tubercle and in proximity of the screw holes number 12. In fact, the highest value is reached at the pubic tubercle as in the SQBP C1 and SPP C2 configuration, but in this configuration the solicitation is the lowest, and reaches 96.2 MPa.

The possible reason of this phenomenon, is that the plate locally leans exclusively on this zone, characterized by the presence of a little spur, and the load transfer to a so little area results in a local

peak of stress. In this configuration, also in proximity of the screw hole number 12, it is possible to note the contact between bone and plate, producing stress up to 20 MPa. Eventually it is also evident that, differently from the SPP C2 configuration, between screws number 10 and 11 higher values (about 20 MPa) are present, compared to the 10 MPa found in the SPP C2 configuration. The maximal stress induced by screw pre-tensioning corresponds to 40.6 MPa, detectable at the screw hole number 11. The increased stress detection in this zone can be directly related to the higher stiffness of the SQBP plate compared to the SPP plate which consequently is subjected to higher strains.

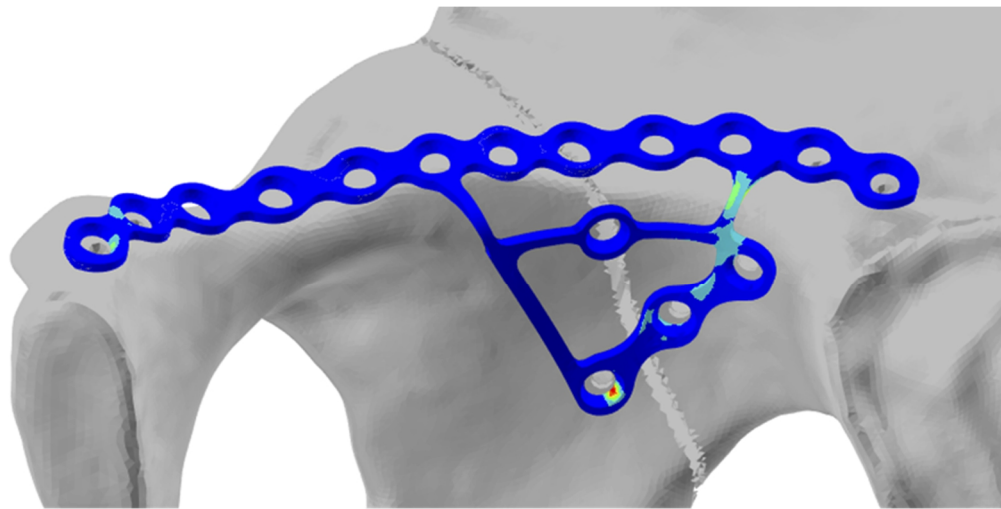
In the following table (Table 3-1) the maximum Von Mises stresses generated by the screw fastening directly on the bone are listed.

Screw hole	SQBP C1 (MPa)	SPP C2 (MPa)	SQBP C2 (MPa)
1	11.4	8.4	10.5
2	16	21.4	13.1
9	-	6.1	5.2
10	-	10.2	20.7
11	10	20.8	40.6
12	10	11.3	13.42
13	11	-	-
14	4.9	-	-
15	7.9	-	-

*Table 3-1 Von Mises stress induced in bone by screws fastening (MPa)*

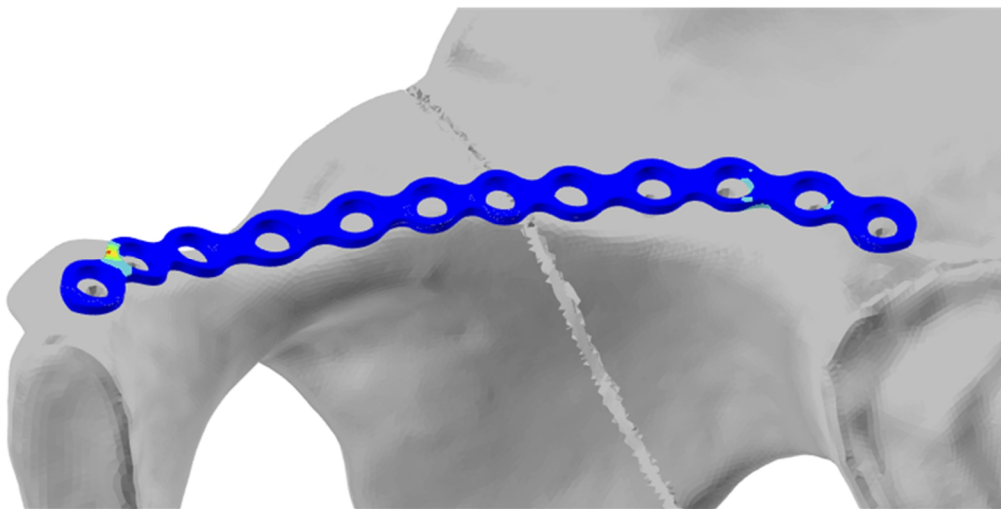
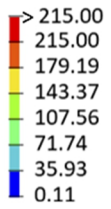
The maximum stress induced by screw fastening in cancellous bone in the SQBP C1 configuration is equal to 5.6 MPa, in the SPP C2 configuration 11.2 MPa and in the SQBP C2 configuration is 1.7 MPa.

In figure 3.4 it is possible to observe the Von Mises stress distribution in the three configurations of plates implemented in this thesis work: SQBP C1, SPP C2 and SQBP C2. As can be derived from the already shown results belonging to the pelvic bone stress, it is feasible to note the different solicitations among these three plates. Although all the three configurations show a maximal stress zone in their inferior side between holes number 1 and 2, where the yield strength (215 MPa [50]) of the stainless steel 304 is reached, the SPP C2 configuration is the one subjected to the widest stressed area. The SQBP C1 combination differently from the SQBP C2 registers a solicitation at the connection between the suprapectineal and infrapectineal portions near the hole number 10 which is around 120 MPa: this is explained by the fastening of the screw 13, 14 and 15 that together with the action of the suprapectineal screws, tend to bend this connection “bridge”. In the SQBP C1 combination in fact, the zone of the hole 15 seems to be highly stressed because of the great effort of the screw 15 to hold together the two stumps. The most stable condition therefore is identifiable in the SPP C2 configuration which reports the lowest Von Mises stress manifestation, as expectable from the bone stresses evaluation.

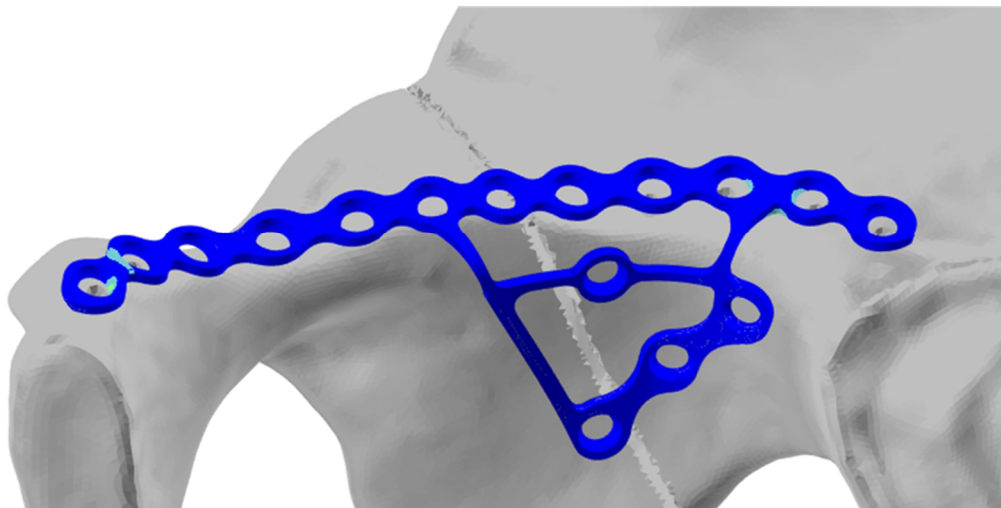


**SQBP  
C1**

Von Mises stress (MPa)



**SPP  
C2**



**SQBP  
C2**

Figure 3.4 Plates Von Mises stress distribution in pretension step

### 3.1.2 Single leg stance loading

During the single leg stance phase, the comparison between SQBP C1 and SPP C2 has reported the results showed in figure 3.5.

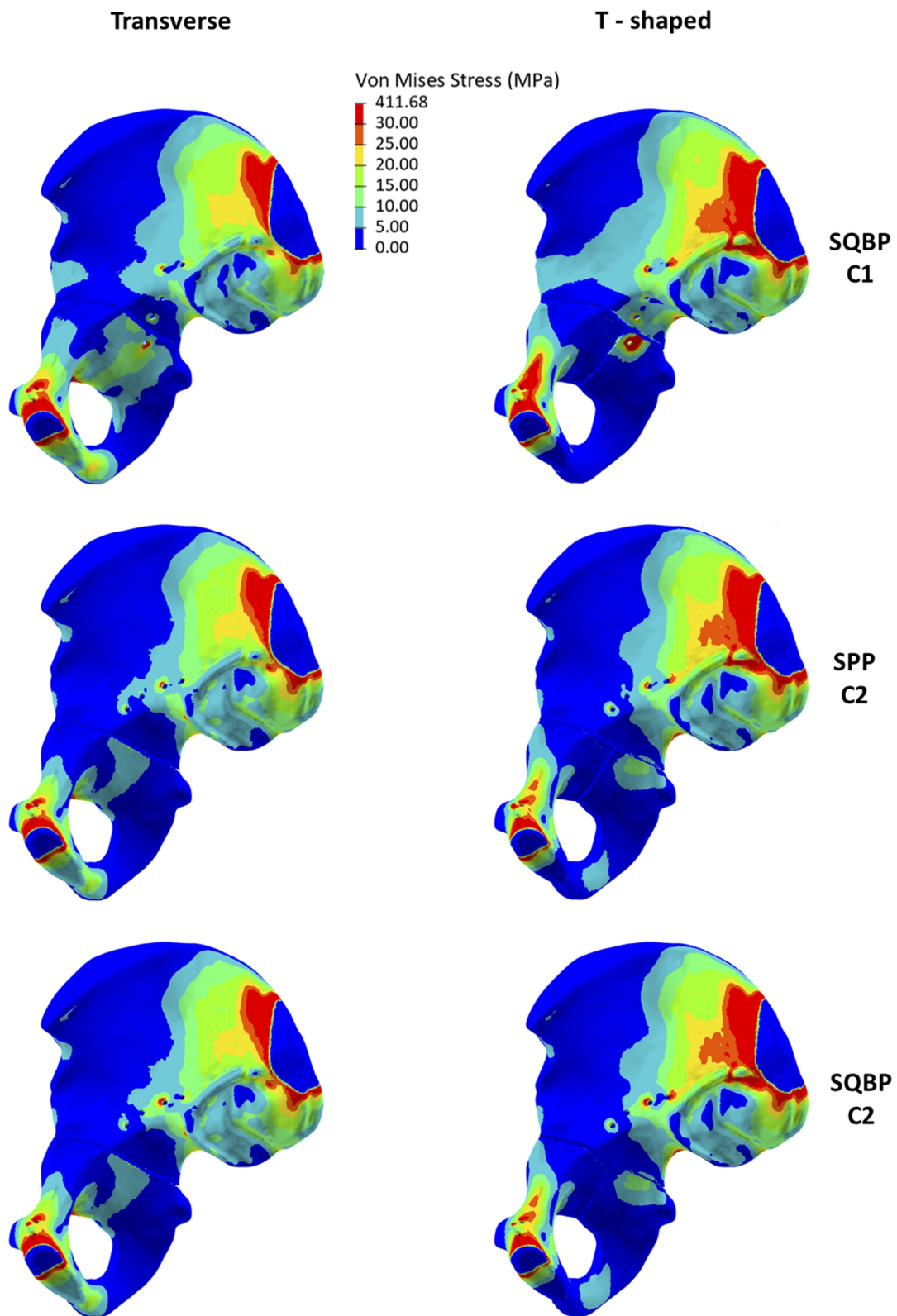


Figure 3.5 Von Mises stress confrontation in hemipelvis (medial view) during pretension step

From a medial view it is possible to see, with a rescaled legend where the red colour identifies values greater than 30 MPa, the focusing on distribution of the stresses over the hemipelvis.

In each model, regions with high values of stress correspond to the ones adopted as constraints (pubic symphysis and iliac crest): in fact here all the degrees of freedom have been bonded so that the immediately closer zone are submitted to a reaction stress for reaching an internal equilibrium.

Furthermore, if the zones of plate-bone contact are considered, it is possible to evaluate that all the three configurations report the highest stress located in the pubic tubercle. Only exception is the T-shaped fracture of the SQBP C1 model, showing a maximum stress of 174.4 MPa near the screw hole number 15. Substantially, it is visible from the medial view, that the high stresses present in proximity of the constrained zones, in all the configurations, decrease moving away along all the directions, reaching a mean of 26 MPa in the iliac wing and almost 10 MPa in the middle ilium and the body of ischium, until they become negligible in correspondence of the fracture gaps. For both models belonging to the SQBP C2 configuration, a clear reduction of the stresses at the pubic tubercle induced by the bone-plate contact is visible, whilst in proximity of the screw hole number 10, middle-low values of stresses (almost 20 MPa) can be noted (Fig. 3.6).

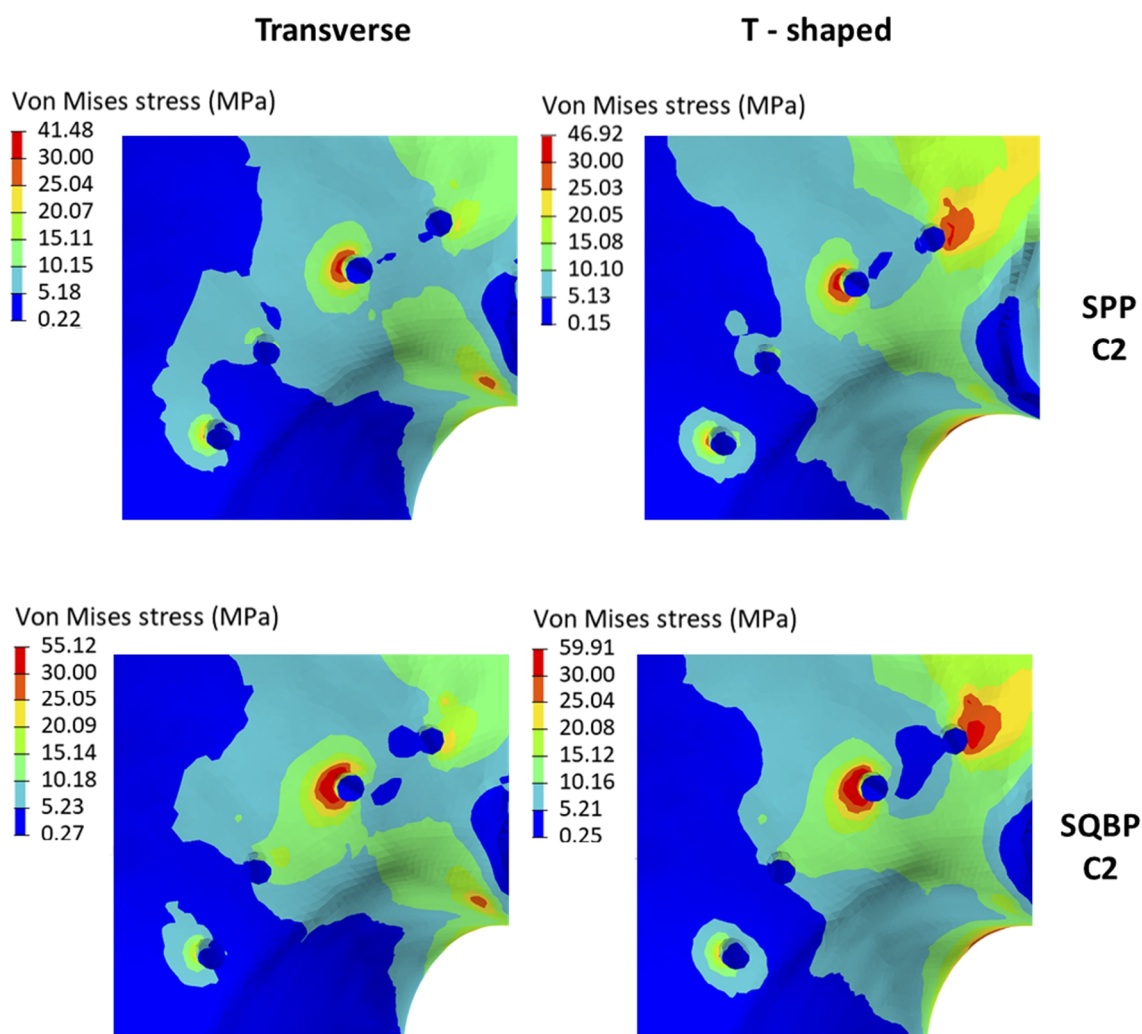


Figure 3.6 Zoom of iliopectineal brim for both C2 configurations

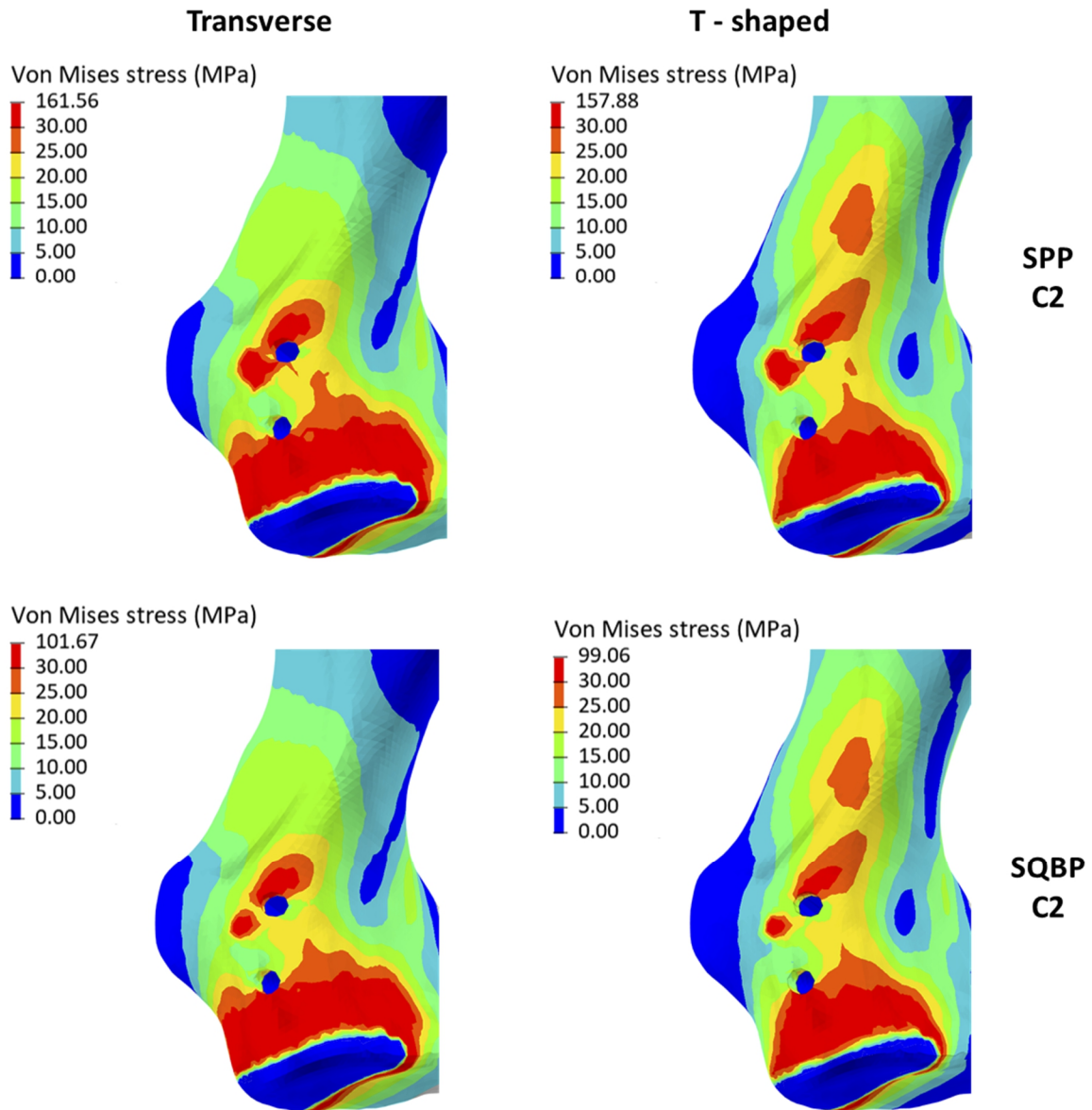


Figure 3.7 Zoom of pubic tubercle for both C2 configurations

The SPP C2 configuration with a transverse fracture shows, in correspondence of the pubic tubercle, a peak value of 161.6 MPa and for the T-shaped one a peak value of 157.9 MPa; conversely, values belonging to the SQBP C2 in the corresponding regions are 101.7 MPa and 99.1 MPa (Fig 3.7) .

Another difference is related to the stress generated to the pelvic ring fracture region of the T-shaped models due to contact forces of the bone stumps: in the SPP C2 configuration values of 411.7 MPa are reached, compared to the 337.8 MPa found in the SQBP C2 configuration.

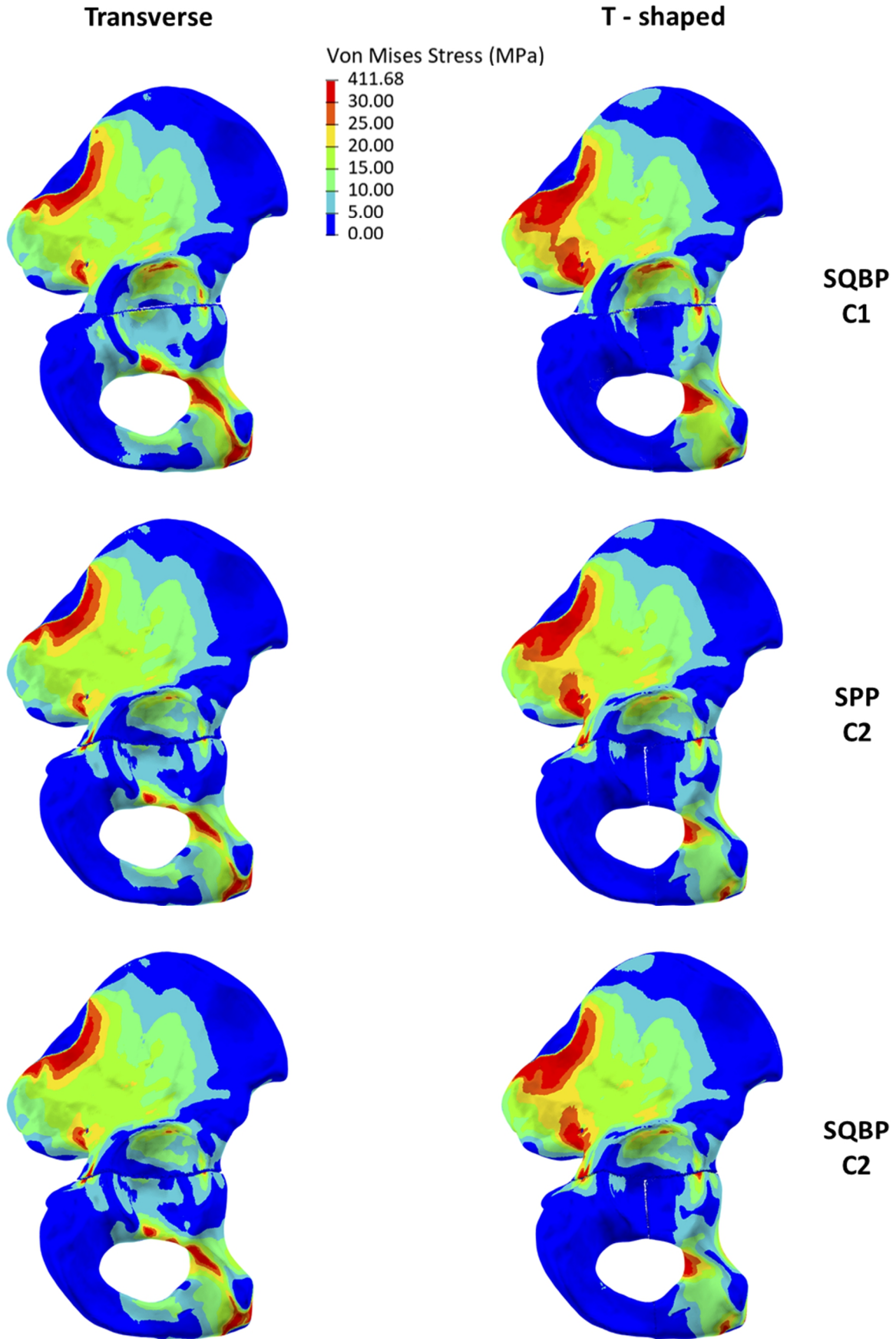


Figure 3.8 Von Mises stress confrontation in hemipelvis (lateral view) during pretension step

Through the representation of the map of stresses on the lateral view, adopting a legend saturated at 30 MPa (Fig. 3.8 above) it is possible to analyse mainly the acetabular cup. Starting with the comparison of the two different internal fixation systems (SQBP C1 vs SPP C2), in all the configuration emerges that the most solicited part in the acetabulum consists in the anther-superior dial, which is determined by the direction of the external applied load. Here in fact, the maximal Von Mises stresses are on average 55 MPa with peaks up to 70 MPa; in the rest of the acetabulum the values remain between 4 MPa (above all in the centre of the acetabulum) and 23 MPa. In each transverse fracture, the distribution of stress appears more uniform, suggesting a more homogeneous load transfer through the bone; this is probably due to the absence of the additional fracture of the T-shaped configuration, that represents an obstacle to the propagation of the stress.

In fact, observing the three models in relation to the fracture type, it can be extrapolated that this one concurs in the determination of the shape of stress distribution: both the T-shaped fractures have very low values of stress in the centre of acetabulum and a similar behaviour at the superior ramus of the pubis; on the contrary, in the two transverse fracture there is the same involvement of the ischio-pubic ramus, where values of 10 MPa are reached, and along the inferior ramus of pubis and in the lower dial of acetabulum where there are peaks of 40 MPa.

As regards the comparison between the SPP C2 and the SQBP C2 configurations, it is possible to note that there are not present significative differences in terms of stress distributions on the bone within the same fracture type: stresses seem indeed to follow the same propagation curves.

Considering the hemipelvis globally, the highest value of stress among the combinations is found in the T-shaped fracture models: 382 MPa for the SQBP C1, 412 MPa for the SPP C2 and 337.8 MPa for the SQBP C2. This phenomenon is directly related to the conformation of the fracture which permits a rigid motion of the bone stumps decreasing frictional contacts; thus, it follows the production of so high Von Mises stresses.

In the following table (Table 3-2) the maximal Von mises stresses found in the specific regions of the pelvis are reported (expressed in MPa).

<b>Model</b>		<b>Acetabulum</b>	<b>Pubic symphysis</b>	<b>Iliac crest</b>	<b>Contact zones plate-bone</b>	<b>Overall</b>
SQBP C1	Transverse	62.4	96.2	74.5	102.1	102.1
	T-shaped	68.1	74.2	87.1	174.4	382
SPP C2	Transverse	30.9	98.2	111.9	161.6	161.6
	T-shaped	70.23	90.8	157.2	157.9	412
SQBP C2	Transverse	32.3	98.3	111.9	101.4	111.9
	T - shaped	70.5	89.3	157.1	99.1	337.8

*Table 3-2 Summary of Von Mises stress peaks in the considered regions of hemipelvis*

## 3.2 Displacements field

In this section the displacement distributions related to the hip bone during both the pre-tensioning and single leg stance steps are presented. The displacement displayed is intended as magnitude value that represents with a unique value all the movements belonging to the three spatial directions.

### 3.2.1 Preloading of the screws

From the comparison between SQBP C1 and SPP C2, it is immediately evident that a maximum displacement equal to 0.067 mm is present at the fractured foramen obturator of the SQBP C1 model (figure 3.9). In the corresponding fracture of the SPP C2 configuration, the same region is characterized by the highest displacement values, but with a more moderate entity (0.02 mm). In the SQBP C1 configuration the transverse fracture reports the minimal displacements compared to the other models. In both fractures of SPP C2, local displacements equal to 0.04 mm are present at the screw hole number 10, and equal to 0.012 mm at the pubic tubercle, as effect of the plate compression.

Conversely, from the comparison between the SPP C2 and the SQBP C2 configurations displacements maps, it is evident that the two groups appear almost coincident, only exception is the magnitude of the displacement. In fact, matching the stress patterns previously presented, the SQBP C2 model shows higher values of displacement at the screw hole number 10 (0.06 mm) and lower values of displacement in correspondence of the pubic tubercle (0.008 mm). Furthermore, in the ischio-pubic ramus it is possible to note a more extended bone surface subjected to a displacement of 0.025 mm.

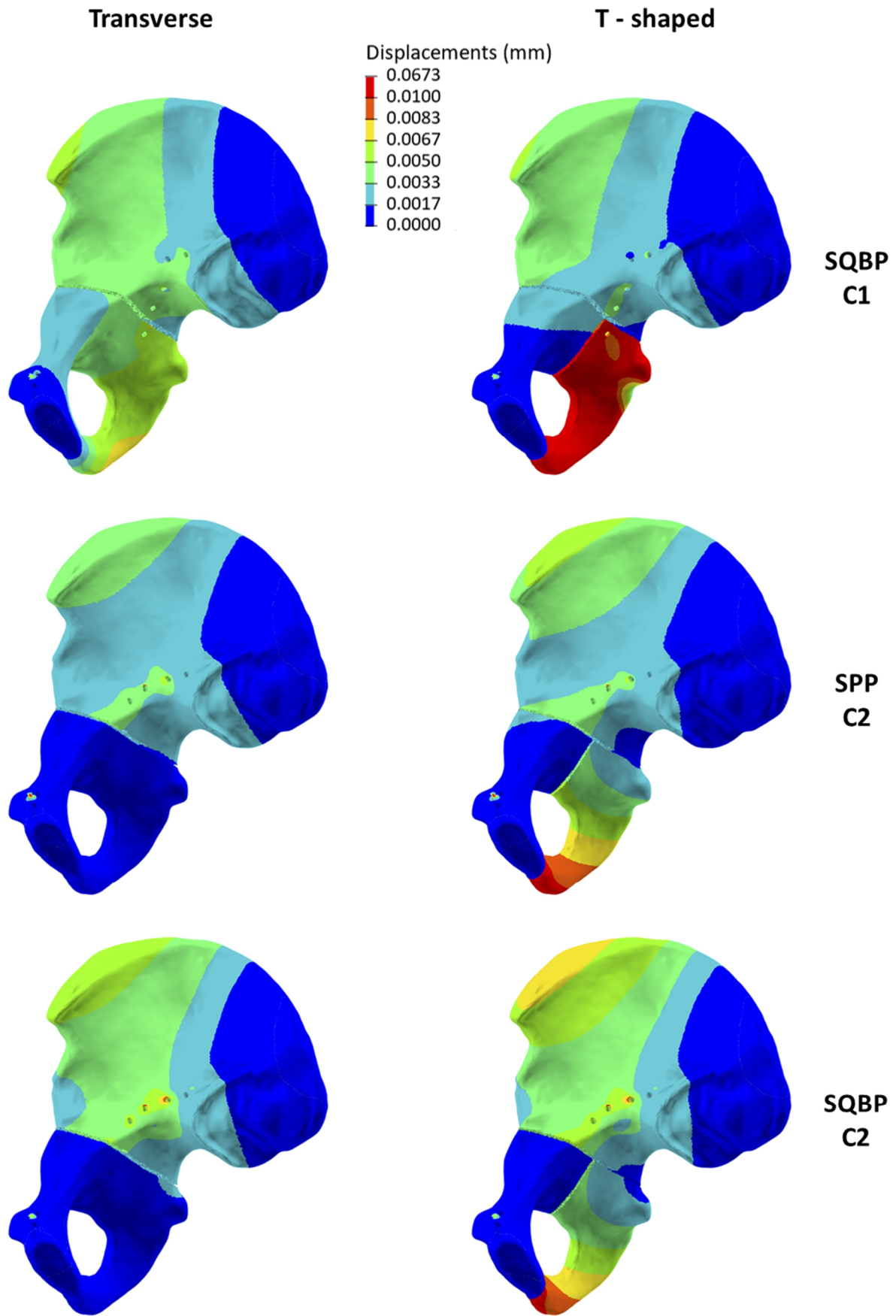


Figure 3.9 Confrontation of displacements field of hemipelvis (medial view) during pretension step

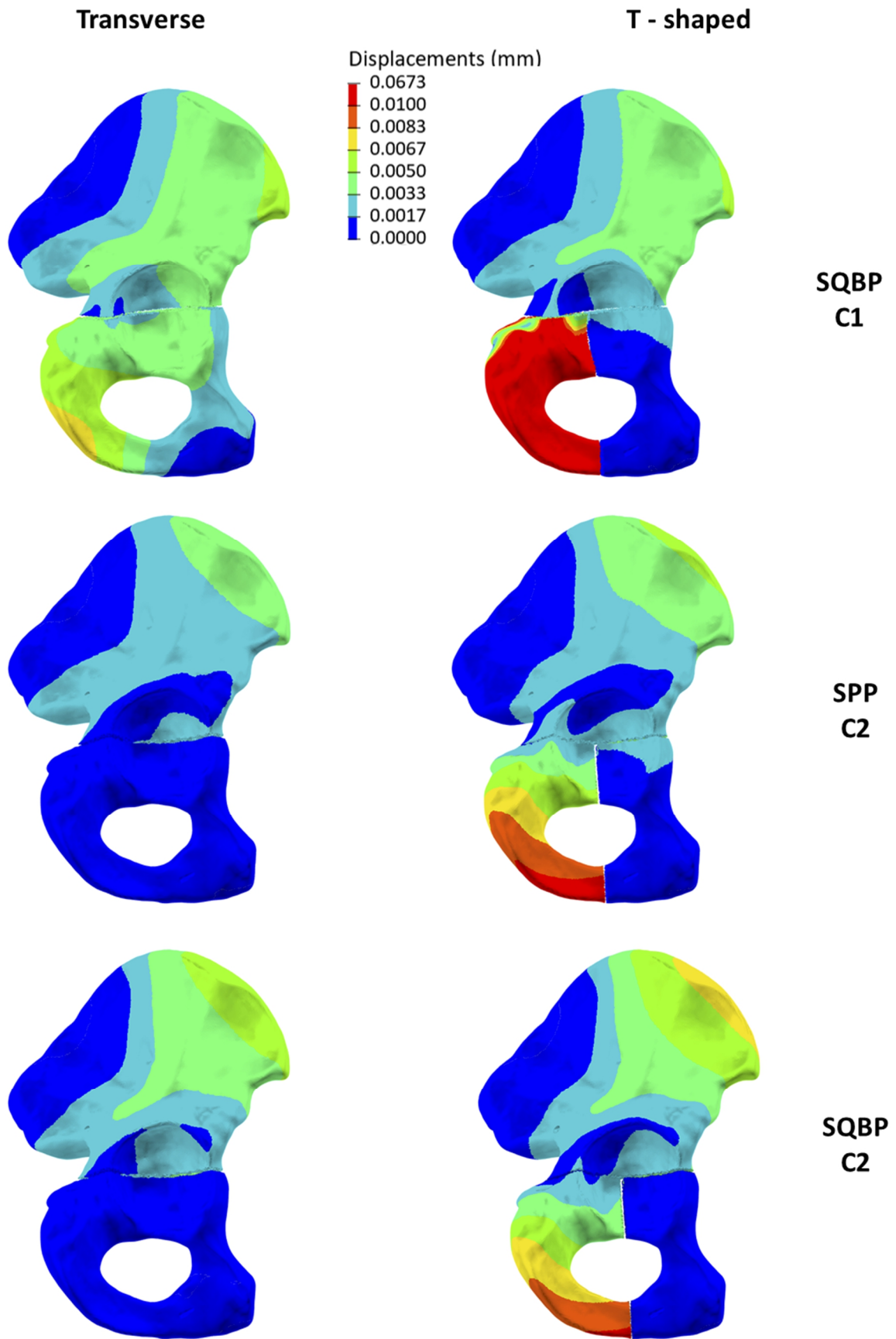


Figure 3.10 Confrontation of displacements field of hemipelvis (lateral view) during pretension step

### ***3.2.2 Single leg stance loading***

When the single leg stance external load is applied to the acetabulum (figure 3.11), it follows that in the two T-shaped fractures of SQBP C1 and SPP C2 configurations phenomena of rotations of the fractured stump are generated. This motion is so elevated that closes a great part of the fracture gap. Substantially, the T-shaped configuration consists of three separated bony blocks, where the one belonging to the pubic symphysis and the one belonging to the iliac crest are externally constrained (see boundary conditions in the previous chapter). The most distal bony stump (the one belonging to ischium) is constrained to the others through the internal fixation system composed of screws and plate; nevertheless, it is subjected to a motion. In relation to the described situation, the SQBP C1 model has the highest magnitude of displacement equal to 3.1 mm, conversely in the SPP C2 model the maximum value is 2.3 mm. The behaviour of the two transverse fractures is similar, with the one fixed with the SQBP C1 plate having the highest displacement equal to 1.2 mm, against 0.9 mm detected in the ischium of the SPP C2 model.

Observing the C2 models (both SPP and SQBP plates), similar behaviours arises. In fact, changing the plate the differences are negligible: in both configurations the transverse fracture reports a maximal value of 0.9 mm and the T-shaped one a maximal displacement equal to 2.3 mm.

Considering the three configurations, the main outcome of the displacement analysis is related to the differences between the two fracture types. In particular, all the T-shaped fracture models show the less stable behaviour.

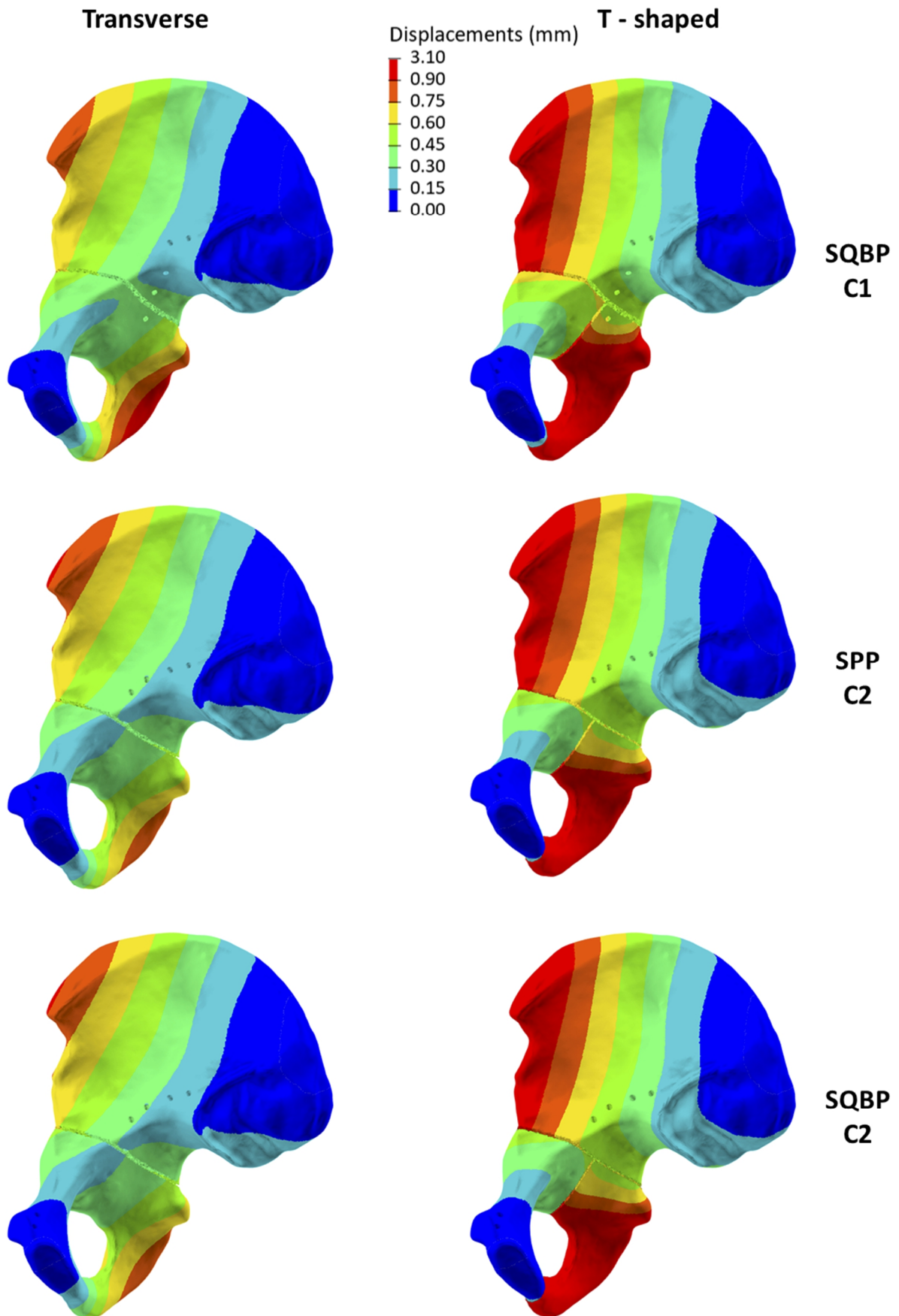


Figure 3.11 Confrontation of displacements field of hemipelvis (medial view) during loading step

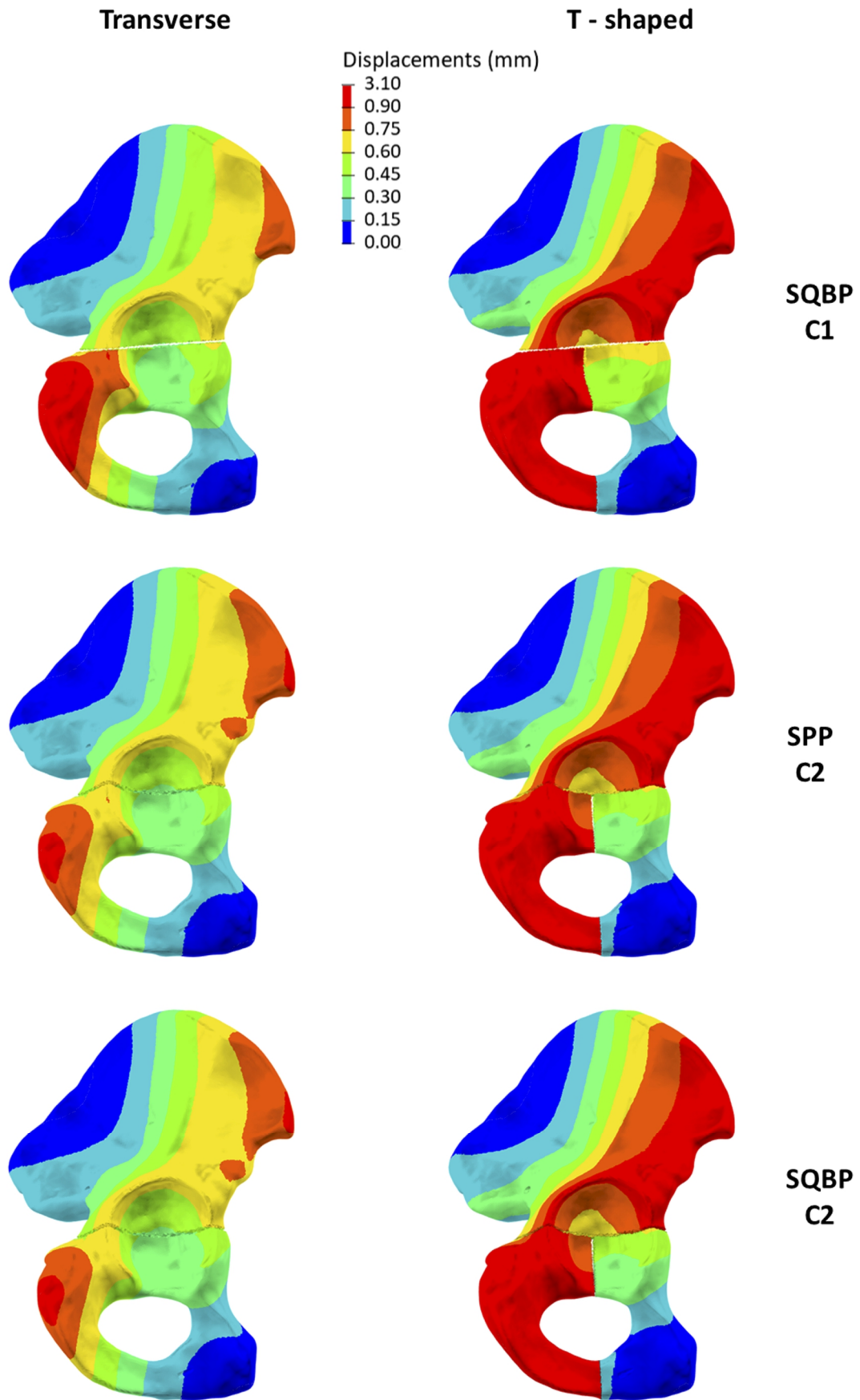


Figure 3.12 Confrontation of displacements field of hemipelvis (lateral view) during loading step

### 3.3 Analysis at fracture gap

The last assessment is the evaluation of the Perren's theory on fracture strain, which will be presented in this section. Here, the couples of points considered in the computation of the incremental distances have been classified into the three ranges defined in the Methods chapter: (1) the optimal range as described by Perren [32], (2) the acceptable range, which is the range of values tending to the optimal behaviour, and (3) the unacceptable range, which accounts for values that are rejected from the previous ranges.

#### 3.3.1 Axial strain

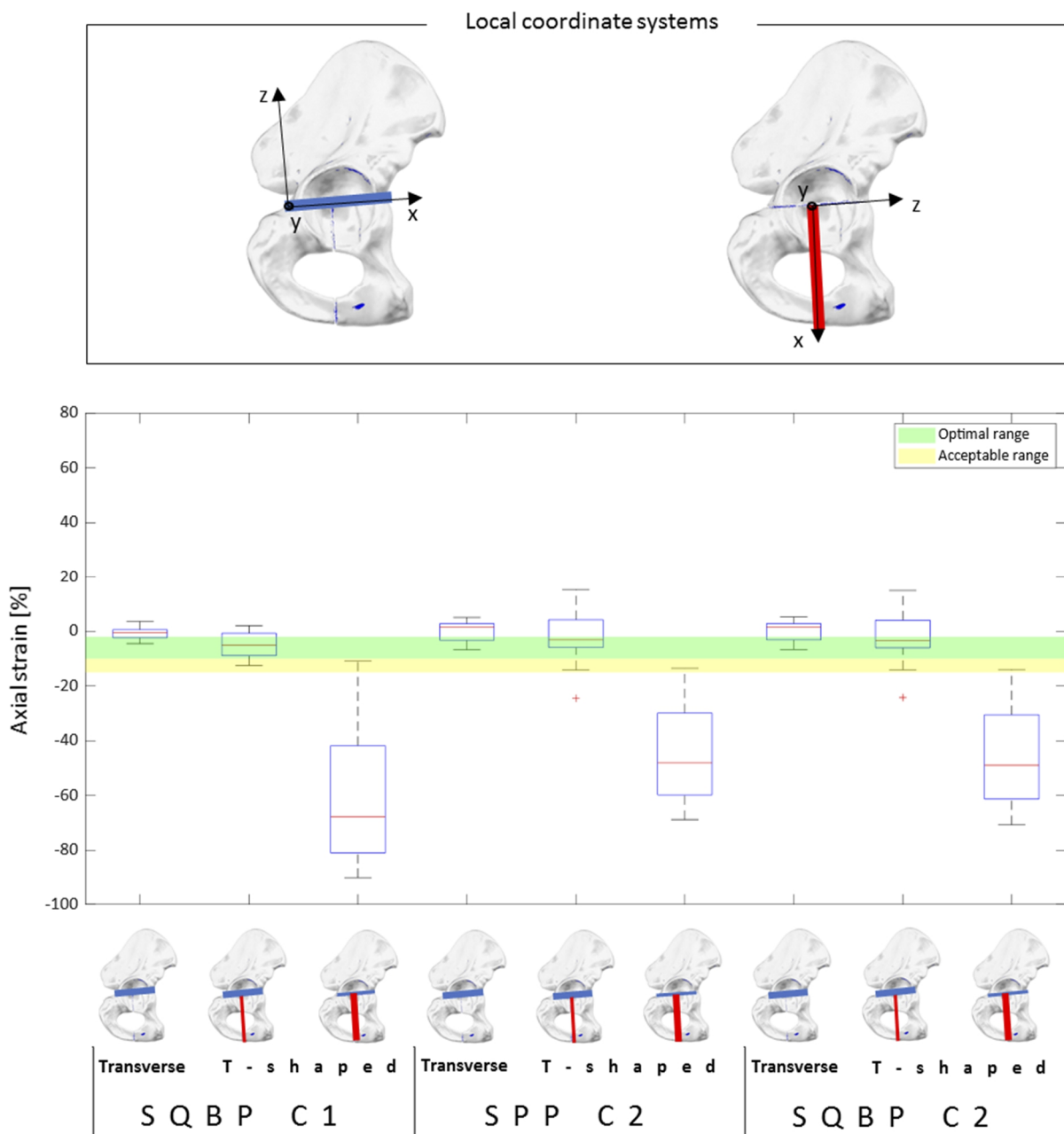


Figure 3.13 Boxplot of axial strain distribution of the three internal fixation configurations

Comparing the models that differ both in terms of plate and screws configuration (SQBP C1 and SPP C2), it is possible to note two main differences regarding the elementary transverse fracture:

1. the median direction of the incremental distances (Figure 3.13) of SPP C2 is mainly oriented towards a minimum axial expansion (median 1.57%) of the fracture gap; conversely SQBP C1 mainly brings the fracture gap towards minimum compressions (median -0.61%).
2. the slightly greater quantity in the SPP C2 model of observations satisfying the optimal range, ascertained by the percentage histogram in Fig. 3.14 (36% against 31% of SQBP C1).

Comparing the T-shaped fracture, in its associated transverse fracture portion (in blue in Fig. 3.13) SQBP C1 shows a better performance, both related to the number of point couples belonging to the optimal range (45.5% versus 41%) and to the acceptability range (68% versus 55%). As far as the associated fracture of the pelvic ring is concerned (in red in Fig. 3.13), a very high axial compression is visible in both models, which generates an almost closure of the fracture gap. The minimal values are indeed respectively -90% (median -68%) for the SQBP C1 model and -69% (median -48%) for the SPP C2 model, which both result outside the optimal and the acceptable range.

Comparing instead the models with screw configurations C2 (SPP C2 and SQBP C2), the same behaviour emerged according to the histogram percentages: 36 % of couples belongs to optimal range for both the transverse elementary fractures, 41 % of occurrences satisfy the optimal range for both the associated transverse fractures and, eventually, only almost 7% of occurrences are within the transition range as regard the two obturator foramen fractures.

### Percentage axial strain

■ Optimal range [-2 -10] %    
 ■ Acceptable range (-10 -15] %    
 ■ Unacceptable range (-15 -∞) %

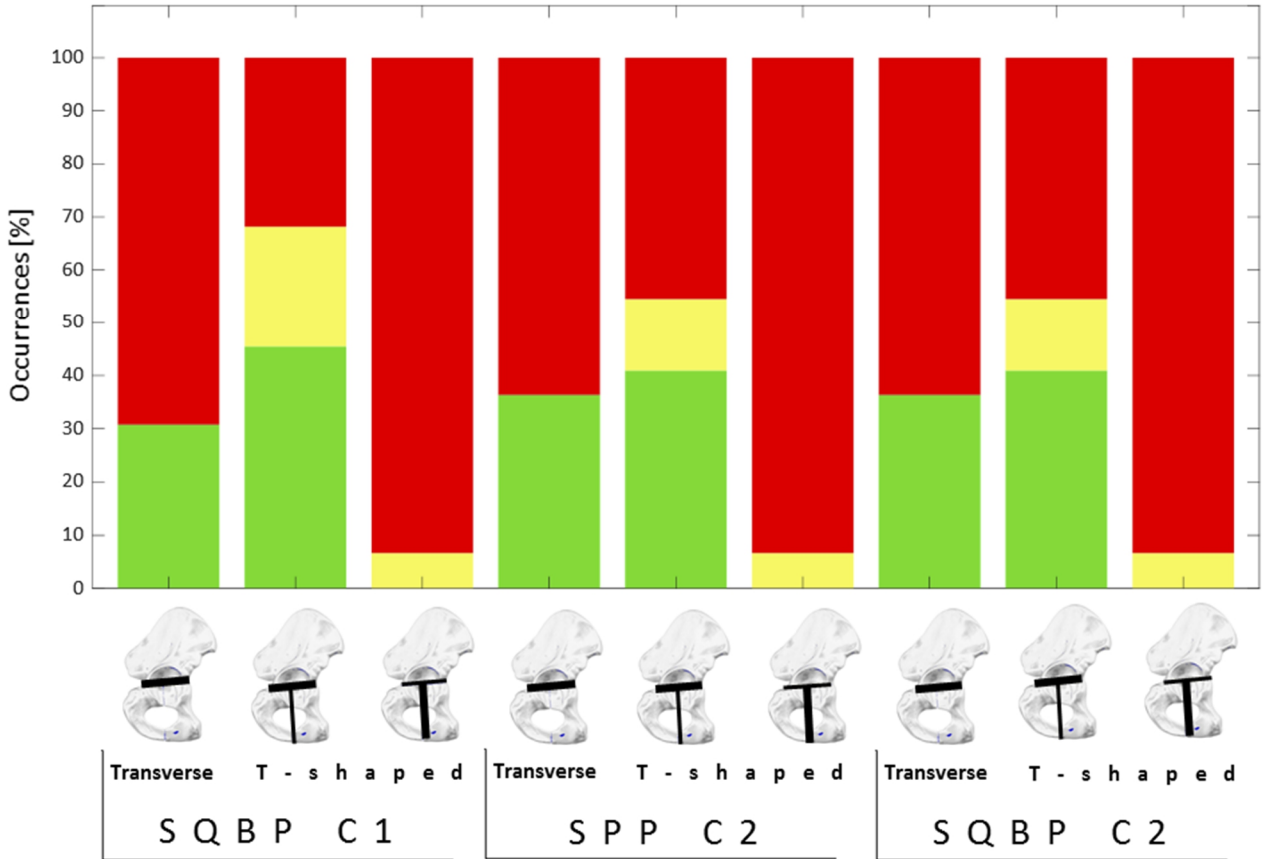


Figure 3.14 Percentage histograms of axial strain occurrences according to the three ranges of the three internal fixation configurations

### 3.3.2 Shear strain

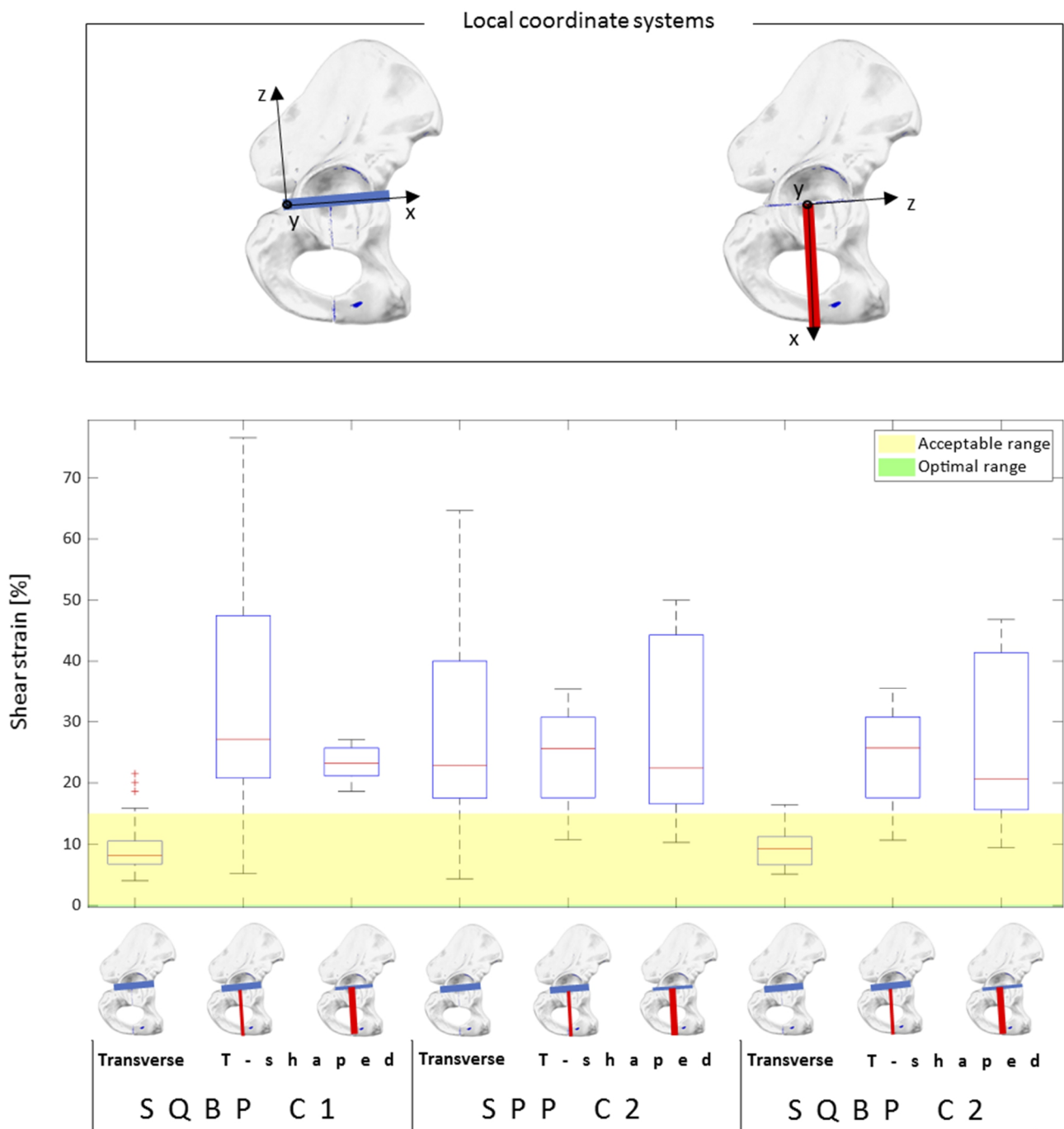


Figure 3.15 Boxplot of shear strain distribution of the three internal fixation configurations

From figure 3.15, showing the distribution of shear strain among the various fractures, it is evident that none of the configurations reported an optimal behaviour in blocking sliding motions of stumps in the fracture plane (0% shear strain). Comparing the models S Q B P C 1 and S P P C 2, when the elementary transverse fracture is considered the former has lower shear strain values and almost 82% of the values are within the acceptable range (0 -15] %, while the latter is characterized by a great variability of shear strain in a range between 4 % and 65 % and with an acceptability percentage of 18% (figure 3.16).

As far as the T-shaped fracture is concerned, in its associated transverse fracture a similar behaviour between the two models is visible: for the SQBP C1 the shear strain values range between 5% and 77%, whilst for the SPP C2 range between 10 % and 35 %. Respectively, the percentage of couples of points within the acceptable range is 9% and 14%. For the associated fracture of the pelvic ring, SQBP C1 values range between 18% and 27%, meaning that no points satisfy the acceptable range; in SPP C2 configuration, on the other hand, the shear strain is wider, between 10% and 50%, but with 20% of the points within the acceptable range.

If the C2 screws configurations models are compared, in order to investigate the incidence of the infrapectineal portion of the SQBP plate, it can be noted that for the T-shaped fracture the differences are minimal: in the transverse fracture the range of shear strain distribution [10% 36%] is almost identical, and it is feasible to assess the same value of median equal to 26% with the same percentage of values belonging to the acceptable range (16.64%). In the pelvic ring fracture, a range of distribution equal to [10% 50%] is reached, with median equal to 22%, for the SPP plate. The SQBP plate reaches a very similar range of values [9% - 47%] with median 21%. For both plates, the same percentage of 20% of the points within the acceptable range was computed.

The substantial difference between the two plate is noticeable in the elementary transverse fracture: SPP plate has an acceptable percentage of 18 % while SQBP plate the percentage increases to 90 %; in this latter, indeed, the range of shear strain is confined between 5 % and 16% with median 9% .

### Percentage shear strain

■ Optimal range [0] %    
 ■ Acceptable range (0 15] %    
 ■ Unacceptable range (15 ∞) %

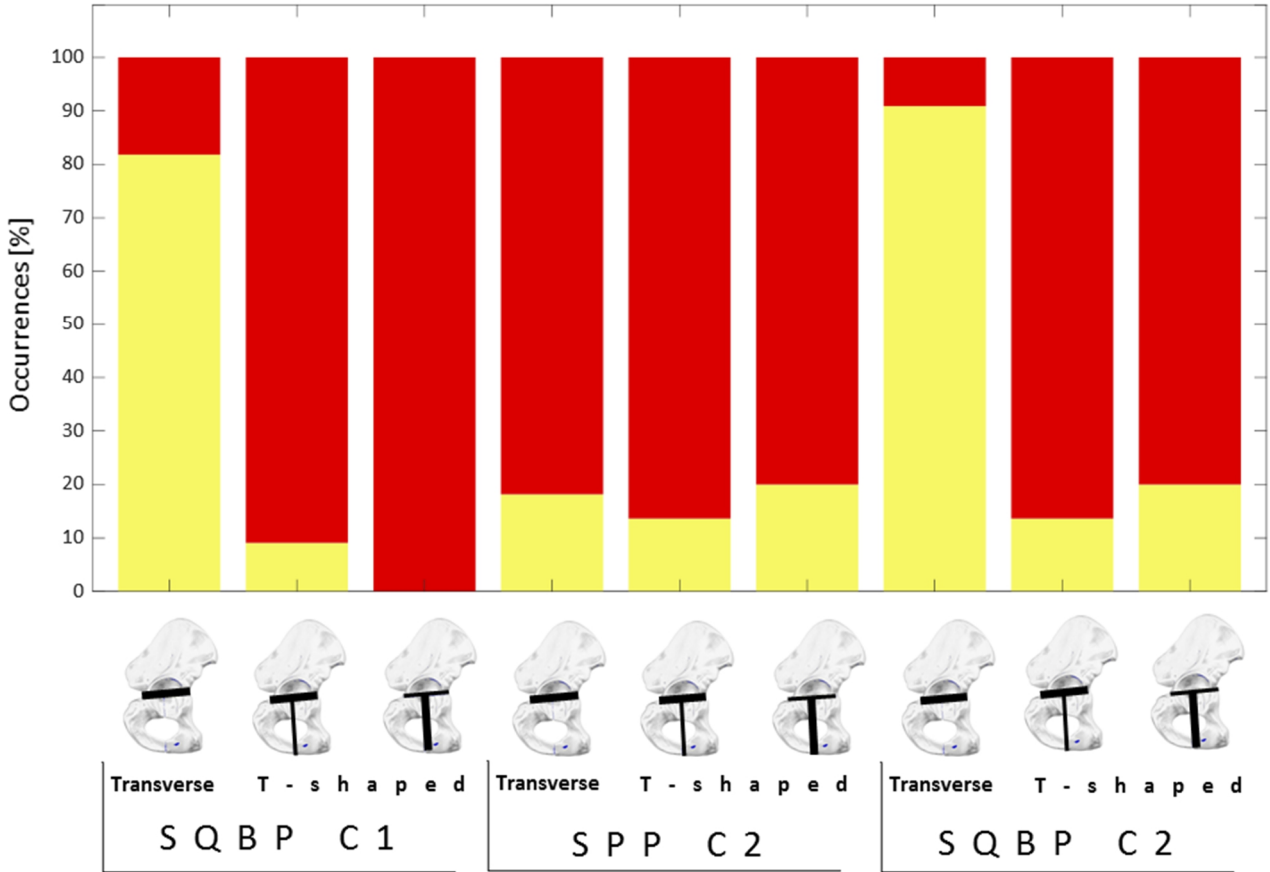
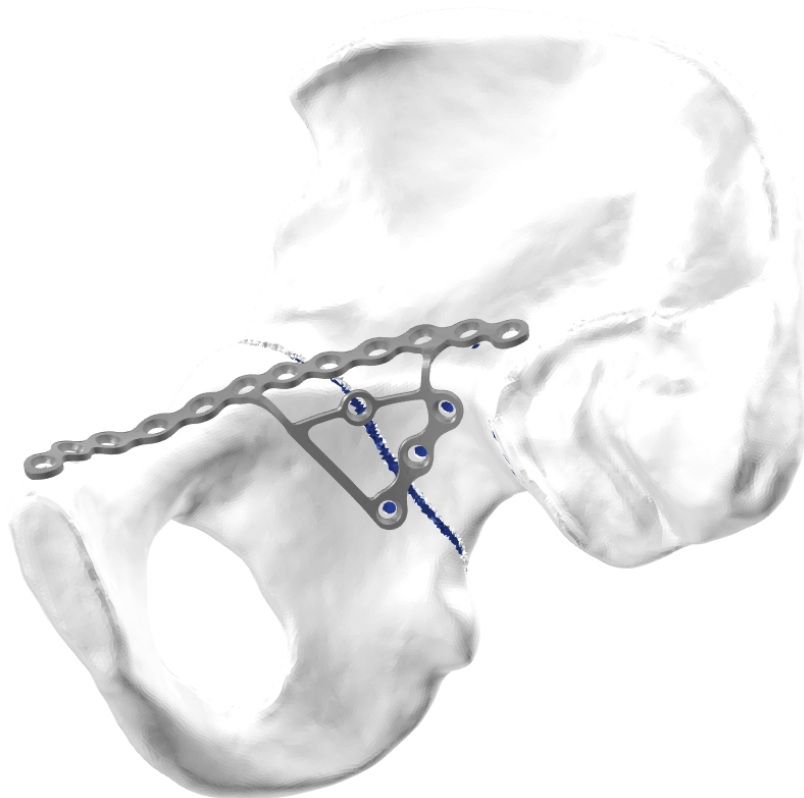


Figure 3.16 Percentage histograms of shear strain occurrences according to the three ranges of the three internal fixation configurations

## 4. Discussion

---

The generation in the FEA environment of the Pro Striker plates design has been a delicate step in this thesis work because it has represented the first task for the implementation of a reliable model able to correctly describe an internal fixation configuration.



*Figure 4.1 Patient specific SQBP plate adapted to the bone shapes*

Observing the generated SQBP plate (Fig. 4.1), its property to follow the articulate shapes of the hip stands out. In fact, due to the adaptation of its geometry to the specific hip model it can be defined as a patient-specific plate. Nowadays, the gold standard in internal fixation plates is represented by the Pro suprapectineal Striker plate, which has a native pre-contouring based on the average sizes of male and female hip bones. This feature allows the surgeon to minimize operation times and risks related to blood loss during surgical intervention [31] with respect to the standard plane plates. Nevertheless, the steps of the plate reconstruction presented in this thesis work could be a forefront conception: they are focused on the possibility to create a 3D CAD plate design totally based on the patient geometry, which perfectly and immediately could fit on the patient own pelvic bone, just by varying geometrical parameters. Although rapid manufacturing techniques are emerging in the orthopaedics devices production, the diffusion of these methodologies is still limited, especially in

the field of load bearing plates [63]. Therefore, if the direct production of this patient specific plate through standard manufacturing technologies would comport realizability difficulties, an alternative approach could be implemented: thanks to the generation of a mold CAD model on the basis of the patient-specific 3D CAD design - obtained in accordance with the procedure described in this work - the surgeon can model the plate on the physical mold manufactured in plastic materials through a low-cost 3D printing [64] thus obtaining a patient-specific plate. This preoperative planning procedure, above all, would abolish any in-situ bending, reducing intervention time and preserving the patient from surgical risks as bleeding and infections [64].

The assessment of the performances of the three configurations of internal fixation reported in this thesis study, has showed, as expected, the presence of several discrepancies. The evaluation of the models, therefore, has been executed taking in consideration primarily the sollicitation on the bone through the examination of different parameters.

The first investigated parameter has been the Von Mises stress. In the pre-tensioning step, the SPP C2 combination reported the highest values: this could be due to the compression of the plate over the relatively small area of the pubic tubercle, resulting therefore in a significative negative effect on the bone. If the SQBP plate is considered, in proximity of the pubic tubercle the stress is reduced, but at the same time it is slightly increased in the region of the ilium characterized by screw hole number 10 and 11: these screws, when fastened, produce higher stresses induced by the less flexibility of the plate over the suprapectineal brim thanks to its additional infrapectineal portion which leads to a greater plate stiffness. On the contrary, by using the SQBP plate with the C1 screws disposition (SQBP C1 combination), also a stress of 3 MPa is produced at the acetabulum which can be considered neglectable.

The different stresses detected in proximity of the screw holes are also explained by considering screw inclination that is determinant to the holding power on the bone [65] and more precisely it is established that the holding power of the screw is maximal when it is inserted at  $90^\circ$  in the bone [66]. The holding power of the screw is not a mechanical property of the screw itself, but it depends on the friction between bone and the screw and it "is related to the shearing strength of the material into which it is inserted" [57].

A mechanism of holding power of the screw can be identified with the so called bending stress of the screw head. This effect is fundamentally detectable with the simultaneal presence of tensile stress and compression stress in proximity of the screw head. Being the screw the element that allows to hold in adhesion the plate to the bone, this phenomenon is generated by the simultaneous contact between screw and bone and between screw head and plate. When a load is applied, that is the pre-tensioning or hip joint reaction force, the screw, sollicitated by the different mechanical responses of bone and plate, is subjected to contact forces that induce this phenomenon [65].

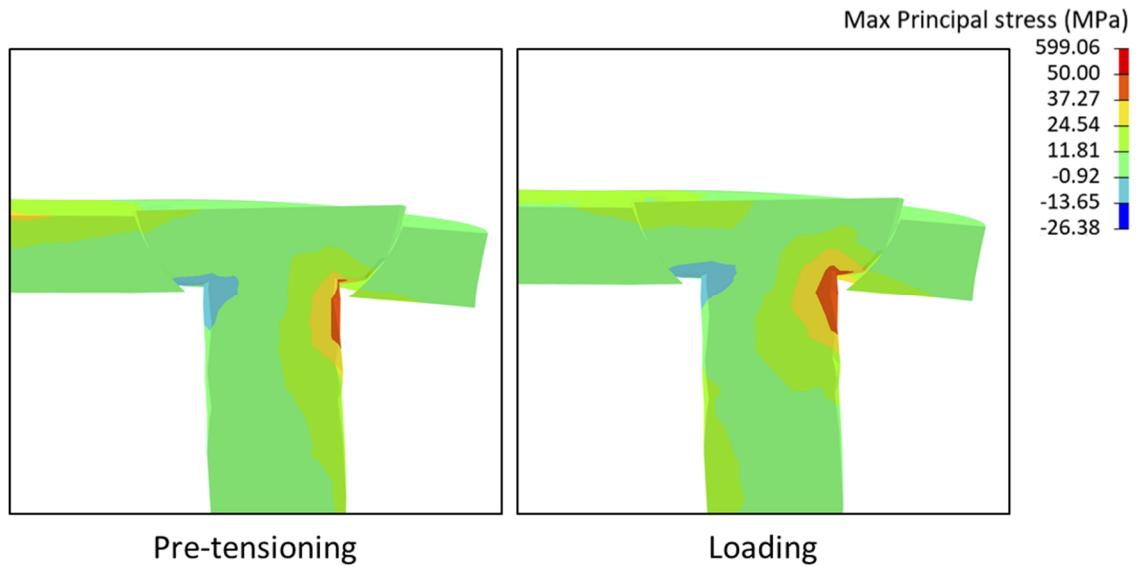


Figure 4.2                      *Bending stresses in proximity of screw head in pre-tensioning step (left) and loading step (right)*

In figure 4.2, the Max principal stresses on a sectioned screw are shown, representing the bending stresses of the screw head: in hotter colours are represented tensile stresses, instead in colder ones the compression stresses.

Considering the loading step, among the three configurations the one with minor solicitation on the cortical bone under the plate is the SQBP C2. The presence of the SQBP plate, having a more extensive surface with respect to the SPP plate, although by using the same configuration of screw placement C2, allows for a higher stress dissipation, with the consequence of not excessively weighting down the bone underneath.

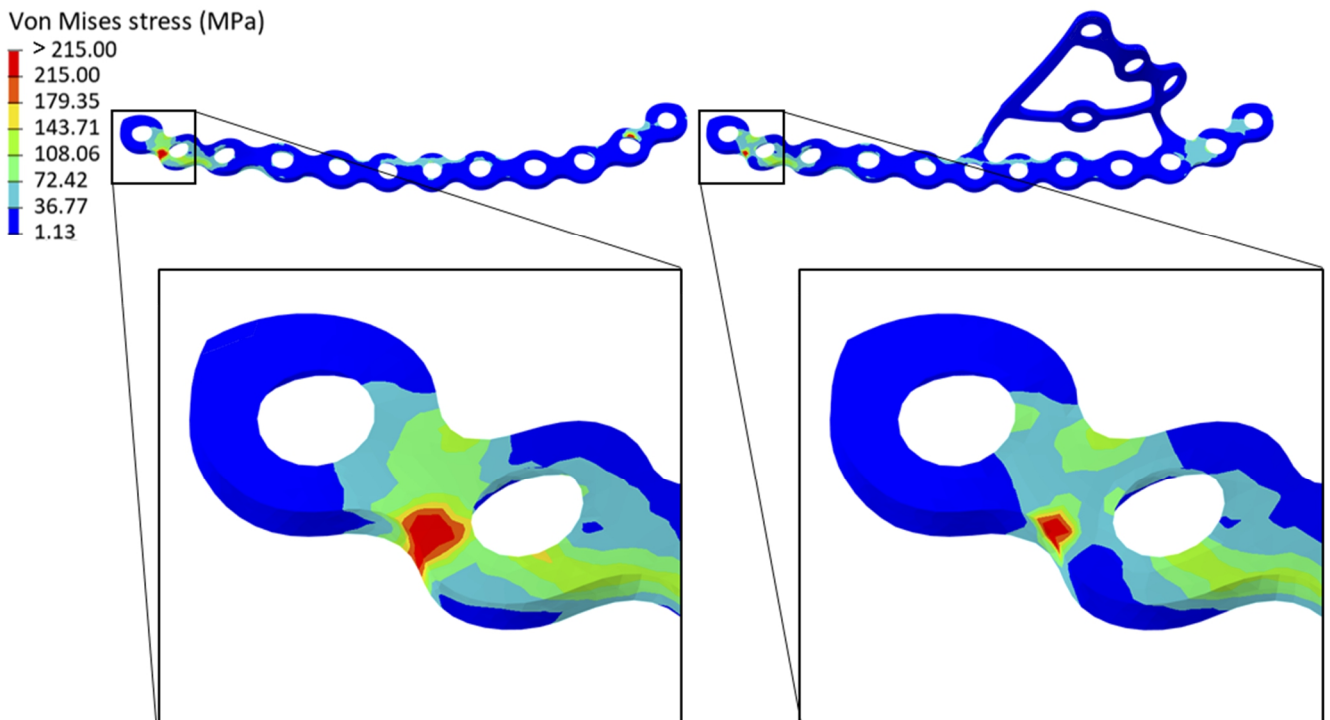


Figure 4.3                      *Von Mises stress maps of SPP plate (left) and SQBP plate (right) with C2 screws configuration during single leg stance*

As can be observable in Fig. 4.3, although the same configurations of screws are considered, it is evident that the stresses present on the two plates are not equivalent. In fact, it is possible to note the presence of stresses acting on the SQBP plate also in the two “bridges” that connect the two suprapectineal and infrapectineal portions, where values of Von Mises stresses of the order of 20 MPa are reached. The most solicited area in both the two C2 (SQBP C2 and SPP C2) configurations is between hole number 1 and 2, where due to modelling imperfections, stresses equal and superior to the yield point (215 MPa [50]) are reached. Nevertheless, from the two zoomed images the more extended area with highest solicitation in the SPP C2 configuration is evident. This outcome endorses the already obtained results about the stress distribution detected on the bone, according which the use of the SPP plate would comport the highest stresses manifestation. The SPP plate furthermore has a more flexible behaviour with respect to the SQBP plate, being more suitable to adapt to the bone shape and so it is able to transfer more easily the load to the bone. The SQBP C2 configuration would result conversely the stiffer and with the lower strains present in the suprapectineal portion, decreasing in this manner lower induced stresses to the bone.

The maps of displacements fields have demonstrated, rather than highlighting significative incongruities among the three internal fixation configurations, mainly differences among the two fractured hemipelvis: with the T-shaped ones the most unstable conditions emerge, mainly related to the high range of motion at the pelvic ring fracture site. The highest values have been detected at the ischiopubic ramus belonging to the SQBP C1 combination (equal to 3.1 mm) further, in terms of magnitude displacements, no significative differences have been found between SPP C2 and SQBP C2 combinations (equal to 2.3 mm).

The different entity of motion of the fractured ischium in the three T-shaped fractured models could explain the lower peak of stress at the pelvic ring fracture region of the SQBP C1 configuration with respect to the SPP C2 one: since in the SQBP C1 configuration the portion of ischium is involved more in this phenomenon of rotation (up to 90% of fracture axial strain detected), the presence of a higher number of contact points between the two stumps would reduce the contact pressure and consequently would diminish also the local peaks of stress. It is dutiful to claim that since the fractures have been produced manually, among the models the fractures conformation is not exactly the same and with the same mesh; this would comport that the entities of the contact points is not constant in all the models, that may lead to the different localization of peaks of stress. Furthermore, the utilize of a denser mesh with smaller elements in the fracture rhyme should be preferable to better appreciate the phenomenon of contact between bony stumps.

Examining instead the entire non fractured hemipelvis shown in fig 4.4, it is possible to make some considerations with respect to the fractured models.

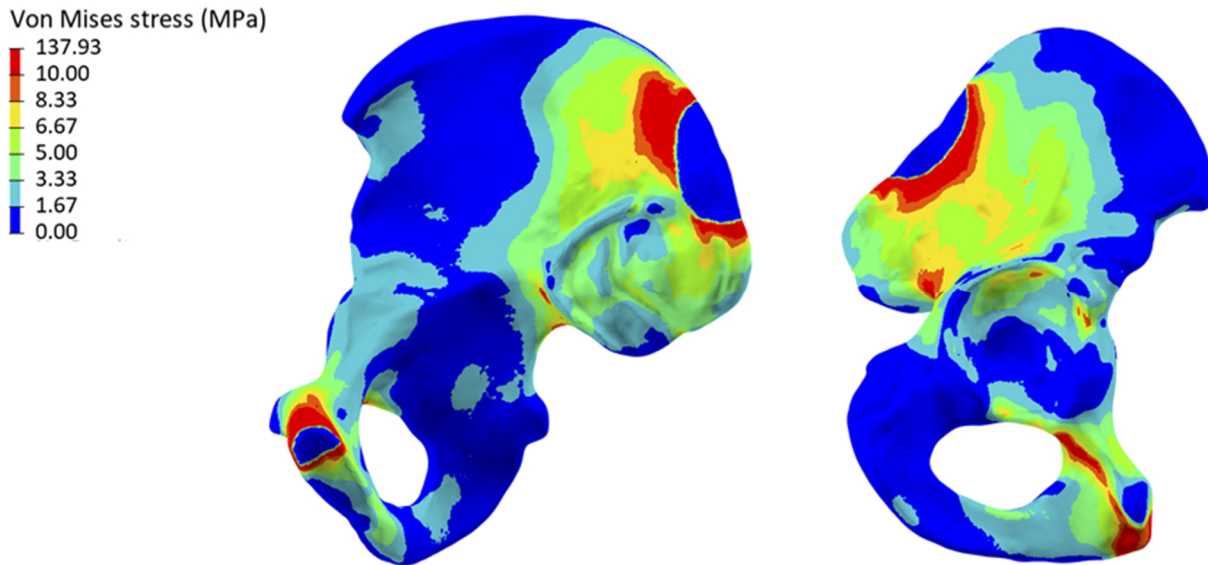


Figure 4.4 Von Mises stress distribution of non-fractured hemipelvis cortical bone in medial (left) and lateral (right) views

As in the fractured hemipelvis, in the non-fractured one (Fig. 4.4) it is possible to find similar features:

- The reaction force areas (pubic symphysis and iliac crest) remain the most solicited zones ;
- A similar mechanism of stress transmission from the femoral head to the acetabular cup through the cartilage: in fact, in all the conditions the most stressed zone of the acetabulum coincides with the anther-superior dial.

Although the modality of transmission is the same, the effective value of stress produced over the acetabulum is different, taking into account a fractured or a non-fractured bone. Differently from the fractured acetabulum where an average Von Mises stress of 55 MPa has been observed, in the intact hemipelvis within the acetabulum, maximal stresses equal to 29 MPa have been detected. In the rest of the acetabulum, instead, it is possible to note minimal stresses: in the centre of acetabulum almost 5 MPa are detected with increasing values moving radially. The minor solicitation of the acetabulum in the normal hemipelvis could be explained by the ability of the bone to dissipate all over its volume the stresses coming from the femoral head.

Nevertheless, when a fracture in the acetabulum involves the area of load transfer, peaks of stress seem to cumulate in proximity of the fracture rhyme. In fact, a possible explanation could be that the fracture gap behaves like a material discontinuity, blocking any stress propagation. Further it could be mentioned that cartilage, when fractured, could lose its specific feature to uniform the load transmission. Another contribution in increasing the stress at the fracture rhyme could be traceable in the screw holding mechanism that would act into a zone of the bone where geometrical discontinuities are present (Fig. 4.5).

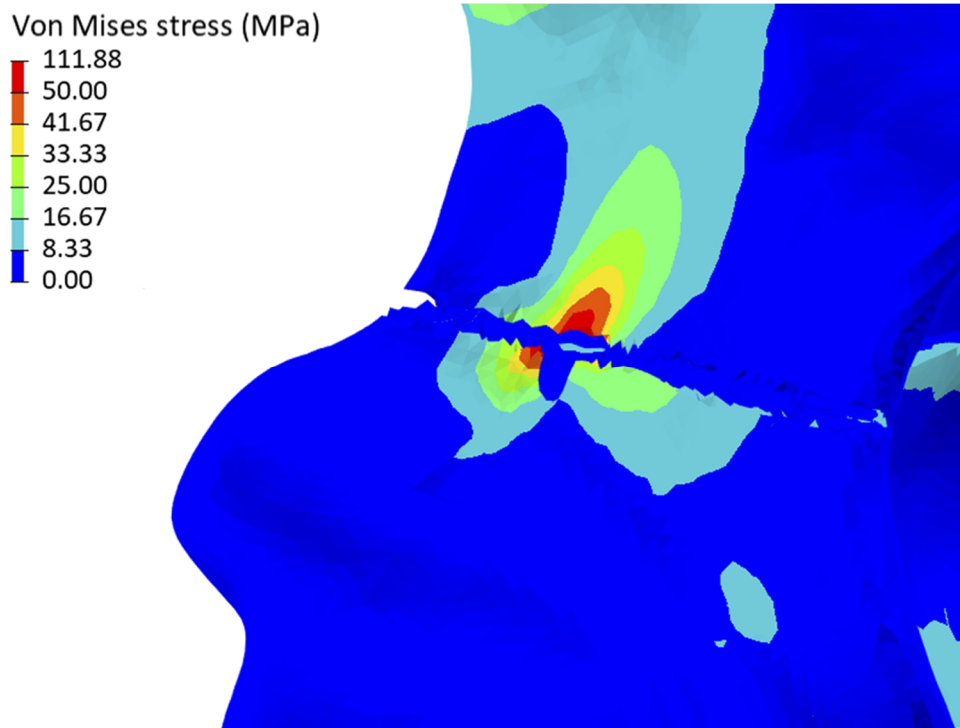


Figure 4.5 Increasing stress at fracture gap site with load transfer

The distribution of stress obtained in the non-fractured acetabulum seems to agree with the theory proposed by Dalstra and Huiskes [67] which affirmed that the most solicited zone in the acetabulum during single leg stance are in the anterior-superior quadrant. Further, in the same study [67], similarly to this thesis work, it is found that also the pubic symphysis and sacroiliac regions with the incisura ischiadica could represent other solicited zones were the load is mainly transmitted [68].

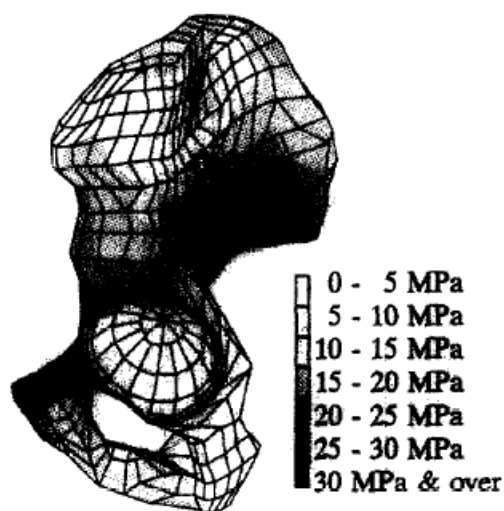


Figure 4.6 Von Mises stress map of cortical bone of hemipelvis during single leg stance according to Dalstra and Huiskes [67]

Goel and colleagues [69] instead, stated that the maximal stress present in a normal acetabulum could be expressed (in MPa) by the formula  $0.57 * Mb$ , where  $Mb$  is the subject body weight. Thus, considering a weight of 100 Kg (as done in this thesis work) the resulting maximum stress would be almost 57 MPa. This value is slightly higher with respect to the one found in this work (29 MPa) but however it has to be interpreted as an indicative one, because of the entity of load applied to the model (it is not applied the exactly same vector of force) and the adopted material properties of cartilage, which are not coincident.

The presence of the cartilage or the muscles acting on the pelvis could interfere with the modality of distribution of the stresses within the hemipelvis, respectively on the acetabulum and in proximity of the insertion point of the muscle.

It is established that cartilage has a primarily role in the capability to distribute uniformly the stress all over the acetabular cup and if for any reason it stops to perform this task, an high stress density would appear in the roof of the socket [69].

Ghosh and colleagues [68] reported that the maximal value of stress induced in the acetabulum during the gait being in the range 30-50 MPa without the presence of cartilage, whilst considering a layer of cartilage it is reduced to 5-15 MPa.

The presence of the muscle instead has incidence mainly on the zone of muscle insertion, such as the iliac crest where two of the most powerful muscle of the hip are attached: the medium and maximus gluteus. Their action permits a stabilization of the hemipelvis because it contrasts the tilt movement of the acetabulum induced by the hip joint reaction force [67]. Opposing to the hip joint reaction force, it is observed that the muscles and ligaments, acting on the hemipelvis, reduce the stresses mainly in correspondence of the pubic symphysis and sacro-iliac region [60].

As showed by Dalstra and Huiskes [67], the pelvic bone behaves like a sandwich, that is all the load is transferred principally on the cortex shell, that having higher elastic modulus is able to support up to 50 times the stresses respect to the trabecular bone. According to the non-fractured hemipelvis implemented in this thesis study, in the cortical bone a maximal von Mises stress is found equal to 138 MPa and in the cancellous bone a maximal value of 11.7 MPa; thus, it is possible to extrapolate that according this thesis job, cortical bone supports almost up to 12 times the stress induced in the cancellous bone. Another difference between cortical and trabecular bone, established by Dalstra and Huiskes [67], is the mismatch of their stress distribution under loading phase. According to them, if in the cortical bone is detected the presence of the so called line of propagation of the stresses that acts from the pubic symphysis to the sacroiliac joint passing through the acetabulum, conversely, in the trabecular bone the maximal stress are reached in the thin wing of ilium and in the acetabulum.

Something similar is evident also in the non-fractured cancellous bone analysed in this thesis study in Fig 4.7.

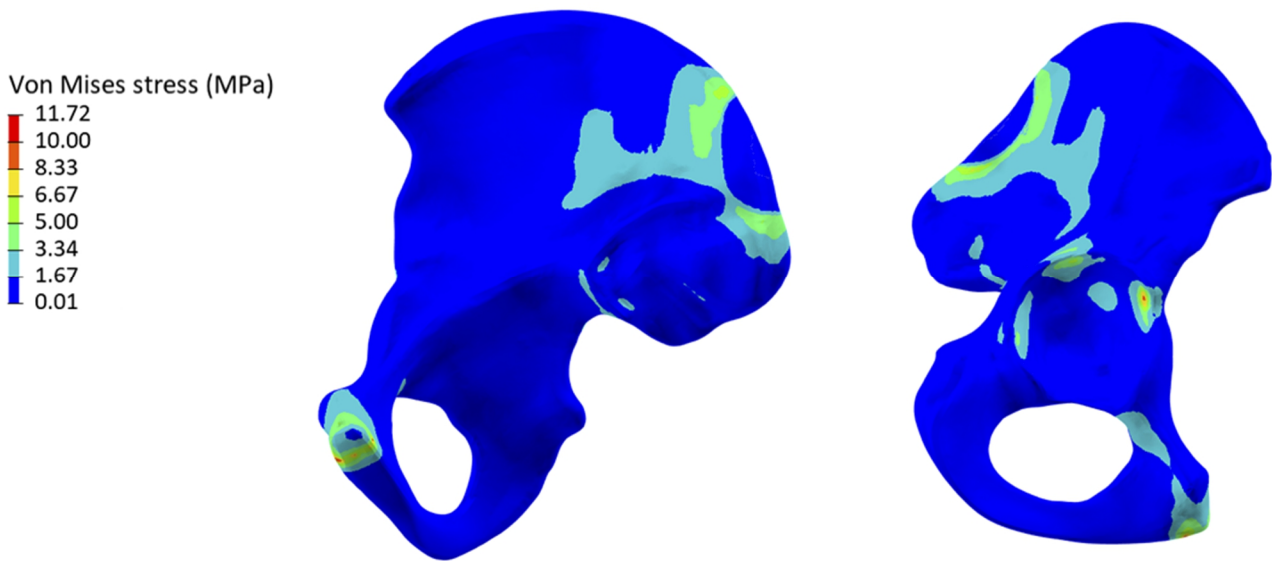


Figure 4.7 Von Mises stress distribution of non-fractured hemipelvis cancellous bone in medial (left) and lateral (right) views

The max value registered in the acetabulum is 8 MPa, instead the maximal value of 11.7 MPa has been detected in the pubic symphysis. It is evident that in the acetabulum the stress is shifted also posteriorly [67] with respect to the cortical bone. The main loaded zones are also the iliac fossa and the wing of ilium which transport the stresses up to the iliac crest.

It is dutiful to stress that this model does not consider any muscular force applied to the hip, but only the hip joint reaction force. Therefore, the resultant stresses at the constrained zones appear higher compared to Dalstra and Huiskes results [67]. As already explained in the chapter two, in this work of thesis, it has been decided to avoid the implementation of any ligaments or muscles in order not to weight down with the use of springs and rigid connections an already complex model, allowing the processing of simulations in a reasonable computational time (40 min adopting intel® Core™ i7 8<sup>th</sup> gen CPU @3.6 GHz with 13 GB RAM dedicated).

These models have obvious limitations, primarily the imposition of fixed boundary conditions. Nevertheless, these assumptions seem not to influence particularly the zone of acetabulum that is the one of higher interest in this study. Moreover, this analysis can also provide interesting information about the modality of internal fixation for acetabular fractures. In fact, the aim of this study was to compare internal fixation configurations rather than trying to understand the effective biomechanics of the hemipelvis.

Taking in consideration the Von Mises yield criterion according which a material starts its yielding process when the Von Mises stress reaches the value known as yield strength, considerations about yielding phenomena of cortical bone can be made. The longitudinal tensile yield strength of cortical bone is found to be equal to 114 MPa [70]. As described in the result chapter, all the six different configurations have been analysed in terms of maximal Von Mises stresses reached in specific regions

of the hemipelvis which are (1) the bonded zone (iliac crest and pubic symphysis), (2) the fracture sites, (3) the bone-plate contact zone and eventually (4) the region of the acetabulum (Table 3-2 in Result chapter). All the models in relation to the acetabulum and pubic symphysis zones seems to remain within the elastic range of the cortical bone solicitation.

As regards the iliac crest, the two models that exceed the yielding point are the T-shaped fracture treated with SQBP C2 and SPP C2 configurations although, as discussed, the absence of muscular structures originating in this region would influence that localized high stress.

The most dangerous situations are detectable at the fracture sites of all the T-shaped models : the so extensive compression over the pelvic ring fracture rhyme, that would induce a so elevated stress could be strictly related to the typology of fixed boundary conditions considered, since the ramus of ischium being the only stump to move. Nevertheless, it can be hypothesized that in a real condition the presence of soft tissues could avoid a so net compression between the two stumps.

As far the bone-plate contact zones are concerned, both the SPP plate combinations and the T-shaped fracture of the SQBP C1 configuration are found to be over the yield strength of cortical bone. This outcome must be ascribed mainly to the already well explained faults of the SPP C2 fixation system and further highlights the weakness points of the SQBP C1 configuration in the treatment of a T-shaped fracture. In these three configurations, theoretically, cortical bone yielding or even material ruptures would happen.

Conversely the only two models that present Von Mises stresses within the elastic behaviour in the hemipelvis globally, are both the two transverse fractures treated with SQBP plate.

Taking into account the results of the interfragmentary movement analysis (IFM), it is feasible to affirm that the infrapectineal portion of the SBQP plate, although not bound with any screw to the bone, can bring improvements in relation to the shear strain reduction of almost 4 times compared to the use of the standard plate (from 65% to 16%). The same usefulness, in the field of axial compressions, however, has not been noticed because the two plates seem to behave in the same way.

The SQBP plate together with the screw configuration C1 achieves the best results in relation to an elementary transverse fracture: it tries to impose an axial compression to the fracture gap (although the optimal range is only reached in 31% of cases) and at the same time it minimizes the shear strain (which is within the acceptable range in 82% of the measurements).

The same behaviour cannot be shifted fully to the transverse associated fracture: although the same combination of plate and screws (SQBP C1) produces an optimal axial compression in 45.5% of the occurrences, however, shear strains are generated reaching up to 77% of the average fracture gap wideness, making unlikely the achieving of secondary stability. This behaviour could be explained by the presence of the further associated fracture of the pelvic ring that modify the trajectory of rigid motion of the bone stumps.

For what concerns the fracture of the pelvic ring, in relation to the axial strain, all the plates and screw configurations are unable to prevent such a high compression of the fracture gap (the SPP C2 combination remains below 70% in compression whilst the SQBP C1 combination comports compression up to 90%); instead from the shear strain point of view it can be seen that reaching the value of 28%, the combination SQBP C1 has the most restrict distribution, probably due to the infrapectineal portion that would hold ischium stump with a better adhesion .

Comparing the three configurations with reference to both shear strain and axial strain, it can be seen that the movement at the fracture gap is dictated not only by the plate itself but also by the typology of fixation screws; in fact, it can be observed that the SQBP C2 combination could offer the best compromise in both elementary and associated fractures. The first configuration of screws (C1) would therefore be disadvantageous on the associated transverse fractures.

# 5. Conclusions

---

This work of thesis based on Finite Element Analysis and focused on the relative comparison of the six models implemented, has provided significative outcomes in terms of internal fixation behaviours. The three parameters adopted to assess the performances of the three internal fixation systems (SQBP C1, SPP C2, SQBP C2) have deccred outcomes compatible with each other. In fact, with the exception of the displacement field parameter by which differences substantially related to fracture typology emerged, from the evaluation of Von Mises stress distributions and IFM analysis, discrepancies between internal fixation combinations have been revealed.

The Von Mises stress distribution identified the SPP C2 configuration as the most inappropriate, since in both transverse and T-shaped fractures the highest values have been reached, even arriving to bone yielding in contact zones with plate. Therefore, it is derived that the SQBP plate could be able to dissipate more easily the stresses coming from the hip joint reaction force, so minimizing repercussions on the bone.

The fracture gap strain assessment has revealed that, in relation to a transverse fracture, the configuration that would more easily promote an indirect healing process is the SQBP C1, since its great ability to minimize shear strain is led by the presence of the infrapectineal portion of the plate. Nevertheless, the configuration SQBP C2 has shown the best compromise considering either the shear and the axial strain.

Fundamentally, a clinical suggestion that could emerge from this study is that in relation to an elementary transverse fracture, adopting the SQBP C1 configuration should be preferable, whilst the most appropriate treatment for T-shaped fractures could be identifiable with the SQBP C2 configuration.

# Bibliography

---

1. Tile M - *Fractures of the pelvis and acetabulum*, 1994.
2. Slooff TJ, Schreurs BW, Buma P et al. - *Impaction morcellized allografting and cement*, 1998.
3. Gansslen A, Pohlemann T, Paul C et al. - *Epidemiology of pelvic ring injuries*, 1996.
4. Melton LJ, Sampson JM, Morrey BF et al. - *Epidemiologic features of pelvic fractures*, 1981.
5. Laird A, Keating JF - *Acetabular fractures: a 16-year prospective epidemiological study*, 2005.
6. Giannoudis PV, Grotz MR, Papakostidis C et al. - *Operative treatment of displaced fractures of the acetabulum*, 2005.
7. Mears DC, Velyvis JH, Chih-Peng C - *Displaced acetabular fractures managed operatively: indicators of outcome*, 2003.
8. Demetriades D, Karaiskakis M, Toutouzas K et al. - *Pelvic fractures: epidemiology and predictors of associated abdominal injuries and outcomes*, 2002.
9. Stein DM, O'Connor JV, Kufera JA et al. - *Risk factors associated with pelvic fractures sustained in motor vehicle collisions involving newer vehicles*, 2006.
10. Dakin GJ, Eberhardt AW, Alonso JE et al. - *Acetabular fracture patterns: associations with motor vehicle crash information*, 1999.
11. Ruedi T, Murphy WM - *AO principles of fracture management*, 2000.
12. Judet R, Judet E, Letournel E - *Fractures of the acetabulum: classification and surgical approach for open reduction. Preliminary report*, 1964.
13. Ganz R, Gill TJ, Gautier E et al. - *Surgical dislocation of the adult hip, a technique of full access to the femoral head and acetabulum without the risk of avascular necrosis*, 2001.
14. Notzli HP, Siebenrock KA, Hempfing A et al. - *Perfusion of femoral head during surgical dislocation of the hip. Monitoring by laser Doppler flowmetry*, 2002.

15. Routt ML Jr, Swiontkowski MF - *Operative treatment of complex acetabular fractures. Combined anterior and posterior exposures during the same procedure*, 1990.
16. Beaulé PE, Dorey FJ, Matta JM - *Letournel classification for acetabular fractures: assessment of interobserver and intraobserver reliability*, 2003.
17. Tile M, Helfet DL, Kellam JF et al. - *Comprehensive classification of fractures in the pelvis and acetabulum*, 1995.
18. Pace A - *Le fratture di acetabolo*, 2011.
19. Durkin A, Sagi HC, Durham R et al. - *Contemporary management of pelvic fractures*, 2006.
20. Croce MA, Magnotti LJ, Savage SA et al. - *Emergent pelvic fixation in patients with exsanguinating pelvic fractures*, 2007.
21. Rommens PM, Hessmann MH - *Staged reconstruction of pelvic ring disruption: differences in morbidity, mortality, radiologic results, and functional outcomes between B1, B2/B3, and C-type lesions*, 2002.
22. Borrelli J, Goldfarb C, Ricci W et al. - *Functional outcome after isolated acetabular fractures*, 2002.
23. Bhandari M, Matta J, Ferguson T - *Predictors of clinical and radiological outcome in patients with fractures of the acetabulum and concomitant posterior dislocation of the hip*, 2006.
24. Matta JM - *Fractures of the acetabulum: accuracy of reduction and clinical results in patients managed operatively within three weeks after the injury*, 1996.
25. Letournel E, Judet R. - *Fractures of the Acetabulum*, 1993.
26. Johnson EE, Matta JM, Mast JW et al. - *Delayed reconstruction of acetabular fractures 21-120 days following injury*, 1994.
27. Tile M - *Pelvic ring fractures: should they be fixed?*, 1988.
28. Cole JD, Bolhofner BR - *Acetabular fracture fixation via a modified Stoppa limited intrapelvic approach. Description of operative technique and preliminary results*, 1994.

29. Tornetta P - *Displaced acetabular fractures: indications for operative and non operative management*, 2001.
30. *PRO pelvis and acetabulum system (brochure)*, 2017.
31. Gras F, Marintschev I, Grossterlinden L et al. - *Anterior intrapelvic approach for acetabular fractures using approach-specific instruments and an anatomical-preshaped 3-dimensional suprapectineal plate*, 2017.
32. Perren SM, *Evolution of the internal fixation of long bone fractures. The scientific basis of biological internal fixation: choosing a new balance between stability and biology*, 2002.
33. Halvachizadeh S, Pape HC - *Perren's strain theory and fracture healing*, 2020.
34. Perren SM - *Fracture healing the evolution of our understanding*, 2008.
35. Wolff J - *Das gesetz der transformation der knochen*, 1892.
36. Frost HM - *Bone "mass" and the "mechanostat": a proposal*, 1987.
37. Elliott DS, Newman KJH, Forward DP et al.- *A unified theory of bone healing and nonunion*, 2016.
38. Caiti G, Dobbe JGG, Bervoets E et al. - *Biomechanical considerations in the design of patient-specific fixation plates for the distal radius*, 2019.
39. HJ Kim, SH Kim, SH Chang - *Finite element analysis using interfragmentary strain theory for the fracture healing process to which composite bone plates are applied*, 2011.
40. Augat P, Burger J, Schorlemmer S et al. - *Shear movement at the fracture site delays healing in a diaphyseal fracture model*, 2003.
41. Claes LE, Meyers N - *The direction of tissue strain affects the neovascularization in the fracture-healing zone*, 2020.
42. Steiner M, Claes L, Ignatius A et al. - *Disadvantages of interfragmentary shear on fracture healing—mechanical insights through numerical simulation*, 2014.
43. Epari DR, Taylor WR, Heller MO et al. - *Mechanical conditions in the initial phase of bone healing*, 2006.
44. Lacroix D, Prendergast PJ - *A mechano-regulation model for tissue differentiation during fracture healing: analysis of gap size and loading*, 2002.
45. Lacroix D, Prendergast PJ, Li G et al. - *Biomechanical model to simulate tissue differentiation and bone regeneration: application to fracture healing*, 2002.

46. Hu P, Wu T, Wang HZ et al. - *Biomechanical comparison of three internal fixation techniques for stabilizing posterior pelvic ring disruption: a 3d finite element analysis*, 2011.
47. Feng x, Qi W, Wang C et al. - *Effect of the screw tightening sequence on the stress distribution of a dynamic compression plate: A pilot finite element study*, 2019.
48. Mechlenburg I, Nyengaard JR, Gelineck J et al. - *Cartilage thickness in the hip joint measured by MRI and stereology*, 2007.
49. Chen YC, Tu YK, Chen LW - *Finite element simulations of bone temperature rise during bone drilling based on a bone analog*, 2013.
50. <http://asm.matweb.com/search/SpecificMaterial.asp?bassnum=MQ304A>
51. Butz KD, Chan DD, Nauman EA et al. - *Stress distributions and material properties determined in articular cartilage from MRI-based finite strains*, 2011.
52. Willing R, Lalone EA, King GJW et al. - *Comparing two constitutive material models of cartilage for hemiarthroplasty articular contact mechanics using computational analyses*, 2012.
53. Lai YS, Chen WC, Huang CH et al. - *Effect of graft strength on knee laxity and graft in-situ forces after posterior cruciate ligament reconstruction*, 2015.
54. Fuller DD - *Theory and practice of lubrication for engineers*, 1956.
55. Shockey JS, von Fraunhofer JA, Seligson D - *A measurement of the coefficient of static friction of human long bones*, 1985.
56. Damm P, Dmyke J, Ackermann R et al. - *Friction in total hip joint prosthesis measured in vivo during walking*, 2013.
57. Hughes AN, Jordan BA - *The mechanical properties of surgical bone screws and some aspects of insertion practice*, 1972.
58. Karnezis IA, Miles AW, Cunningham JL - *Axial preload in external fixator half-pins: a preliminary mechanical study of an experimental bone anchorage system*, 1999.
59. Beaupré GS, Carter DR, Orr TE et al. - *Stresses in plated long-bones: the role of screw tightness and interface slipping*, 1988.
60. Pankaj P, Howie CR, Usmanic AS et al. - *Finite element modelling of the pelvis: Inclusion of muscular and ligamentous boundary conditions*, 2007.

61. Yao F, He y, Quian H et al. - *comparison of biomechanical characteristics and pelvic ring stability using different fixation methods to treat pubic symphysis diastasis*, 2015.
62. Bergmann G, Bender A, Dymke J et al. - *standardized loads acting in hip implants*, 2016.
63. Zanetti EM, Aldieri A, Terzini M et al. - *Additively manufactured custom load-bearing implantable devices: grounds for caution*, 2017.
64. Chana-Rodríguez F, Mañanes RP, Rojo-Manaute J et al. - *3D surgical printing and pre contoured plates for acetabular fractures*, 2016.
65. Johnson A - *Humeral fracture fixation techniques: a fea comparison of locking and compression techniques with cadaveric pullout comparison of cortical compression and internal locking screws*, 2007.
66. Robert KQ 3<sup>rd</sup>, Chandler R, Baratta RV - *The effect of divergent screw placement on the initial strength of plate-to-bone fixation*, 2003.
67. Dalstra M, Huiskes R - *Load transfer across the pelvic bone*, 1995.
68. Ghosh R, Pal B, Ghosh D et al. - *Finite element analysis of a hemi-pelvis: the effect of inclusion of cartilage layer on acetabular stresses and strain*, 2015.
69. Goel VK, Valliappan S, Svensson NL - *Stresses in the normal pelvis*, 1978.
70. Black J - *Handbook of biomaterial properties*, 1998.